

AEDC-TR-71-51

Cy1



**TRIPLE COLLISION EFFECTS  
IN THE THERMAL CONDUCTIVITY AND VISCOSITY  
OF MODERATELY DENSE GASES  
PART II**

**D. T. Gillespie and J. V. Sengers**

**Institute for Molecular Physics  
University of Maryland  
College Park, Maryland**

**March 1971**

This document has been approved for public release and  
sale; its distribution is unlimited.

**ARNOLD ENGINEERING DEVELOPMENT CENTER  
AIR FORCE SYSTEMS COMMAND  
ARNOLD AIR FORCE STATION, TENNESSEE**

PROPERTY OF U S AIR FORCE  
AEDC LIBRARY  
F40600-71-C-0002

# *NOTICES*

When U. S. Government drawings specifications, or other data are used for any purpose other than a definitely related Government procurement operation, the Government thereby incurs no responsibility nor any obligation whatsoever, and the fact that the Government may have formulated, furnished, or in any way supplied the said drawings, specifications, or other data, is not to be regarded by implication or otherwise, or in any manner licensing the holder or any other person or corporation, or conveying any rights or permission to manufacture, use, or sell any patented invention that may in any way be related thereto.

Qualified users may obtain copies of this report from the Defense Documentation Center.

References to named commercial products in this report are not to be considered in any sense as an endorsement of the product by the United States Air Force or the Government.

TRIPLE COLLISION EFFECTS  
IN THE THERMAL CONDUCTIVITY AND VISCOSITY  
OF MODERATELY DENSE GASES  
PART II

D. T. Gillespie and J. V. Sengers  
Institute for Molecular Physics  
University of Maryland  
College Park, Maryland

This document has been approved for public release and  
sale; its distribution is unlimited.

## FOREWORD

The research reported herein was sponsored by the Arnold Engineering Development Center (AEDC), Air Force Systems Command (AFSC). The research was conducted at the Institute for Molecular Physics of the University of Maryland from September 1, 1968 to August 31, 1970 under delivery order F40600-69-C-0002. Air Force project monitor for this project was 1st Lt. Michael G. Buja, AEDC (DYR). The Program Element was 61102F and the Project 8951. The manuscript was submitted for publication November 1, 1970.

The present research report is concerned with the formulation and evaluation of collision integrals needed for the prediction of transport properties of compressed gases. Some of the highlights of this research were discussed in a paper entitled, "Three-Particle Collisions in the Theory of Transport Properties of Gases" [Proceedings of the Fifth Symposium on Thermophysical Properties, C. F. Bonilla, ed., The American Society of Mechanical Engineers, New York, N. Y., 1970, pp. 42-54]. In part under the same delivery order, a study was initiated of the experimental viscosity of compressed nitrogen and argon in collaboration with Professor J. Kestin of Brown University; this research is not yet fully completed and will be incorporated in a subsequent technical report.

The authors want to thank Miss Jean I-Jeng Chu for her assistance in checking the equations and computer coding reported in Chapter V. The research reported in Chapter III concerning the number of collisions between three gas molecules was conducted in collaboration with Dr. W. R. Hoegy of the Goddard Space Flight Center in Greenbelt, Maryland. The computer calculations leading to the results reported in Tables IV and VI were carried out on a UNIVAC 1108 computer at the Computer Science Center of the University of Maryland.

The reproducibles used in the reproduction of this report were supplied by the authors.

This technical report has been reviewed and is approved.

Michael G. Buja  
First Lieutenant, USAF  
Research and Development  
Division  
Directorate of Technology

Harry L. Maynard  
Colonel, USAF  
Director of Technology

## ABSTRACT

Calculations of transport properties of dilute gases are always based on the Boltzmann equation. The Boltzmann equation accounts only for the effects of collisions between two gas molecules. To predict transport properties of moderately dense gases one needs to determine the effects of collisions among more than two gas molecules. The present report studies the contributions to the transport properties caused by collisions among three gas molecules. It is demonstrated that the first density correction to the transport properties can be represented by a series of collision integrals associated with, one, two, three and four collisions between three gas molecules. Numerical studies for calculating the dominant collision integrals are made for a gas of hard spherical molecules.

## TABLE OF CONTENTS

Foreword . . . . .	ii
Abstract . . . . .	iii
List of Tables . . . . .	vii
List of Figures . . . . .	viii
<i>Chapter</i>	<i>Page</i>
I. SCOPE OF THIS RESEARCH . . . . .	1
1.1 Introduction . . . . .	1
1.2 Highlights of This Research . . . . .	4
II. REVIEW OF THE BASIC EQUATIONS . . . . .	10
2.1 Equations Governing the Transport Coefficients in the Dilute Limit. The "Binary Collision Inner Product". . . . .	11
2.2 Equations Governing the Transport Coefficients to First Order in Density. The "Triple Collision Inner Product". . . . .	22
III. SEQUENCES OF MOLECULAR COLLISIONS . . . . .	31
3.1 Definitions and Nomenclature . . . . .	33
3.2 Some Important Theorems . . . . .	38
IV. ANALYSIS OF THE TRIPLE COLLISION INNER PRODUCT . . . . .	43
4.1 Introduction . . . . .	43
4.2 Separation of Spatial and Dynamical Correlations. Expansion in Effective Number of Collisions. . . . .	55
4.3 Consequences for the Transport Coefficients . . . . .	87
V. NUMERICAL CALCULATIONS OF THE "EXCLUDED VOLUME" CONTRIBUTIONS TO THE TRANSPORT PROPERTIES. . . . .	91
5.1 Equivalence of the "Double-Overlap" Contribution with Enskog's Approximation. . . . .	91
5.2 Evaluation of the "Single-Overlap" Contribution. Refinement of Enskog. . . . .	95

VI. DISCUSSION OF RESULTS . . . . . 132

    6.1 Summary of Accomplishments. . . . . 132

    6.2 Outlook. . . . . 137

APPENDIX A. THEOREMS ON THE DYNAMICS OF THREE HARD  
            SPHERE MOLECULES . . . . . 141

References . . . . . 156

## LIST OF TABLES

<i>Table</i>	<i>Page</i>
I The coefficients for the first and second Sonine approximations to the solution of the linearized Boltzmann equation for hard sphere molecules . . . . .	19
II The Sonine polynomials . . . . .	19
III Dynamical quantities for the single-overlap collision sequence, expressed in terms of the integration variables in equation (5-27) . . . .	110
IV Monte Carlo estimates of the single-overlap triple collision integrals, and the consequent fractional corrections to the Enskog values for $\lambda_1$ , $\eta_1$ and $D_1$ in the first(1) and second(2) Sonine approximations . . . . .	127
V Expansion of the triple collision integrals . .	134
VI Numerical results for the single-overlap terms . . . . .	134

## LIST OF FIGURES

<i>Figure</i>	<i>Page</i>
1 A collision between two hard sphere molecules. . .	13
2 The excluded volume determining the linear density term in $g(\sigma)$ . . . . .	28
3 Representation of (a) an interacting collision, (b) a non-interacting penetrating collision, (c) a non-interacting separating collision, and (d) an explicit overlap. . . . .	35
4 Example of a three-particle collision sequence.. .	36
5 Illustrating the addition of two collision sequence diagrams. . . . .	38
6 Diagram of Lemma 1. . . . .	40
7 Diagrams for the operators $T_{\mu}^{(2)}(12)$ . . . . .	46
8 Diagrams for the operators $T_{\mu}^{(3)}(12;13)$ . . . . .	47
9 Diagrams $R_{11} \equiv R_1$ and $R_{12}$ . . . . .	53
10 The six $v$ -diagrams. . . . .	54
11 Illustrating the relation between the vari- ables at the first and second collisions. . . . .	62
12 All $v$ -diagrams containing at least one double-overlap collision. . . . .	65
13 All $v$ -diagrams containing at least one single-overlap collision. . . . .	67
14 Equivalent double-overlap diagrams. . . . .	69
15 Diagram for $(\phi, \psi)_1^{(3)}$ . . . . .	70
16 Summation of the single-overlap diagrams. . . . .	72
17 Diagram for $(\phi, \psi)_2^{(3)}$ . . . . .	75

18	All $\nu$ -diagrams not containing an overlap collision. . . . .	77
19	Diagrams for $(\phi, \psi)_3^{(3)}$ . . . . .	80
20	Four-collision diagrams: class (i). . . . .	82
21	Four-collision diagrams: top row, class (ii); bottom row, class (iii). . . . .	83
22	Diagrams for $(\phi, \psi)_4^{(3)}$ . . . . .	86
23	Integrating variables for $(\phi, \psi)_1^{(3)}$ . . . . .	92
24	Integrating variables for $(\phi, \psi)_2^{(3)}$ . . . . .	98
25	The variable $\hat{k}_{21}$ in $(\phi, \psi)_2^{(3)}$ . . . . .	105
26	The variable $\vec{r}_{31}$ in $(\phi, \psi)_2^{(3)}$ . . . . .	107
27	The variable $\vec{w}_{31}$ in $(\phi, \psi)_2^{(3)}$ . . . . .	107
28	Diagram of Lemma 1. . . . .	141
29	Diagram used in proof of Lemma 1. . . . .	143
30	Diagram used in proof of Theorem I. . . . .	147

CHAPTER I  
SCOPE OF THIS RESEARCH

1.1 Introduction

For many engineering applications, reliable information on the transport properties of compressed gases is required. This research is part of a continuing effort to develop methods to calculate the transport properties of gases as a function of pressure or density. In order to pursue this goal we are attempting to derive such methods from the rigorous foundations of statistical mechanics. Our approach is in many ways analogous to the virial expansion for the equation of state and the thermodynamic properties. We recall that, for a gas in equilibrium, the product of the pressure  $P$  and volume  $V$  can be expanded in a power series in terms of the density  $\rho$ :

$$PV = RT + A_1\rho + A_2\rho^2 + \dots \quad (1-1)$$

The "virial coefficients"  $A_k$  can be expressed in terms of molecular cluster integrals which are integrals over the positions of  $k$  simultaneously interacting gas molecules. They can be calculated for molecules with a given interaction potential.

Similarly, we attempt to represent the thermal conductivity  $\lambda$  and the viscosity  $\eta$  by expansions in terms of the density  $\rho$ :

$$\lambda = \lambda_0 + \lambda_1 \rho + \lambda_2' \rho^2 \log \rho + \lambda_2 \rho^2 + \dots$$

$$\eta = \eta_0 + \eta_1 \rho + \eta_2' \rho^2 \log \rho + \lambda_2 \rho^2 + \dots$$
(1-2)

The new expansion (1-2) for the transport properties differs from the virial expansion (1-1) for the equilibrium properties in two important aspects:

1. The theory predicts that the expansion for the transport properties contains not only simple powers of  $\rho$ , but also terms which depend logarithmically on  $\rho$  [1,2,3]. These extra terms lead to some complicating features and we shall need to assess their effect. In this and a subsequent technical report we shall give some arguments indicating that the coefficients of the  $\log \rho$  term are small.
2. The coefficients  $\lambda$  and  $\eta$  determine the response of the gas to the presence of a gradient in temperature or fluid velocity. Microscopically, these coefficients are related to the dynamical interactions among the molecules. While the coefficients  $A_k$  of the virial series are determined by relatively simple "configurational integrals", the coefficients of the expansions (1-2) are determined by fairly complicated "collision integrals". At the present, the structure of these collision integrals is poorly understood.

The transport coefficients  $\lambda_0$  and  $\eta_0$  in the dilute gas limit ( $\rho \rightarrow 0$ ) are determined by the Boltzmann equation. Using a procedure introduced by Chapman and Enskog [4,5],  $\lambda_0$  and  $\eta_0$  are obtained in terms of "binary collision integrals". Calculation of these binary collision integrals has become a routine procedure, and tabulated values are available for many forms of the intermolecular potential.

The approximate nature of the Boltzmann equation is due to the fact that it considers only uncorrelated binary collisions. That is, if two molecules are aimed to collide, the Boltzmann equation assumes that they will eventually collide; similarly, if two molecules are not aimed to collide, the Boltzmann equation assumes that they will never collide. These assumptions clearly fail at higher densities, where, as a result of "interfering" collisions with other molecules, two molecules which are originally aimed to collide may in fact not collide, and two molecules which are originally not aimed to collide may eventually do so. Therefore, to extend the theory to higher densities, collision processes involving more than two molecules must be accounted for.

In the past decade many attempts have been made to generalize the Boltzmann equation to higher densities. However, all such attempts have been on a rather formal level. Thus it becomes our task to judge these developments, to derive expressions for the collision integrals determining the coefficients in the density expansion (1-2) for the transport properties, and

to explore procedures for calculating these collision integrals.

In this technical report we focus our attention on the first density corrections  $\lambda_1$  and  $\eta_1$  in (1-2). A knowledge of these first density coefficients would enable us to predict the transport properties up to pressures of the order of 100 atmospheres.

A calculation of the first density corrections requires an analysis of collisions among three gas molecules. A treatment of "genuine" triple collisions, such as those leading to the association and dissociation of bounded states, is deferred to a later stage in this research program. Here we consider the effect on the transport properties of those triple collisions which are *sequences of successive binary collisions involving three molecules*.

In view of the complexity of this task, our initial analysis must be restricted to a gas of *hard spherical molecules*. Although this model is somewhat unrealistic, it nevertheless provides valuable insight as to how the various collision sequences contribute to the transport coefficients of the gas. Our ultimate goal of course is to calculate the density dependence of the transport properties of more realistic gases.

## 1.2 Highlights of This Research

The research program outlined above was initiated in a previous technical report AEDC-TR-69-68 [6]. We shall refer to that report as I.

In the past a few attempts have been made to propose a tentative theory for the density dependence of the transport properties. The most important approximate theory is the one proposed by Enskog for a gas of hard spherical molecules [7]. This theory assumes that the probability of finding two molecules involved in a collision, when the gas is *not* in equilibrium, is the same as when the gas *is* in equilibrium.

All approximate theories developed thus far avoid an explicit analysis of collision sequences involving more than two molecules. The research reported in I and the present report yields, for the first time, actual *calculations* of transport collision integrals which include the effects of collisions among more than two gas molecules.

The preliminary calculations reported in I revealed that the theory of Enskog is not strictly correct, but it does provide a good first approximation to the first density coefficients. While this result represented a major discovery, its physical origin was far from clear. Furthermore, the calculations reported in I revealed that substantial cancellations occurred among the contributions from the various three-particle collision sequences. These results indicated that, despite the fact that our formulation of the transport integrals was mathematically correct, we did not grasp sufficiently well the "physics" of the problem. As a consequence we were unable to refine the approximate Enskog theory in a systematic way, nor was it clear how the prediction method

could be extended to account for successive collisions between more realistic gas molecules.

In the present report we show how these questions can be answered by considering three-particle collision integrals containing respectively, one, two, three and four binary collisions among the three molecules. Present indications are that this expansion converges rapidly, and the first term accounts for 90 to 95% of the first density correction.

To appreciate the physical meaning of this expansion we again make the analogy with the virial expansion (1-1) for the equation of state and the thermodynamic properties. For a gas in equilibrium the velocities of the molecules are uncorrelated; that is, the velocities of the molecules are independent and determined by the Maxwell-Boltzmann distribution. As a result the virial coefficients  $A_k$  are related to cluster integrals that contain only the *positions* of the molecules. In the dilute gas limit, the equation of state is that of a perfect gas:  $PV=RT$ . In this approximation it is assumed that the positions of the molecules are also random. This assumption fails at higher densities since the *excluded volume* associated with molecules of finite size leads to correlations among the positions of the molecules.

For a gas that is not in equilibrium both the positions and the velocities are correlated. At low densities, the transport coefficients of a gas are given approximately by the Chapman-Enskog theory [ $\lambda_0$  and  $\eta_0$  in (1-2)]. This approximate theory is akin to the perfect gas law, in that it assumes

no correlations in either the positions or the velocities of the molecules. The assumption that the velocities are uncorrelated is sometimes referred to as the assumption of *molecular chaos*. In order to calculate the transport properties at higher densities we have to account for excluded volume effects in the position distribution, and also for deviations from molecular chaos in the velocity distribution. With the foregoing points in mind, our new expansion procedure for calculating the first density correction to the transport properties may be characterized in the following way: The first term in the expansion takes into account the excluded volume effects for the positions of three molecules, but no deviations from molecular chaos for their velocities. The next term accounts for the excluded volume effects for two molecules and a first deviation from molecular chaos in which the velocities are correlated by two successive binary collisions among the three molecules. The higher order terms contain no excluded volume effects, but increased deviations from molecular chaos caused by three and four successive collisions among the three molecules. It turns out that the first term in this expansion of the first density coefficients coincides *precisely* with the Enskog theory.

In the course of our investigations, several theorems were discovered leading to significant simplifications in the calculations of the transport integrals. In particular we were able to prove that, for a calculation of transport coefficients, one does *not* need to consider more than *four* successive collisions

among three gas molecules. Although this theorem is strictly valid for hard spherical molecules, the analysis strongly suggests that the contributions from five and more successive collisions will be negligibly small for more realistic gas molecules as well. Furthermore, it turns out that the matrix of collision integrals is *symmetric*, so it suffices to calculate only half the elements of the matrix.

In summary, the results obtained for this report represent a significant advance in our ability to calculate transport collision integrals accounting for sequences of collisions involving three gas molecules. Moreover, the results are in such a form that methods to extend the theory to higher densities and to generalize the procedure to more complicated molecules begin to suggest themselves. For a more detailed discussion of the results the reader is referred to Chapter VI.

While developing the theory further, we have also made a close examination of the density dependence of transport properties for those gases where experimental information is available. In I we developed some criteria as to how information could be extracted from the experimental data for a meaningful comparison of theory and experiment. As a result we presented tables of first density coefficients for both the thermal conductivity and shear viscosity [8]. During the present research efforts, new very precise results were obtained for the density dependence of the viscosity of argon and nitrogen. These studies were carried out in collaboration with Professor Kestin and Mr. Paykoc at Brown University, and will be presented in another technical

report to be prepared in the near future. The present report is limited to a comprehensive account of our methods to calculate the required transport collision integrals.

CHAPTER II  
REVIEW OF THE BASIC EQUATIONS

In Chapter II of our previous report I[6], the basic equations determining the transport coefficients of a gas of hard sphere molecules were presented and discussed in some detail. In the present chapter we review these equations, since they form the basis for our subsequent work. Inasmuch as these equations and their underlying formalism are rather complicated, we have made several changes in notation and format in an attempt to obtain greater pedagogical clarity. We shall now write all equations directly in terms of the number density of molecules  $n$  and the molecular diameter  $\sigma$ , instead of the molecular covolume  $b\rho$ ; these quantities are related by the equation [cf. (2.3-8) of I]

$$\frac{5}{8}b\rho = \frac{5}{12}\pi\sigma^3n \quad (2-1)$$

More importantly, we shall introduce the "binary collision inner product" and the "triple collision inner product" as the fundamental entities which determine the zeroth-order density and first-order density parts of the transport coefficients. We shall see that our understanding of the origin and magnitude of the linear terms in the density expansions of the transport coefficients depends mainly upon how deeply we can analyze the physics and mathematics of the general "triple collision inner product".

2.1 Equations Governing the Transport Coefficients in the Dilute Limit. The "Binary Collision Inner Product".

The Boltzmann equation for the rate of change of the single-particle distribution function  $f(\vec{r}_1, \vec{v}_1; t)$  of a dilute gas is [4]

$$\frac{\partial f}{\partial t} + \vec{v}_1 \cdot \frac{\partial f}{\partial \vec{r}_1} = J(ff) \quad (2-2)$$

Here the term  $J(ff)$  represents the effects of uncorrelated binary collisions among the molecules [cf. p.10 of I for a description of  $J(ff)$ ]. In order to obtain a solution  $f$  valid to first order in the gradients of the local temperature  $T(\vec{r}_1, t)$  and the local mean velocity  $\vec{u}(\vec{r}_1, t)$  -- i.e., a solution sufficient to determine the thermal conductivity  $\lambda_0$  and the shear viscosity  $\eta_0$  -- one assumes for  $f$  the form [6]

$$f(\vec{r}_1, \vec{v}_1; t) = f_0(V_1) \left( 1 - \vec{A}(\vec{v}_1) \cdot \frac{\partial \log T}{\partial \vec{r}_1} - \vec{B}(\vec{v}_1) : \frac{\partial \vec{u}}{\partial \vec{r}_1} \right) \quad (2-3)$$

Here,  $\vec{v}_1$  is the "thermal velocity" of molecule 1,

$$\vec{v}_1 \equiv \vec{v}_1 - \vec{u}(\vec{r}_1, t) \quad (2-4)$$

$f_0(V_1)$  is the Maxwell-Boltzmann distribution function,

$$f_0(V_1) = n \left( \frac{m}{2\pi kT} \right)^{3/2} e^{-mV_1^2/2kT} \quad (2-5)$$

where  $m$  is the mass of a molecule and  $k$  is Boltzmann's constant, and finally,  $\vec{A}(\vec{v}_1)$  and  $\vec{B}(\vec{v}_1)$  are respectively vector- and

tensor-valued functions of velocity whose forms must be such that (2-3) satisfies (2-2) to first order in the gradients of  $T$  and  $\vec{u}$ . One thus finds that  $\vec{A}$  and  $\vec{B}$  must satisfy the equations [6]

$$I_2 \vec{A}(\vec{V}_1) = f_0(V_1) \left( \frac{mV_1^2}{2kT} - \frac{5}{2} \right) \vec{V}_1 \quad (2-6)$$

and

$$I_2 \vec{B}(\vec{V}_1) = f_0(V_1) \frac{m}{kT} \vec{V}_1^{\circ} \vec{V}_1 \quad (2-7)$$

where  $\vec{V}_1^{\circ} \vec{V}_1$  is the traceless tensor  $\vec{V}_1 \vec{V}_1 - \overline{V_1^2}/3$ , and where  $I_2$  is the "linearized binary collision operator". For hard sphere molecules of diameter  $\sigma$ , the operator  $I_2$  acting on a general function  $\psi(\vec{V}_1)$  produces [cf. (2.8-8) of I]

$$I_2 \psi(\vec{V}_1) = -\sigma^2 \int d\vec{V}_2 d\hat{k}_{21} |\vec{V}_{21} \cdot \hat{k}_{21}| f_0(V_1) f_0(V_2) \sum_{n=1}^2 \psi(\vec{V}_n) \quad (2-8)$$

The quantities appearing in this equation are related to each other through the binary collision sequence depicted in Fig.1. The variable  $\vec{V}_2$  is the thermal velocity of molecule 2,  $\vec{V}_{21} \equiv \vec{V}_2 - \vec{V}_1$ , and  $\hat{k}_{21}$  locates molecule 2 relative to molecule 1 according to

$$\sigma \hat{k}_{21} = -(\vec{r}_2 - \vec{r}_1) \quad (2-9)$$

Since  $\hat{k}_{21}$  is a unit vector, then  $|\vec{r}_2 - \vec{r}_1| = \sigma$ , implying that we are spatially constraining molecules 1 and 2 to be just touching

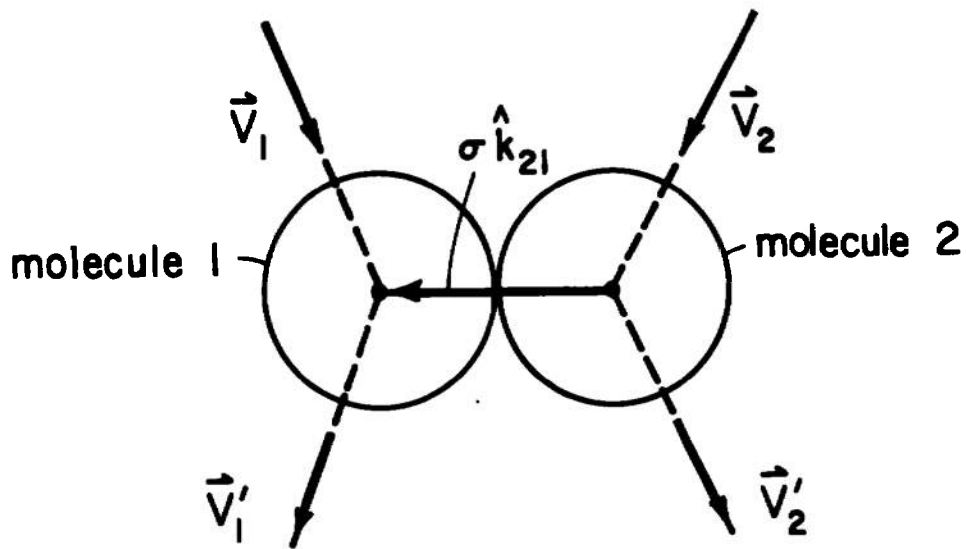


Figure 1. A collision between two hard sphere molecules.

each other; in other words, in (2-8) molecules 1 and 2 are "colliding" with perihelion or "collision vector"  $\hat{k}_{21}$  [see Fig.1].

The operator  $T(12)$  in (2-8) has two forms, depending on whether the two molecules are converging ( $\vec{V}_{21} \cdot \hat{k}_{21} > 0$ ) or diverging ( $\vec{V}_{21} \cdot \hat{k}_{21} < 0$ ). Specifically, if the molecules are *diverging*, then  $T(12)$  acting on a general function  $F$  of the velocities  $\vec{V}_1$  and  $\vec{V}_2$  produces zero:

$$\vec{V}_{21} \cdot \hat{k}_{21} < 0: \quad T(12)F(\vec{V}_1, \vec{V}_2) = 0 \quad (2-10a)$$

if the molecules are *converging*, however, then

$$\vec{V}_{21} \cdot \hat{k}_{21} > 0: \quad T(12)F(\vec{V}_1, \vec{V}_2) = F(\vec{V}'_1, \vec{V}'_2) - F(\vec{V}_1, \vec{V}_2) \quad (2-10b)$$

where  $\vec{V}'_1$  and  $\vec{V}'_2$  are the velocities of the molecules after the collision:

$$\left. \begin{aligned} \vec{V}'_1 &= \vec{V}_1 + \vec{V}_{21} \cdot \hat{k}_{21} \hat{k}_{21} \\ \vec{V}'_2 &= \vec{V}_2 - \vec{V}_{21} \cdot \hat{k}_{21} \hat{k}_{21} \end{aligned} \right\} \quad (2-11)$$

For later purposes it will be illustrative to regard  $T(12)$  as being the sum of two "velocity replacement" operators,

$T_n^{(2)}(12)$  and  $T_i^{(2)}(12)$ , which we shall denote generally by

$T_\mu^{(2)}(12)$ :

$$T(12) = \sum_{\mu=n,i} T_\mu^{(2)}(12) \quad (2-12)$$

According to (2-10a), when molecules 1 and 2 are *not* aimed to collide, then  $T_i^{(2)}(12) = T_n^{(2)}(12) = 0$ ; according to (2-10b), when molecules 1 and 2 *are* aimed to collide, then

$$\begin{aligned} T_i^{(2)}(12)F(\vec{V}_1, \vec{V}_2) &= F(\vec{V}'_1, \vec{V}'_2) \\ T_n^{(2)}(12)F(\vec{V}_1, \vec{V}_2) &= -F(\vec{V}_1, \vec{V}_2) \end{aligned} \quad (2-13)$$

where  $\vec{V}'_1$  and  $\vec{V}'_2$  are given by (2-11). Our motivation for introducing the  $T_\mu^{(2)}(12)$  operators, is as follows. Let us associate the index  $\mu=i$  with an "interacting" collision, in which molecules 1 and 2 are deflected in the usual way with their final velocities  $\vec{V}'_1$  and  $\vec{V}'_2$  given by (2-11); similarly, let us associate the index  $\mu=n$  with a "non-interacting" collision, in which molecules 1 and 2 pass through each other

undeflected so that their final velocities are  $\vec{V}'_1 = \vec{V}_1$  and  $\vec{V}'_2 = \vec{V}_2$ . Then we may write for *either* index  $\mu$ .

$$\vec{V}_{21} \cdot \vec{k}_{21} < 0: \quad T_{\mu}^{(2)}(12)F(\vec{V}_1, \vec{V}_2) = 0 \quad (2-14a)$$

$$\vec{V}_{21} \cdot \vec{k}_{21} > 0: \quad T_{\mu}^{(2)}(12)F(\vec{V}_1, \vec{V}_2) = (-1)^{\mu} F(\vec{V}'_1, \vec{V}'_2) \quad (2-14b)$$

where  $(-1)^{\mu} = +1$  or  $-1$  according to whether the  $\mu$ -collision is interacting or non-interacting, and where  $\vec{V}'_1$  and  $\vec{V}'_2$  are *now* the final velocities for the  $\mu$ -collision. A more precise mathematical definition of these operators has been given by Ernst et al [9].

With the linearized Boltzmann operator  $I_2$  thus defined, one next proceeds to solve equations (2-6) and (2-7) for the functions  $\vec{A}$  and  $\vec{B}$  respectively. The solution  $\vec{A}$  governs the linear response of the distribution function  $f$  to a gradient in the temperature, and in fact it determines the dilute-limit thermal conductivity  $\lambda_0$  according to [cf. (2.1-18) of I]

$$\lambda_0 = \frac{k}{3} \int d\vec{V}_1 \vec{A}(\vec{V}_1) \cdot \left[ f_0(V_1) \left( \frac{mV_1^2}{2kT} - \frac{5}{2} \right) \vec{V}_1 \right] \quad (2-15)$$

Similarly, the solution  $\vec{B}$  governs the linear response of the distribution function to a gradient in the mean velocity, and it determines the dilute limit viscosity  $\eta_0$  according to [cf. (2.1-19) of I]

$$\eta_0 = \frac{kT}{10} \int d\vec{V}_1 \vec{B}(\vec{V}_1) : \left[ f_0(V_1) \frac{m}{kT} \vec{V}_1 \vec{V}_1 \right] \quad (2-16)$$

By virtue of equations (2-6) and (2-7), it is seen that equations (2-15) and (2-16) can also be written

$$\lambda_0 = \frac{k}{3} \int d\vec{V}_1 \vec{A}(\vec{V}_1) \cdot I_2 \vec{A}(\vec{V}_1)$$

$$\eta_0 = \frac{kT}{10} \int d\vec{V}_1 \vec{\vec{B}}(\vec{V}_1) : I_2 \vec{\vec{B}}(\vec{V}_1)$$

We are thus led to define the *binary collision inner product* of two functions  $\phi(\vec{V}_1)$  and  $\psi(\vec{V}_1)$  by

$$(\phi, \psi)^{(2)} \equiv \int d\vec{V}_1 \phi(\vec{V}_1) * I_2 \psi(\vec{V}_1) \quad (2-17)$$

where  $*$  denotes the dot product if  $\phi$  and  $\psi$  are vectors, and the double dot product if they are tensors. With this notation, the above equations for  $\lambda_0$  and  $\eta_0$  take the compact forms

$$\lambda_0 = \frac{k}{3} (\vec{A}, \vec{A})^{(2)} \quad (2-18)$$

$$\eta_0 = \frac{kT}{10} (\vec{\vec{B}}, \vec{\vec{B}})^{(2)} \quad (2-19)$$

Therefore, once  $\vec{A}(\vec{V}_1)$  and  $\vec{\vec{B}}(\vec{V}_1)$  have been found,  $\lambda_0$  is given essentially by the binary collision inner product of  $\vec{A}$  with itself, while  $\eta_0$  is given essentially by the binary collision inner product of  $\vec{\vec{B}}$  with itself.

An explicit expression for the binary collision inner product can be obtained by substituting the formula for  $I_2$  given in (2-8) into the definition (2-17), and then symmetrizing with respect to the velocities. Defining

$$\Phi(\vec{V}_1, \vec{V}_2) \equiv \sum_{n=1}^2 \phi(\vec{V}_n) \quad \text{and} \quad \Psi(\vec{V}_1, \vec{V}_2) \equiv \sum_{n=1}^2 \psi(\vec{V}_n) \quad (2-20)$$

we obtain in this way

$$(\phi, \psi)^{(2)} = - \frac{\sigma^2}{2} \int d\vec{v}_1 d\vec{v}_2 d\hat{k}_{21} |\vec{v}_{21} \cdot \hat{k}_{21}| f_0(v_1) f_0(v_2) \{ \Phi(\vec{v}_1, \vec{v}_2) * T(12) \Psi(\vec{v}_1, \vec{v}_2) \} \quad (2-21)$$

If we write T(12) as in (2-14), this becomes

$$(\phi, \psi)^{(2)} = - \frac{\sigma^2}{2} \sum_{\mu=i, n} \int d\vec{v}_1 d\vec{v}_2 d\hat{k}_{21} |\vec{v}_{21} \cdot \hat{k}_{21}| f_0(v_1) f_0(v_2) \{ \Phi(\vec{v}_1, \vec{v}_2) * T_{\mu}^{(2)}(12) \Psi(\vec{v}_1, \vec{v}_2) \} \quad (2-22)$$

Alternatively, we can use (2-10) to write the binary collision inner product as

$$(\phi, \psi)^{(2)} = - \frac{\sigma^2}{2} \int_{\vec{v}_{21} \cdot \hat{k}_{21} > 0} d\vec{v}_1 d\vec{v}_2 d\hat{k}_{21} |\vec{v}_{21} \cdot \hat{k}_{21}| f_0(v_1) f_0(v_2) \{ \Phi(\vec{v}_1, \vec{v}_2) * [\Psi(\vec{v}'_1, \vec{v}'_2) - \Psi(\vec{v}_1, \vec{v}_2)] \} \quad (2-23)$$

where  $\vec{v}'_1$  and  $\vec{v}'_2$  are given in terms of the integration variables by (2-11).

In practice, one does not solve (2-6) and (2-7) for  $\vec{A}(\vec{v}_1)$  and  $\vec{B}(\vec{v}_1)$  *exactly*, but only in some "Nth Sonine approximation"; that is,  $\vec{A}$  and  $\vec{B}$  are written as linear combinations of N Sonine polynomials, and the optimum values of the expansion coefficients are found by a variational procedure. If these Sonine expansions are written as [cf. (2.2-10) of I]

$$\vec{A}_N(\vec{v}_1) = - \frac{15}{32} \sqrt{\frac{2}{\pi}} \frac{1}{n\sigma^2} \sum_{k=1}^N a_k(N) S_{3/2}^{(k)}(w_1^2) \vec{w}_1 \quad (2-24)$$

$$\vec{B}_N(\vec{v}_1) = + \frac{5}{8} \sqrt{\frac{2}{\pi}} \frac{1}{n\sigma^2} \sqrt{\frac{m}{2kT}} \sum_{k=0}^{N-1} b_k(N) S_{5/2}^{(k)}(w_1^2) \vec{w}_1 \vec{w}_1 \quad (2-25)$$

where we have defined the dimensionless velocity  $\vec{W}_i$  by

$$\vec{W}_i \equiv \sqrt{\frac{m}{2kT}} \vec{V}_i \quad (2-26)$$

then one finds that the expansion coefficients for  $N=1$  and  $N=2$  are as shown in Table I [4]. The explicit formulae for the Sonine polynomials which we shall be using are give in Table II [4]. We remark that the complicated looking factors in front of the summation signs in (2-24) and (2-25) were chosen merely in order to make  $a_1(1)=b_0(1)=1$ , for hard sphere molecules.

If we now substitute the Sonine expansions (2-24) and (2-25) into (2-18) and (2-19), we can obtain the well-known results [cf. (2.2-13) of I]

$$\lambda_0(N) = \frac{k}{3} (\vec{A}_N, \vec{A}_N)^{(2)} = \frac{75}{64} \frac{1}{\sigma^2} \sqrt{\frac{k^3 T}{m\pi}} a_1(N) \quad (2-27)$$

$$\eta_0(N) = \frac{kT}{10} (\vec{B}_N, \vec{B}_N)^{(2)} = \frac{5}{16} \frac{1}{\sigma^2} \sqrt{\frac{mkT}{\pi}} b_0(N) \quad (2-28)$$

for the  $N$ th Sonine approximations to  $\lambda_0$  and  $\eta_0$  respectively. We remark, however, that these results are actually obtained by substituting the Sonine expansions for  $\vec{A}_N$  and  $\vec{B}_N$  directly into (2-15) and (2-16), rather than into (2-18) and (2-19). Of course, the coefficients  $a_k(N)$  and  $b_k(N)$  in the expansions (2-24) and (2-25) were obtained by evaluating integrals which are essentially binary collision inner products between the various Sonine polynomials, as was indicated in I.

TABLE I

The coefficients for the first and second Sonine approximations (2-24) and (2-25) to the solution of the linearized Boltzmann equation for hard sphere molecules.

<u>N=1</u>	$a_1(1) = 1$	$b_0(1) = 1$
<u>N=2</u>	$\left\{ \begin{array}{l} a_1(2) = 1 + \frac{1}{44} \\ a_2(2) = \frac{1}{11} \end{array} \right.$	$\left\{ \begin{array}{l} b_0(2) = 1 + \frac{3}{202} \\ b_1(2) = \frac{6}{101} \end{array} \right.$

TABLE II

The Sonine Polynomials

General: 
$$S_n^{(k)}(X) = \sum_{j=0}^k \frac{(-1)^j (k+n)!}{(j+n)! (k-j)! j!} X^j$$

k=0: 
$$S_n^{(0)}(X) = 1$$

k=1: 
$$S_n^{(1)}(X) = (n+1) - X$$

k=2: 
$$S_n^{(2)}(X) = \frac{(n+1)(n+2)}{2} - (n+2)X + \frac{1}{2}X^2$$

In the following chapters, we shall indicate how the calculation of the first order density quantities proceeds along lines parallel to the foregoing binary collision inner product formalism. Thus, an appreciation of (a) the definition of the binary collision inner product in (2-17), (b) its relation to the zeroth-order transport coefficients in (2-18) and (2-19), and (c) its mathematical structure in (2-21)-(2-23), will enable us to see more clearly what is involved in determining the first order density corrections to the transport coefficients.

Finally, we wish to point out an important feature of the binary collision inner product in (2-17): it is *symmetric*, in that

$$\boxed{(\phi, \psi)^{(2)} = (\psi, \phi)^{(2)}} \quad (2-29)$$

provided that  $\phi$  and  $\psi$  are either both even or both odd functions of velocity. This can be proved most easily using equation (2-23): Changing the integrating variables from  $\vec{V}_1, \vec{V}_2$  to  $\vec{V}'_1, \vec{V}'_2$  and noting from (2-11) that

$$\begin{aligned} d\vec{V}'_1 d\vec{V}'_2 &= d\vec{V}_1 d\vec{V}_2 \\ \vec{V}'_{21} \cdot \hat{k}_{21} &= -\vec{V}_{21} \cdot \hat{k}_{21} \\ V_1'^2 + V_2'^2 &= V_1^2 + V_2^2 \end{aligned} \quad (2-30)$$

(2-23) can be written as

$$\begin{aligned} (\phi, \psi)^{(2)} &= -\frac{\sigma^2}{2} \int_{\vec{V}'_{21} \cdot \hat{k}_{21} < 0} d\vec{V}'_1 d\vec{V}'_2 d\hat{k}_{21} |\vec{V}'_{21} \cdot \hat{k}_{21}| f_0(V_1') f_0(V_2') \\ &\quad \{ \phi(\vec{V}_1, \vec{V}_2) * [\Psi(\vec{V}'_1, \vec{V}'_2) - \Psi(\vec{V}_1, \vec{V}_2)] \} \end{aligned} \quad (2-31)$$

Here,  $\vec{V}_1$  and  $\vec{V}_2$  are given in terms of the integrating variables by the inverse of equations (2-11):

$$\left. \begin{aligned} \vec{V}_1 &= \vec{V}'_1 + \vec{V}'_{21} \cdot \hat{k}_{21} \hat{k}_{21} \\ \vec{V}_2 &= \vec{V}'_2 - \vec{V}'_{21} \cdot \hat{k}_{21} \hat{k}_{21} \end{aligned} \right\} \quad (2-32)$$

If we now make a second change of variables from  $\vec{V}'_1, \vec{V}'_2$  to the negative of these quantities, then because  $\phi$  and  $\psi$  are assumed to have the same parity,

$$\phi(-\vec{X}) * \psi(-\vec{Y}) \equiv \phi(\vec{X}) * \psi(\vec{Y})$$

the only change in (2-31) is that the "<" sign in the integration limit becomes a ">" sign. Finally, we interchange the primed and unprimed velocity variables throughout; the resulting equation is then identical to the original expression (2-23), save only for an interchange of the primed and unprimed velocities inside the braces. If this equation and (2-23) are added together and the result divided by 2, we obtain

$$\begin{aligned} (\phi, \psi)^{(2)} &= \frac{\sigma^2}{4} \int_{\vec{V}'_{21} \cdot \hat{k}_{21} > 0} d\vec{V}'_1 d\vec{V}'_2 d\hat{k}_{21} |\vec{V}'_{21} \cdot \hat{k}_{21}| f_0(V_1) f_0(V_2) \\ &\quad \{ [\phi(\vec{V}'_1, \vec{V}'_2) - \phi(\vec{V}_1, \vec{V}_2)] * [\psi(\vec{V}'_1, \vec{V}'_2) - \psi(\vec{V}_1, \vec{V}_2)] \} \end{aligned} \quad (2-33)$$

Since (2-33) is manifestly symmetric in  $\phi$  and  $\psi$ , the property (2-29) follows immediately.

## 2.2 Equations Governing the Transport Coefficients to First Order in Density. The "Triple Collision Inner Product".

The "generalized Boltzmann equation" to first order in the density  $n$  is [2,10]

$$\frac{\partial f}{\partial t} + \vec{v}_1 \cdot \frac{\partial f}{\partial \vec{r}_1} = J(ff) + J_1(ff) + K(fff) \quad (2-34)$$

This equation differs from the ordinary Boltzmann equation (2-2) only by the addition of the two terms on the right. The term  $J_1(ff)$  accounts for the "spatial inhomogeneity" caused by the fact that the centers of two colliding molecules are not at the same point, but are separated by a distance  $\sigma > 0$ . As the notation suggests, the term  $J_1(ff)$  is essentially a binary collision term. The term  $K(fff)$ , however, represents the effects of correlated binary collision sequences involving three molecules, and is the subject of our present investigation. The precise form of  $K(fff)$  has been set down and discussed in I [see equations (2.4-1)-(2.4-4) of I].

Corresponding to the three collision terms on the right of (2-34), the transport coefficients take the forms

$$\lambda = \lambda_0 + \frac{4}{5}\pi\sigma^3 n\lambda_0 + n\lambda_1 \quad (2-34)$$

$$\eta = \eta_0 + \frac{8}{15}\pi\sigma^3 n\eta_0 + n\eta_1 \quad (2-36)$$

We see that the terms  $J_1(ff)$  and  $K(fff)$  *each* contribute terms to the transport coefficients which are linear in the density.

The contributions of  $J_1(ff)$  are known exactly in terms of  $\sigma, n$  and the zeroth order quantities [4], but the contributions of  $K(fff)$  remain to be determined.

A derivation of formal expressions for  $\lambda_1$  and  $\eta_1$  has been given in I [cf. Section 2.4 and Appendix A of I]. Briefly, what is involved is as follows: Just as one constructs from  $J(ff)$  a "linearized binary collision operator"  $I_2$  so one constructs from  $K(fff)$  a "linearized triple collision operator"  $I_3$  [cf. (2.4-5) and (2.4-6) of I]. As originally obtained,  $I_3$  is a 12-dimensional integral operator; after performing one rather intricate integration [cf. Appendix A of I], one obtains an 11-dimensional "surface integral" form for  $I_3$ :

$$I_3 \psi(\vec{V}_1) = -\frac{\sigma^5}{2} \int d\vec{V}_2 d\vec{V}_3 d\hat{k}_{21} d\vec{r}_{31} |\vec{V}_{21} \cdot \hat{k}_{21}| f_0(V_1) f_0(V_2) f_0(V_3) \cdot T(123) \prod_{n=1}^3 \psi(\vec{V}_n) \quad (2-37)$$

[Note:  $I_3$  here corresponds to  $b\rho I_3$  in I.] We call attention to the similarity in forms between this expression for  $I_3$  and  $I_2$  given in (2-8). The integrating variables in (2-37) and the operator  $T(123)$  are related to certain sequences of binary collisions involving *three* molecules, just as the integrating variables in (2-8) and the operator  $T(12)$  are related to certain sequences of binary collisions involving *two* molecules. Since a detailed description of the relevant three-particle collision sequences requires a specialized nomenclature, we shall postpone a deeper analysis of the quantities appearing in (2-37) until after this nomenclature has been developed in

Chapter III. For now, it suffices only to realize that the theory provides us with a well-defined "linearized triple collision operator"  $I_3$ , which is a generalization of the linearized binary collision operator  $I_2$ .

Now, in Sec. 2.4 of I it is shown that  $\lambda_1$  and  $\eta_1$  are given by [cf. (2.4-11) of I]

$$n\lambda_1 = -\frac{k}{3} \int d\vec{V}_1 \vec{A}(\vec{V}_1) \cdot I_3 \vec{A}(\vec{V}_1) \quad (2-38)$$

$$n\eta_1 = -\frac{kT}{10} \int d\vec{V}_1 \vec{\vec{B}}(\vec{V}_1) : I_3 \vec{\vec{B}}(\vec{V}_1) \quad (2-39)$$

[Note:  $n\lambda_1$  here corresponds to  $b\rho\lambda_1$  in I, and similarly for  $n\eta_1$ .] Here  $\vec{A}$  and  $\vec{\vec{B}}$  are the *same* functions we encountered in the previous section -- i.e., the solutions to (2-6) and (2-7). Defining, then, the *triple collision inner product* of two functions  $\phi(\vec{V}_1)$  and  $\psi(\vec{V}_1)$  by

$$(\phi, \psi)^{(3)} \equiv \int d\vec{V}_1 \phi(\vec{V}_1) * I_3 \psi(\vec{V}_1) \quad (2-40)$$

where, as in (2-17), \* denotes the dot product if  $\phi$  and  $\psi$  are vectors, and the double dot product if they are tensors, we may evidently write (2-38) and (2-39) in the compact forms

$$n\lambda_1 = -\frac{k}{3} (\vec{A}, \vec{A})^{(3)} \quad (2-41)$$

$$n\eta_1 = -\frac{kT}{10} (\vec{\vec{B}}, \vec{\vec{B}})^{(3)} \quad (2-42)$$

The only differences between these formulae for  $n\lambda_1$  and  $n\eta_1$  and the formulae in (2-18) and (2-19) for  $\lambda_0$  and  $\eta_0$  are:

(i) the minus signs, and (ii) the fact that the inner products are now taken with respect to  $I_3$  rather than  $I_2$ . Since  $\vec{A}$  and  $\vec{B}$  are the *known* solutions of the ordinary Boltzmann equation, then further progress from equations (2-41) and (2-42) evidently requires a thorough understanding of the triple collision inner product in (2-40); it is to this end that our present work is directed. If the expression for  $I_3$  in (2-37) is inserted into the definition (2-40), and the resulting expression then symmetrized with respect to the velocities, we obtain [cf. (2-21)]

$$\begin{aligned}
 (\phi, \psi)^{(3)} &= - \frac{\sigma^5}{3!} \int d\vec{V}_1 d\vec{V}_2 d\vec{V}_3 d\hat{k}_{21} d\vec{r}_{31} \\
 &\quad |\vec{V}_{21} \cdot \hat{k}_{21}| f_0(V_1) f_0(V_2) f_0(V_3) \quad (2-43) \\
 &\quad \{ \phi(\vec{V}_1, \vec{V}_2, \vec{V}_3) * T(123) \psi(\vec{V}_1, \vec{V}_2, \vec{V}_3) \}
 \end{aligned}$$

Here we have defined, in analogy with (2-20),

$$\phi(\vec{V}_1, \vec{V}_2, \vec{V}_3) \equiv \sum_{n=1}^3 \phi(\vec{V}_n); \quad \psi(\vec{V}_1, \vec{V}_2, \vec{V}_3) \equiv \sum_{n=1}^3 \psi(\vec{V}_n) \quad (2-44)$$

The interrelations among the integrating variables in (2-43), and the precise definition of the operator  $T(123)$ , will be explained in detail in Sec. 4.1.

At this point it is pertinent to recall that the earliest (and to date the most meaningful) attempt to account for the density dependence of the transport coefficients was made by Enskog [7]. Enskog correctly assessed the "spatial inhomogeneity" corrections in (2-35) and (2-36) -- i.e., the  $J_1$ -terms -- and

in addition he derived an *approximation* for the triple collision corrections  $\lambda_1$  and  $\eta_1$ . An explanation of the basis of the Enskog theory for  $\lambda_1$  and  $\eta_1$  is given in Sec. 2.3 of I, and we shall quickly review that explanation here:

When a gas is in equilibrium, the probability to find two molecules at a given separation  $r_{21}$  is independent of the velocities of the molecules, and is determined by the radial distribution function  $g(r_{21})$ . The Enskog theory essentially assumes that this still holds true when the gas is *not* in equilibrium, in that  $g(\sigma)$  gives the probability to find two molecules in contact ( $r_{21}=\sigma$ ) even in the presence of gradients. As a consequence, the quantity  $f_0(V_1)f_0(V_2)$  in (2-8) gets replaced by  $g(\sigma)f_0(V_1)f_0(V_2)$ , implying that the linearized Boltzmann operator  $I_2$  gets replaced by  $g(\sigma)I_2$ ; this in turn replaces the solutions  $\vec{A}$  and  $\vec{B}$  of (2-6) and (2-7) by  $\vec{A}/g(\sigma)$  and  $\vec{B}/g(\sigma)$ , respectively. Consequently, from (2-15) and (2-16), we find for the thermal conductivity and shear viscosity the results

$$\lambda_E = \lambda_0/g(\sigma) \qquad \eta_E = \eta_0/g(\sigma) \qquad (2-45)$$

Now, the quantity  $g(\sigma)$  can be expressed as a function of the density  $n$  by a well-known virial expansion,

$$g(\sigma) = 1 + \frac{5}{12}\pi\sigma^3 n + \dots \qquad (2-46)$$

In a gas of hard spheres, spatial correlations are due to the finite size of the molecules, which does not allow molecules

to overlap each other. Therefore, the various terms in the expansion (2-46) are determined by integrals over "forbidden" configurations involving increasing numbers of molecules. In particular, the coefficient  $5\pi\sigma^3/12$  is the volume where a third molecule 3 would overlap with both of two colliding molecules 1 and 2, as illustrated in Fig.2. Inserting now the above expansion for  $g(\sigma)$  into (2-45), we find for the Enskog estimates of  $\lambda_1$  and  $\eta_1$

$$\lambda_1 \approx -\frac{5}{12}\pi\sigma^3\lambda_0 \equiv \lambda_{1E}, \quad \eta_1 \approx -\frac{5}{12}\pi\sigma^3\eta_0 \equiv \eta_{1E} \quad (2-47)$$

A comparison of these results with equations (2-18), (2-19), (2-41) and (2-42) reveals that *the effect of the Enskog theory is to approximate the triple collision inner product according to*

$$(\phi, \psi)^{(3)} \approx \frac{5}{12}\pi\sigma^3 n(\phi, \psi)^{(2)} \equiv (\phi, \psi)_E^{(3)} \quad (2-48)$$

Our subsequent analysis of the triple collision inner product will shed considerable light on the relation of this approximation to the exact theory.

Earlier work by Sengers [12,13] as reported in I, has indicated that the Enskog approximation for  $\lambda_1$  and  $\eta_1$  is probably in error by only about 5% or so. For this reason it will be advantageous to measure the first density corrections to  $\lambda$  and  $\eta$  in units of  $|\lambda_{1E}|$  and  $|\eta_{1E}|$  respectively. Thus, using (2-47), we write (2-35) and (2-36) as

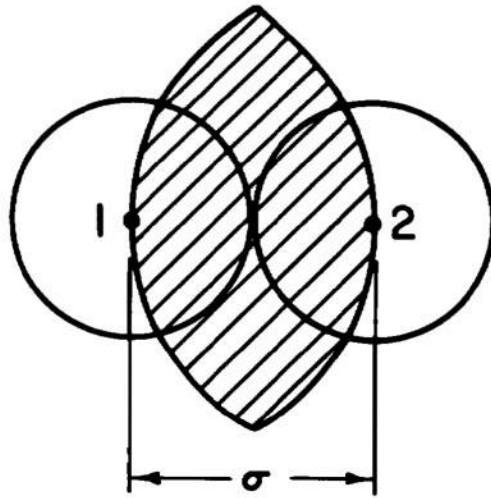


Figure 2. The excluded volume determining the linear density term in  $g(\sigma)$ .

$$\lambda = \lambda_0 \left[ 1 + \frac{5}{12} \pi \sigma^3 n \left( \frac{48}{25} + \lambda_1 / |\lambda_{1E}| \right) \right] \quad (2-49)$$

$$\eta = \eta_0 \left[ 1 + \frac{5}{12} \pi \sigma^3 n \left( \frac{32}{25} + \eta_1 / |\eta_{1E}| \right) \right] \quad (2-50)$$

Our eventual aim, then, is to evaluate the dimensionless quantities  $\lambda_1 / |\lambda_{1E}|$  and  $\eta_1 / |\eta_{1E}|$ , and in particular to determine *why* and *by how much* these quantities differ from the Enskog estimate of -1.

Our present numerical calculations will be keyed to the Sonine approximations of the functions  $\vec{A}$  and  $\vec{B}$  in (2-24) and (2-25). Consequently, our formulae will have to indicate

the degree  $N$  of the approximation, with higher values of  $N$  indicating a more accurate approximation. Thus, equations (2-49) and (2-50) will be written more explicitly as

$$\lambda(N) = \lambda_0(N) \left[ 1 + \frac{5}{12} \pi \sigma^3 n \left( \frac{48}{25} + \lambda_1(N) / |\lambda_{1E}(N)| \right) \right] \quad (2-51)$$

$$\eta(N) = \eta_0(N) \left[ 1 + \frac{5}{12} \pi \sigma^3 n \left( \frac{32}{25} + \eta_1(N) / |\eta_{1E}(N)| \right) \right] \quad (2-52)$$

Here,  $\lambda_0(N)$  and  $\eta_0(N)$  are given by (2-27) and (2-28), and these quantities multiplied by  $5\pi\sigma^3/12$  give  $|\lambda_{1E}(N)|$  and  $|\eta_{1E}(N)|$ . The quantities  $\lambda_1(N)$  and  $\eta_1(N)$  are obtained by substituting the expansions (2-24) and (2-25) into formulae (2-41) and (2-42) respectively. Upon carrying out these steps we obtain the results

$$\frac{\lambda_1(N)}{|\lambda_{1E}(N)|} = \frac{-1}{a_1(N)} \sum_{k, \ell=1}^N a_k(N) a_\ell(N) \left[ S_{3/2}^{(k)}(W_1^2) \vec{W}_1, S_{3/2}^{(\ell)}(W_1^2) \vec{W}_1 \right]^{(3)} \quad (2-53)$$

$$\frac{\eta_1(N)}{|\eta_{1E}(N)|} = \frac{-1}{b_0(N)} \sum_{k, \ell=0}^{N-1} b_k(N) b_\ell(N) \left[ S_{5/2}^{(k)}(W_1^2) \vec{W}_1^\circ \vec{W}_1, S_{5/2}^{(\ell)}(W_1^2) \vec{W}_1^\circ \vec{W}_1 \right]^{(3)} \quad (2-54)$$

where we have now defined the *dimensionless triple collision inner product*  $[\phi, \psi]^{(3)}$  by

$$[\phi, \psi]^{(3)} \equiv \frac{3}{10\pi} \sqrt{\frac{m}{\pi kT}} \frac{1}{n^3 \sigma^5} (\phi, \psi)^{(3)} \quad (2-55)$$

It is most convenient to use  $(\phi, \psi)^{(3)}$  in our *theoretical* work and  $[\phi, \psi]^{(3)}$  in our *numerical* work. According to (2-55), these two

quantities are identical except for a known factor, so no difficulty should arise in switching from one to the other. The dimensionless nature of  $[\phi, \psi]^{(3)}$  can be seen directly from (2-53) and (2-54); it can also be seen if we insert into (2-43) the explicit forms of the  $f_0(V_{\perp})$  functions [see (2-5)] and then change to the dimensionless velocity variables  $\vec{W}_{\perp}$  [see (2-26)]. In this way we obtain the expression

$$[\phi, \psi]^{(3)} = \frac{-3\sqrt{2}}{60\pi^6} \int d\vec{W}_1 d\vec{W}_2 d\vec{W}_3 d\hat{k}_{21} d\vec{r}_{31} \\ |\vec{W}_{21} \cdot \hat{k}_{21}| \exp(-W_1^2 - W_2^2 - W_3^2) \\ \{ \Phi(\vec{W}_1, \vec{W}_2, \vec{W}_3) * T(123) \Psi(\vec{W}_1, \vec{W}_2, \vec{W}_3) \} \quad (2-56)$$

where  $\Phi$  and  $\Psi$  are as defined in (2-44). As we shall point out later, the variable  $\vec{r}_{31}$  is actually a position vector divided by  $\sigma$ ; thus, *all* the integrating variables in (2-56) are dimensionless. Inasmuch as the forms for  $\phi$  and  $\psi$  appearing in (2-53) and (2-54) are also dimensionless, it follows that (2-56) is a completely dimensionless expression, and therefore suitable for numerical analysis.

Our program now is as follows: After developing the requisite "collision sequence" formalism in Chapter III, we shall give the precise definition of  $(\phi, \psi)^{(3)}$  in Sec. 4.1. Then, in Sec. 4.2, we shall derive a more physically meaningful form for  $(\phi, \psi)^{(3)}$ . Finally, in Chapter V, we shall present our current numerical results as to the magnitudes of the unknown terms in (2-51) and (2-52).

## CHAPTER III

## SEQUENCES OF MOLECULAR COLLISIONS

In order to see how collisions among more than two molecules affect the transport coefficients, it is necessary to introduce a suitable nomenclature and notation to specify sequences of collisions. The reason we must take special pains in this regard is that the three-particle collision sequences which contribute to the triple collision inner product  $(\phi, \psi)^{(3)}$  are found to contain so-called "non-interacting collisions", in which the molecules are allowed to pass through each other without any deflection of their paths. The generalization of the concept of "collision" to cover the non-interacting as well as the interacting varieties introduces some important new concepts, and these must be clearly understood if we are to gain insight into the nature of the triple collision inner product.

The fact that non-interacting collisions play an important role in the theory, even though such collisions would not really occur in a gas of hard spheres, may seem strange at first sight. In order to get some notion as to *why* we are forced to deal with these non-occurring entities, let us recall that the approximate nature of the Boltzmann equation is due to the fact that it considers only uncorrelated binary collisions. In other words, the Boltzmann equation assumes that if two molecules are aimed to collide then they will eventually collide, and if two molecules are not aimed to collide then they will never collide.

Thus, the Boltzmann equation has ignored the possibility of "interfering" collisions. For example, two molecules which are originally aimed to collide may be prevented from doing so because one of the molecules is deflected by a third molecule; similarly, two molecules originally not aimed to collide may be knocked together by a third molecule. *In so ignoring these interfering collisions, the Boltzmann equation has essentially treated them as though they were non-interacting.*

Therefore, in order to improve upon the Boltzmann equation results, we must systematically assess the contributions of various collision sequences containing non-interacting collisions. This situation actually has a precedent in conventional statistical mechanics: We recall that the density dependence of an *equilibrium* property of a gas is determined by a "virial expansion", such as that indicated for the equilibrium radial distribution function in (2-46). The coefficients in such an expansion are determined completely by integrations over various *forbidden spatial configurations* of the molecules -- i.e., configurations in which molecules are overlapping. Analogously, we shall find that the density dependence of the *transport* properties of a gas is determined mainly (although not exclusively) by integrations over various *forbidden collision sequences* -- i.e., sequences containing non-interacting collisions.

### 3.1 Definitions and Nomenclature

The *action sphere* of a hard sphere molecule (in a gas of like molecules) is a sphere concentric about the molecule whose radius is equal to the molecular diameter. By definition, two molecules are *colliding* when the center of one molecule lies on the surface of the action sphere of the other molecule. Two molecules are *overlapping* when the center of one molecule lies inside the action sphere of the other molecule. For simplicity, we shall henceforth measure all distances in units of the molecular diameter  $\sigma$ ; thus, the centers of two molecules in a collision will be exactly separated by their unit collision vector  $\hat{k}$ , and the action spheres of all molecules have unit radius.

A "collision", for our purposes, is always one of three *types*: interacting, non-interacting penetrating, and non-interacting separating. In an *interacting collision* between two molecules with velocities  $\vec{V}_1$  and  $\vec{V}_2$  and collision vector  $\hat{k}_{21}$ , the velocities change in accordance with the laws of mechanics (2-11); in words, the velocities just after an interacting collision are obtained from the velocities just before the collision by interchanging the velocity components along the collision vector  $\hat{k}_{21}$ . In a *non-interacting collision*, the velocities of the molecules do not change, and each molecule moves as though the other were not present. Evidently, non-interacting collisions always occur in pairs, corresponding to when the center of one molecule enters the action sphere of

the other molecule and to when it leaves this action sphere. Thus, we distinguish between a non-interacting *penetrating* and a non-interacting *separating* collision, depending on whether the molecules are overlapping just after or just before the collision. It is clear that a penetrating collision is always followed by a continuous period of overlapping which is eventually terminated by a separating collision, and it is also clear that these two collisions occur at different times and with different collision vectors. Nevertheless, it is occasionally convenient to consider the two collisions together, and so we define a *complete collision* to be either a single interacting collision or a concomittant pair of non-interacting collisions.

A *collision sequence* is defined to be a succession of collisions in which the *order* and *types* of the collisions are specified.

We represent collisions and collision sequences by simple line diagrams. These diagrams can roughly be thought of as space-time plots of the centers of the molecules, with the time-axis vertical and the (one-dimensional) space-axis horizontal. The time and space axes are usually not indicated explicitly, but we shall adopt the convention that time increases when the diagrams are read from top to bottom. In Figs. 3a, 3b and 3c we show how we represent the three basic collisions defined above. Each collision occurs at time  $t=t_0$ , and we can imagine that the centers of the molecules are connected by a collision vector  $\hat{k}_{21}$  at  $t_0$ . In Fig. 3a, we indicate the abrupt change

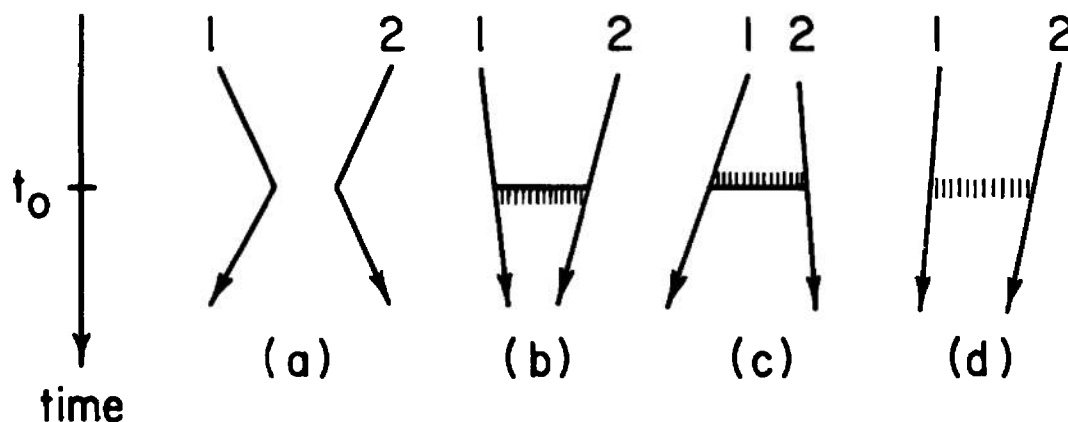


Figure 3. Representation of (a) an interacting collision, (b) a non-interacting penetrating collision, (c) a non-interacting separating collision, and (d) an explicit overlap.

in velocities in an interacting collision. In Figs. 3b and 3c the velocities do not change, but we place hash marks just below/above the collision time in the non-interacting penetrating/separating collision diagram to indicate that the overlap occurs just after/before the collision. We note that upon time-reversal, an interacting collision remains interacting, whereas a penetrating collision becomes a separating collision and vice-versa. It is occasionally advantageous to indicate explicitly that two molecules are overlapping at some time  $t=t_0$ , and we do this by connecting their lines with hash marks, as shown in Fig. 3d.

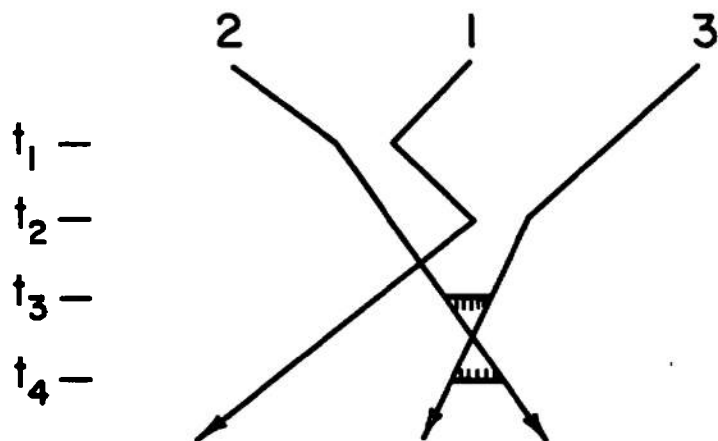


Figure 4. Example of a three-particle collision sequence.

Using the foregoing symbolic representations, we can construct diagrams representing *sequences* of binary collisions. Thus, for example, the diagram in Fig. 4 represents a three-particle collision sequence in which a 1-2 interacting collision occurs at time  $t_1$ , a 1-3 interacting collision occurs at time  $t_2 > t_1$ , a 2-3 penetrating collision occurs at time  $t_3 > t_2$ , and a 2-3 separating collision occurs at time  $t_4 > t_3$ . We must emphasize two points in connection with the collision sequence diagram in Fig. 4:

(i) The diagram says nothing about the sizes of the time-intervals,  $t_2 - t_1$ ,  $t_3 - t_2$ ,  $t_4 - t_3$ , but requires only that they be

positive -- i.e., that the collisions occur in the order indicated.

(ii) The diagram is completely non-committal about the occurrence or non-occurrence of any additional non-interacting collisions. For instance, an additional 1-2 non-interacting collision at any time  $t > t_2$ , or a 2-3 non-interacting collision at any time  $t < t_1$  (either is in fact dynamically possible), may or may not occur. If it is desired to exclude such additional collisions from the class of collision sequences represented by a given diagram, the appropriate restrictions must be explicitly stated.

Item (ii) allows us occasionally to combine or "add" several diagrams to form a single diagram. An example is shown in Fig. 5. The diagrams in Figs. 5a and 5b differ only in the ordering of the 2-3 separating collision and the 1-3 interacting collision. The "sum" of these diagrams may be represented by the diagram in Fig. 5c, which evidently includes both possibilities.

It will be convenient to introduce two further definitions. A *single-overlap collision* is a collision of any type (i.e., interacting, penetrating or separating) between two molecules which occurs while a third molecule overlaps with *one* of the colliding molecules. For example, the 1-2 collisions in Figs. 5a, 5b and 5c, and the 1-3 collision in Fig. 5b are single-overlap collisions. Similarly, a *double-overlap collision* is a collision of any type between two molecules which occurs while a third molecule overlaps with *both* colliding molecules.

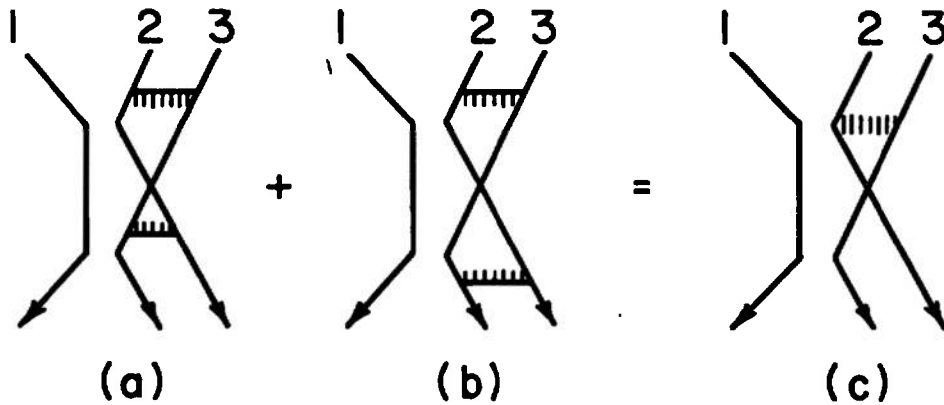


Figure 5. Illustrating the addition of two collision sequence diagrams.

We shall find in Sec. 4.2 that this concept of an "overlap" collision" is of central importance in the analysis of the triple collision inner product.

### 3.2 Some Important Theorems

In this section we present some lemmas and theorems for collision sequences involving three identical hard sphere molecules. These theorems will greatly simplify our analysis of the triple collision inner product in Sec. 4.2.

To date, pertinent studies concerning the motion of three hard spheres have been limited to interacting collisions [14, 15]. Since, as explained at the beginning of this chapter, we shall

be dealing with collisions of both the interacting and non-interacting varieties, it is necessary to develop the subject from a fresh point of view. The development which follows is due to W. R. Hoegy and the present authors [17, 18].

To begin with, there are several "obvious theorems" or "rules" that follow almost immediately from the definition of a collision. For example, we shall frequently invoke the

*Recollision Rule:* After two spheres have collided, they cannot recollide in another complete collision before one of the two spheres undergoes an interacting collision with the third sphere.

In addition to such more or less obvious restrictions, there are several restrictions that are not of a trivial nature. For example, we have

*Lemma 1.* In the collision sequence defined by the diagram in Fig. 6, it is not possible for spheres 2 and 3 to collide or overlap in the time interval  $t_1 \leq t \leq t_5$ .

Note that this lemma also rules out a 2-3 collision or overlap for  $t_1 < t < t_4$  if the 1-2 collision at  $t_4$  were interacting instead of penetrating; it also rules out a 2-3 collision or overlap for  $t_2 \leq t \leq t_5$  if the 1-2 collision at  $t_2$  were interacting instead separating. A proof of this lemma is presented in Appendix A.

As a consequence of Lemma 1, we have

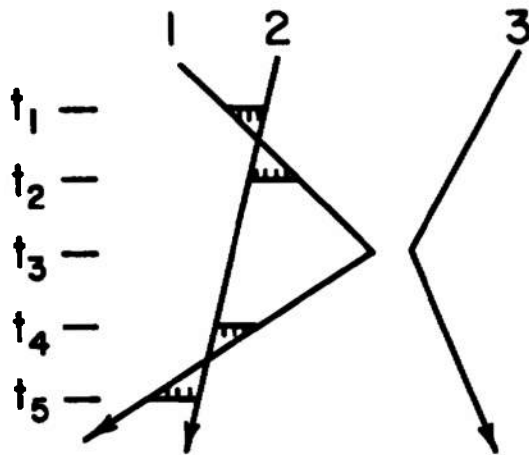


Figure 6. Diagram of Lemma 1.

*THEOREM I. If a three-particle collision sequence contains at least one single-overlap collision, then it cannot contain more than three complete collisions.*

This same theorem is trivially valid for a three-particle collision sequence containing a *double-overlap* collision. Theorem I tells us, for example, that no further collisions are dynamically possible in any of the diagrams in Fig. 5. To prove Theorem I, one considers all three-particle collision sequences with at least one overlap collision and at least four complete collisions, and one finds that every such sequence violates Lemma 1. A proof of Theorem I is given in Appendix A.

We now turn our attention to collision sequences that contain *no* overlap collisions. This means that all *complete* collisions will be separated, so that in between a concomittant pair of non-interacting collisions between two molecules, no other collision with the third molecule will take place. In such cases we indicate an interacting collision between molecule *a* and molecule *b* by  $(ab)^i$ , a complete non-interacting collision by  $(ab)^n$ , and a sequence of such collisions by a left-to-right juxtaposition of these symbols. Thus, e.g., the sequence in Fig. 4 would be denoted by  $(12)^i(13)^i(23)^n$ . Moreover, we shall write  $(ab)$  to denote a complete collision between *a* and *b* which is either interacting or non-interacting:

$$(ab) \equiv (ab)^i + (ab)^n \quad (3-1)$$

Using this notation, we quote the following two lemmas.

*Lemma 2.* Not dynamically possible are the three-particle collision sequences

$$(12)(13)^i(12)^i(13)$$

$$(12)(13)^i(23)^i(12)$$

*Lemma 3.* Not dynamically possible are the three-particle collision sequences

$$(12)(13)^i(12)^i(23)^i(12)$$

$$(23)(12)^i(13)^i(12)^i(23)$$

Lemmas 2 and 3 were stated by Sandri and co-workers [14] and proved in detail by Murphy and Cohen [15]. Implicit in

these lemmas is the fact that any sequence, constructed by inserting non-interacting collisions between any of the collisions in the sequences excluded, is also not dynamically possible [16].

From Lemmas 1,2 and 3 one may then establish

*THEOREM II. If a three-particle collision sequence contains no single-overlap collisions, then it cannot contain more than four complete collisions.*

Again, the proof proceeds by showing that any collision sequence of the kind contemplated violates one of the lemmas. The proof of Theorem II is given in Appendix A. Combining Theorems I and II, we have the theorem that no three-particle collision sequence can contain more than four complete collisions. This theorem was discovered by Hoegy and Sengers [18].

In the proof of Theorem II, one finds as a corollary that there are in fact *only two* dynamically independent sequences with four complete collisions, namely

$$(12)(13)^i(12)^i(23) \quad \text{and} \quad (12)(13)^i(12)^n(23) \quad (3-2)$$

In other words, any sequence of four complete collisions either is one of the above sequences, or else is obtainable therefrom by interchanging numerical labels and/or reversing time. This is a generalization of the previously discovered fact [14,15] that the only possible sequence of four *interacting* collisions is  $(12)^i(13)^i(12)^i(23)^i$ .

## CHAPTER IV

## ANALYSIS OF THE TRIPLE COLLISION INNER PRODUCT

4.1 Introduction

In statistical mechanics one derives the density expansion of the equilibrium pair distribution function  $g(r)$  by making a "cluster expansion" of the partition function [5]. In an analogous way, the first density correction to the Boltzmann operator  $I_2$  can be obtained by making a "cluster expansion" of the Liouville operator, as was first pointed out by Green and Cohen [19,20,21]. This procedure leads eventually to the triple collision operator  $I_3$  which was written down in equation (2-37). In that equation, the variables  $\vec{V}_1, \vec{V}_2$  and  $\vec{V}_3$  may be regarded as the velocities of three isolated molecules 1, 2 and 3, while the variables  $\hat{k}_{21}$  and  $\vec{r}_{31}$  locate molecules 2 and 3 relative to 1 according to

$$\hat{k}_{21} = -(\vec{r}_2 - \vec{r}_1)/\sigma \quad \text{and} \quad \vec{r}_{31} = (\vec{r}_3 - \vec{r}_1)/\sigma \quad (4-1)$$

It will be noted that these position variables are measured in units of the molecular diameter  $\sigma$ . Moreover, since  $\hat{k}_{21}$  is a unit vector, then we are evidently constraining molecules 1 and 2 spatially so that they are "colliding" [cf. our definition of "collision" in Sec. 3.1]. Strictly speaking, the five-dimensional volume element  $|\vec{V}_{ij} \cdot \hat{k}_{ij}| d\hat{k}_{ij} d\vec{r}_{kj}$  in (2-37) should refer to *any* colliding pair  $i$ - $j$ , and we should really write down two more integrals for the pairs 1-3 and 2-3. However, it is sufficient for our purposes to carry out the integrations

only for the pair indicated, and to take account of the permutations by introducing a factor of 3 at a later stage; nevertheless, it should be kept in mind that  $I_3$  is completely symmetrical in the particle labels.

Our real interest here is not so much in the triple collision *operator* but in the triple collision *inner product*, which one forms using this operator according to (2-40). An explicit expression for  $(\phi, \psi)^{(3)}$  which is totally symmetric in the molecule labels was given in (2-43), and for convenience we write that expression again here:

$$\begin{aligned}
 (\phi, \psi)^{(3)} = & - \frac{\sigma^5}{3!} \int d\vec{V}_1 d\vec{V}_2 d\vec{V}_3 d\hat{k}_{21} d\vec{r}_{31} \\
 & |\vec{V}_{21} \cdot \hat{k}_{21}| f_0(V_1) f_0(V_2) f_0(V_3) \quad (4-2) \\
 & \{ \phi(\vec{V}_1, \vec{V}_2, \vec{V}_3) * T(123) \psi(\vec{V}_1, \vec{V}_2, \vec{V}_3) \}
 \end{aligned}$$

where

$$\phi(\vec{V}_1, \vec{V}_2, \vec{V}_3) \equiv \sum_{n=1}^3 \phi(\vec{V}_n); \quad \psi(\vec{V}_1, \vec{V}_2, \vec{V}_3) \equiv \sum_{n=1}^3 \psi(\vec{V}_n) \quad (4-3)$$

Evidently, the triple collision inner product is a fourteen dimensional integral over the velocities and relative positions of three isolated molecules, with molecules 1 and 2 in contact. The integration runs over the whole of this fourteen dimensional space, although, as we shall see momentarily, the operator  $T(123)$  vanishes everywhere except in certain select subregions of this space. The factors  $f_0(V_i)$  are, as before, simple Maxwell-Boltzmann functions [cf. (2-5)].

In defining the operator  $T(123)$ , it is helpful to first recall how the operator  $T(12)$  appearing in the binary collision inner product (2-21) is defined. We noted in (2-12) that  $T(12)$  could be regarded as the sum of two "velocity replacement operators":

$$T(12) = \sum_{\mu=n,i} T_{\mu}^{(2)}(12) \quad (4-4)$$

Using the diagrammatic notation introduced in Chapter III, we may associate these two operators with the two "two-particle collision sequence diagrams" shown in Fig. 7. With the aid of these two diagrams, the expression for  $(\phi, \psi)^{(2)}$  in (2-22) may be understood as follows: For each  $\mu$ -term, the integrating variables  $\vec{V}_1, \vec{V}_2$  and  $\hat{k}_{21}$  in (2-22) are the velocities and relative positions of the molecules instantaneously before (above) the 1-2 collision indicated in diagram  $\mu$ . The operator  $T_{\mu}^{(2)}(12)$  is different from zero *only* when  $\vec{V}_1, \vec{V}_2$  and  $\hat{k}_{21}$  are such that the corresponding  $\mu$ -collision sequence can be realized; the condition for this for *either*  $\mu$ -diagram is simply that the molecules be aimed to collide, or  $\vec{V}_{21} \cdot \hat{k}_{21} > 0$ . When this condition is satisfied,  $T_{\mu}^{(2)}(12)$  acting on a function of the initial velocities  $\vec{V}_1$  and  $\vec{V}_2$  replaces these velocities by the final velocities *in diagram*  $\mu$ , with the proviso that an overall minus sign is introduced when the collision is non-interacting.

Similarly, the operator  $T(123)$  in (4-2) can be considered as a sum of *twelve* velocity replacement operators,

$$T(123) = 3! \sum_{\mu} T_{\mu}^{(3)}(12;13) \quad (4-5)$$

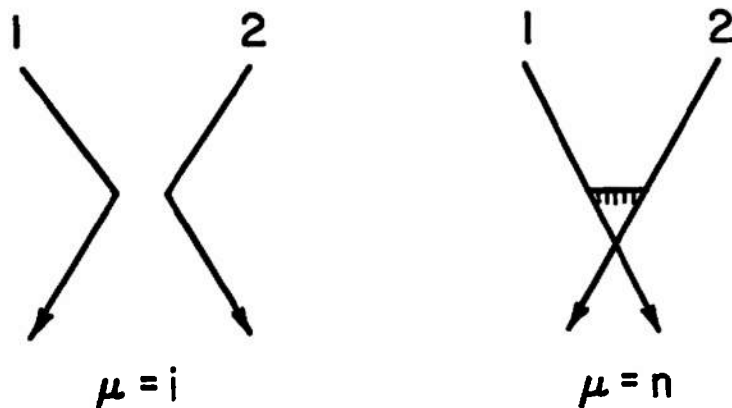


Figure 7. Diagrams for the operators  $T_{\mu}^{(2)}(12)$ .

each of which is defined relative to a particular *three-particle collision sequence diagram*. The twelve diagrams are shown in Fig. 8. We restrict ourselves to collision sequences in which the first collision is a 1-2 collision and the second collision is a 1-3 collision; since the triple collision inner product is symmetric in the molecules, other permutations are accounted for by the factor  $3!$  in (4-5). Concerning the diagrams in Fig. 8, we make the following observations:

Each diagram requires that the three molecules undergo at least three collisions of a specified *type* (either interacting or non-interacting penetrating) and in a specified *time order*. We shall number these three required collisions

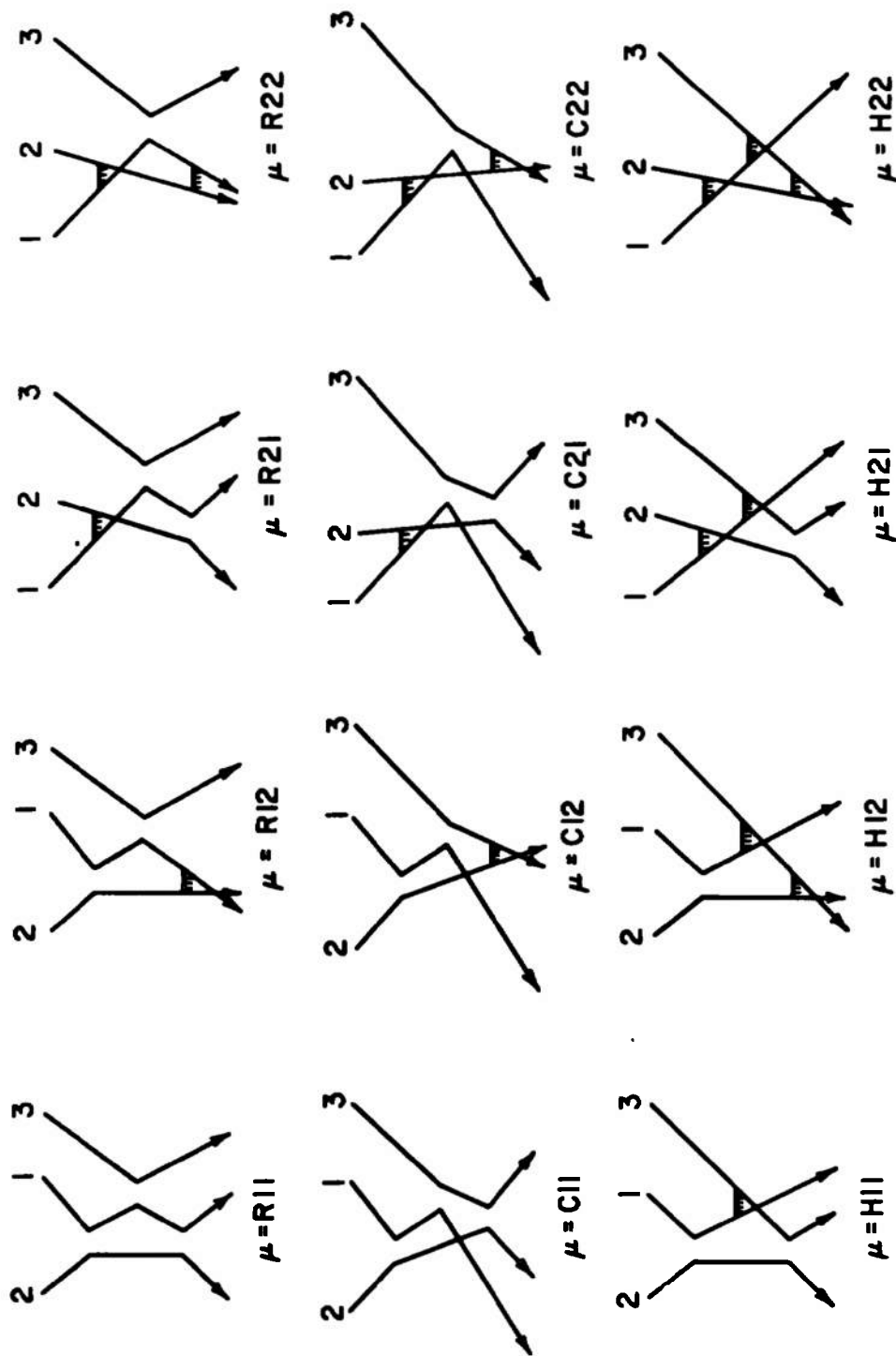


Figure 8. Diagrams for the operators  $T_{\mu}^{(3)}(12;13)$ .  
 [Note that these diagrams are subject to the restrictions stated in the text].

in the order in which they occur (i.e., from top to bottom). Each diagram is labelled by a letter and two numbers. The first number is either 1 or 2 according to whether the *first* collision is interacting or penetrating, and the second number similarly describes the *third* collision. The diagrams with the letter R are "recollision" diagrams, in that the third collision involves the same pair (1 and 2) that made the first collision. The diagrams with the letter C are "cyclic collision" diagrams, in that the third collision involves the third pair (2 and 3). The diagrams with the letter H are "hypothetical cyclic collision" diagrams, in that, like the C diagrams the third collision involves molecules 2 and 3 but unlike the C diagrams the second collision is non-interacting. (It will be noted that a corresponding set of "hypothetical recollision" diagrams is not dynamically possible because of the Recollision Rule).

It must be emphasized, however, that the specific collision sequences relative to which the operators  $T_{\mu}^{(3)}(12;13)$  are defined are *not* completely specified by the diagrams in Fig. 8. As demonstrated in I, the theory imposes the following two restrictions on these diagrams [22]:

*First Collision Restriction:* No collisions of any kind are allowed to occur before (above) the "first" collision in any  $\mu$ -diagram.

*Real Collision Restriction:* In diagrams R11, R12, C11

and C12, no additional collisions of any kind are allowed to occur before the "third" collision.

Additional non-interacting collisions which do not violate these restrictions are permitted to occur. *Some* additional collisions will *necessarily* occur -- namely, the separating collisions which naturally follow the required penetrating collisions; in this connection, we note that the  $\mu$ -diagrams do *not* specify when these separating collisions are to occur. *Other* additional non-interacting collisions may or may not occur: for example, a 2-3 non-interacting collision may occur between the first and second collisions in diagrams C21 and C22, but such a collision must be explicitly excluded from diagrams C11 and C12 because of the Real Collision Restriction; the same holds true for a 1-2 non-interacting collision between the second and third collisions in the C-diagrams.

The integrating variables in (4-2) refer to the velocities and relative positions of the three molecules instantaneously before (above) the "first" collision in each  $\mu$ -diagram, and we define the subvolumes  $\Omega_\mu$  by

$$\Omega_\mu \equiv \text{set of all points } (\vec{V}_1, \vec{V}_2, \vec{V}_3, \hat{k}_{21}, \vec{r}_{31}) \text{ for which} \\ \text{a collision sequence of the type described in} \\ \text{diagram } \mu \text{ can occur (subject to the First Col-} \\ \text{lision and Real Collision Restrictions).} \quad (4-6)$$

Note that a given point in the 14-dimensional space spanned by the integrating variables in (4-2) may lie in none, one,

or more than one of the subvolumes  $\Omega_\mu$ . The operators  $T_\mu^{(3)}$  are now defined analogously to the operators  $T_\mu^{(2)}$  in (2-14):

$$\text{outside } \Omega_\mu: T_\mu^{(3)}\Psi(\vec{V}_1, \vec{V}_2, \vec{V}_3) = 0 \quad (4-7a)$$

$$\text{inside } \Omega_\mu: T_\mu^{(3)}\Psi(\vec{V}_1, \vec{V}_2, \vec{V}_3) = (-1)^\mu \Psi(\vec{V}'_1, \vec{V}'_2, \vec{V}'_3) \quad (4-7b)$$

where  $(-1)^\mu = +1$  or  $-1$  according to whether diagram  $\mu$  has an even or odd number of required non-interacting collisions, and where  $\vec{V}'_i$  is the velocity of molecule  $i$  at the end of the  $\mu$  collision sequence. In the cases  $\mu=R11$  and  $\mu=C11$ , the theory (as developed in I) requires that *if* more interacting collisions can occur after the third collision, then  $\vec{V}'_i$  is to be the velocity of molecule  $i$  after *all* additional collisions have taken place; for  $\mu \neq R11$  and  $\mu \neq C11$ , however,  $\vec{V}'_i$  denotes the velocities after the third required collision, regardless of the possibility of any subsequent collisions [22].

If we insert (4-5) into (4-2), we will evidently obtain an expression for  $(\phi, \psi)^{(3)}$  which is very analogous to the expression for  $(\phi, \psi)^{(2)}$  in (2-22):

$$\begin{aligned} (\phi, \psi)^{(3)} = & -\sigma^5 \sum_{\mu} \int d\vec{V}_1 d\vec{V}_2 d\vec{V}_3 d\hat{k}_{21} d\vec{r}_{31} \\ & |\vec{V}_{21} \cdot \hat{k}_{21}| f_0(V_1) f_0(V_2) f_0(V_3) \quad (4-8) \\ & \{ \phi(\vec{V}_1, \vec{V}_2, \vec{V}_3) * T_\mu^{(3)}(12;13) \Psi(\vec{V}_1, \vec{V}_2, \vec{V}_3) \} \end{aligned}$$

The advantage of this expression is that it conveys in a physical, yet mathematically precise, way the structure of

the triple collision inner product. At the same time, it reveals how the triple collision inner product appears as a fairly natural generalization of the binary collision inner product in (2-22).

Of more usefulness for computational purposes would be an expression for  $(\phi, \psi)^{(3)}$  which is analogous to (2-23). To this end, we first define

$$\vec{V}_i(j_\mu) = \text{velocity of particle } i \text{ immediately after} \\ \text{the } j\text{th required collision in diagram } \mu. \quad (4-9)$$

In particular, we shall write  $j_\mu = 0_\mu$  to denote the velocity region before the first collision, and we shall write

$$\bar{3}_\mu = \begin{cases} \text{velocity region after the } \textit{last} \\ \text{collision for } \mu=R11 \text{ and } \mu=C11; \\ \text{velocity region } 3_\mu \text{ for all other } \mu. \end{cases} \quad (4-10)$$

For brevity, we shall also write

$$\Phi(j_\mu) \equiv \Phi(\vec{V}_1(j_\mu), \vec{V}_2(j_\mu), \vec{V}_3(j_\mu)) \quad (4-11)$$

and similarly for  $\Psi$ . In this notation,  $\Psi(\vec{V}_1', \vec{V}_2', \vec{V}_3')$  in (4-7b) becomes simply  $\Psi(\bar{3}_\mu)$ , and (4-8) takes the form

$$(\phi, \psi)^{(3)} = -\sigma^5 \sum_{\mu} \int_{\Omega_{\mu}} d\vec{V}_1(0_{\mu}) d\vec{V}_2(0_{\mu}) d\vec{V}_3(0_{\mu}) d\hat{k}_{21} d\vec{r}_{31} \\ |\vec{V}_{21}(0_{\mu}) \cdot \hat{k}_{21}| f_0(V_1) f_0(V_2) f_0(V_3) \\ \{ (-1)^{\mu} \Phi(0_{\mu}) * \Psi(\bar{3}_{\mu}) \} \quad (4-12)$$

In (4-12), we have used the fact that the velocities in the product of the Maxwell-Boltzmann functions can be referred to *any* velocity region in diagram  $\mu$ , because of conservation of energy [cf. the remarks following (4-17)]. In order to explain our next step, consider the diagrams of R11 and R12 in Fig. 9. We indicate schematically the integrating variables and the various velocity regions for these diagrams in this figure. Now, the conditions to be satisfied by the integration variables in order to obtain the collision sequence R12 are evidently *identical* to the conditions for R11, since the initial variables do not care whether the third collision is interacting or penetrating; thus,

$$\Omega_{R12} = \Omega_{R11} \equiv \Omega_{R1} \quad (4-13)$$

Moreover, for any given point  $(\vec{v}_1(0_{R1}), \vec{v}_2(0_{R1}), \vec{v}_3(0_{R1}), \hat{k}_{21}, \vec{F}_{31})$  inside  $\Omega_{R1}$ , it is clear that the velocities in regions 1 and 2 of these diagrams will coincide exactly, while the velocities in region 3 of R12 will coincide with the velocities in region 2 of R11. Consequently, we may relate the R12-term in (4-12) directly to diagram R11, which we now *relabel*  $v=R1$ , and we write  $\Psi(2_{R1})$  in place of  $\Psi(3_{R12})$ . The integrands for R11 and R12 can then be added directly, provided we take account of the extra minus sign in front of the R12 integrand. Clearly, we can similarly combine every pair of  $\mu$ -diagrams whose labels differ only in the last digit. In this way we write (4-12) in the form

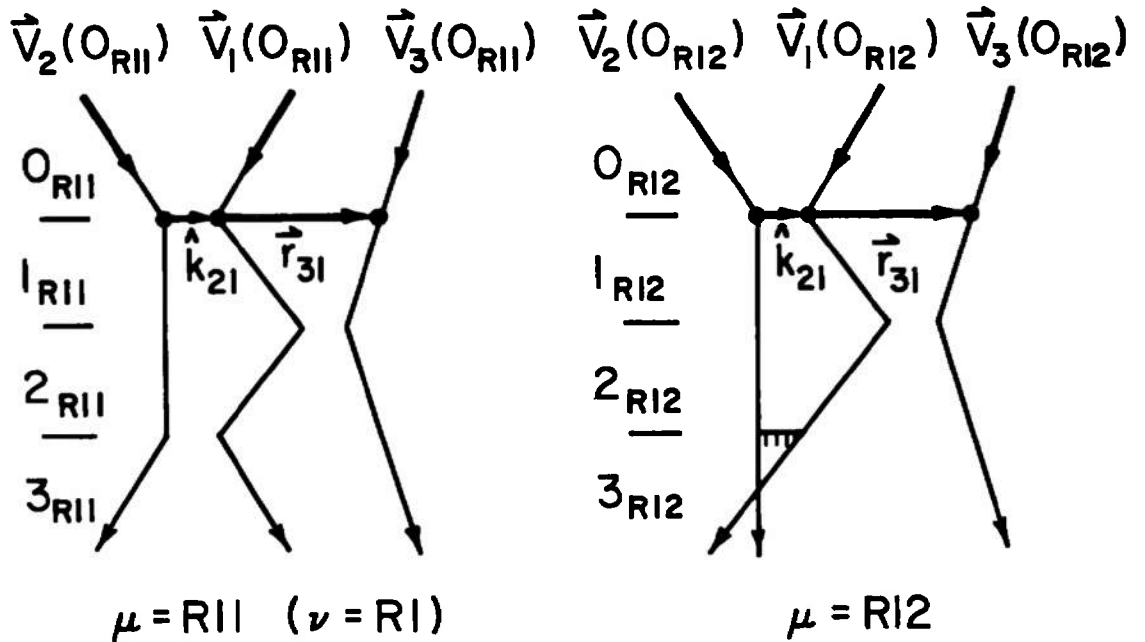


Figure 9. Diagrams R11≡R1 and R12.

$$\begin{aligned}
 (\phi, \psi)^{(3)} = & -\sigma^5 \sum_{\nu} \int_{\Omega_{\nu}} d\vec{v}_1(0_{\nu}) d\vec{v}_2(0_{\nu}) d\vec{v}_3(0_{\nu}) d\hat{k}_{21} d\vec{r}_{31} \\
 & |\vec{v}_{21}(0_{\nu}) \cdot \hat{k}_{21}| f_0(v_1) f_0(v_2) f_0(v_3) \\
 & \{ (-1)^{\nu} \phi(0_{\nu}) * [\Psi(\vec{3}_{\nu}) - \Psi(2_{\nu})] \} \quad (4-14)
 \end{aligned}$$

where the sum now runs over the *six*  $\nu$ -diagrams R1≡R11, R2≡R21, C1≡C11, etc., shown in Figure 10. This form for  $(\phi, \psi)^{(3)}$  is the desired analogue to (2-23), and it is the form in which the triple collision integrals were first presented in earlier publications [6,13,22]. It must be emphasized that the restrictions mentioned earlier in connection with the  $\mu$ -diagrams still

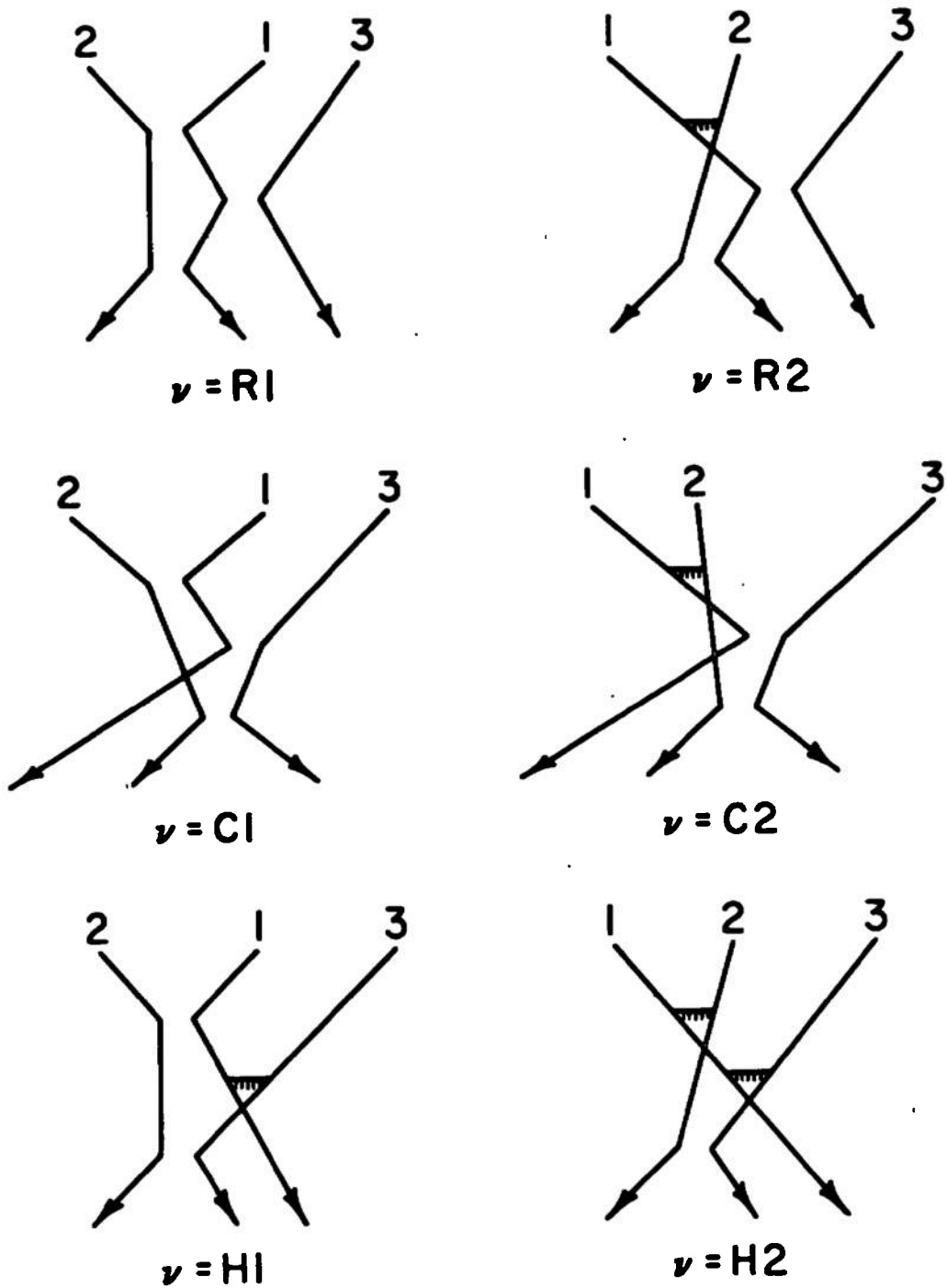


Figure 10. The six  $v$ -diagrams. [Note that these diagrams are subject to the restrictions stated in the text].

apply to the  $v$ -diagrams, the First Collision Restriction applying to all the  $v$ -diagrams and the Real Collision Restriction applying to diagrams R1 and C1 only. We also want to stress the *dual role* played by the  $v$ -diagrams in regard to the six integrals in (4-14): on the one hand, these diagrams serve to define the volume  $\Omega_v$  over which each of the integrals is taken; on the other hand, these diagrams determine the functional dependence of the velocities  $\vec{V}_i(2_v)$  and  $\vec{V}_i(\bar{3}_v)$  upon the integrating variables.

We note that our restriction to hard spheres has thus far been a restriction only on the *duration* of a binary collision, in that we have assumed only "instantaneous interactions" [23]. This restriction excludes the consideration of genuine triple collisions, in which three molecules collide simultaneously. However, the expression in (4-14) and the associated diagrams in Fig. 10 correctly account for the effects of sequential binary collisions for *any* short-range potential with a hard core.

#### 4.2 Separation of Spatial and Dynamical Correlations. Expansion in Effective Number of Collisions.

The expression for the triple collision inner product in (4-14), as a sum of six integrals corresponding to the six  $v$ -diagrams in Fig. 10, suffers from several drawbacks. In particular we mention:

1. Although the triple collision inner product is symmetric [18], it is not true that the six triple collision integrals in (4-14) are individually symmetric [22]. It would be better if  $(\phi, \psi)^{(3)}$  were expressed as a sum of terms which are separately symmetric in  $\phi$  and  $\psi$ .

2. As reported in I [see Sec. 2.7 of I], preliminary numerical calculations have revealed that substantial cancellations occur among the contributions of the six  $v$ -integrals. It would be better if  $(\phi, \psi)^{(3)}$  were expressed as a sum of integrals whose individual contributions were ordered according to some physically sensible scheme.

3. The integration regions  $\Omega_v$  are defined by the diagrams in Fig. 10 *subject to* the First Collision Restriction and the Real Collision Restriction. These extra conditions on the collision sequence diagrams are a nuisance in numerical computation. It would be better if we could use a set of diagrams that are defined without any externally imposed restrictions.

The above observations suggest that the decomposition of  $(\phi, \psi)^{(3)}$  in (4-14), although mathematically correct, is physically not the most desirable one. Part of the problem here is that the diagrams in Fig. 10 do not adequately distinguish between *correlations in positions* and *correlations in velocities*. We recall that, for a gas in equilibrium, the velocities of the molecules are uncorrelated; thus, the density dependence of the equilibrium properties are completely due to spatial correlations, which, for a gas of hard spheres are related to the exclusion of

configurations where the molecules are *overlapping* [cf. Fig.2]. Reasoning by analogy, we may expect that spatial correlation effects on the *non-equilibrium* properties of a gas (such as the transport coefficients) will be related to the exclusion of collision sequences containing *overlap collisions*; collision sequences which do not contain overlap collisions would then represent the effects of velocity correlations.

In light of the foregoing considerations, we now reconsider the  $v$ -diagrams in Fig. 10. We first "decompose" each of these diagrams into its several more specific diagrams, in which we take account of the possible additional collisions that may take place. Next, we recombine or "resum" these specific diagrams, grouping them according to the following criteria:

- (a) diagrams with at least one double-overlap collision;
  - (b) diagrams with at least one single-overlap collision, but no double-overlap collision;
  - (c) diagrams with no overlap collisions and specifying only three complete collisions;
  - (d) diagrams with no overlap collisions and specifying four complete collisions.
- (4-15)

In view of Theorems I and II of Chapter III [cf. Appendix A], we note that these groupings are indeed mutually exclusive and collectively exhaustive. We may then write the triple-collision inner product in the form

$$(\phi, \psi)^{(3)} = \sum_{k=1}^4 (\phi, \psi)_k^{(3)} \quad (4-16)$$

where the four terms represent the contributions from the four groupings (a), (b), (c), (d), respectively. It will be noted that the presence of a double-overlap collision in a collision sequence already implies the occurrence of two additional complete collisions, namely, the two non-interacting collisions which gave rise to the two overlaps; since Theorem I permits a maximum of three complete collisions in such circumstances, we conclude that those collision sequences falling into group (a), and contributing to the term  $(\phi, \psi)_1^{(3)}$ , will effectively contain only *one* collision (namely, the double-overlap collision). Similarly, the presence of a single-overlap collision in a sequence implies the occurrence of one additional complete collision, so that by Theorem I those collision sequences falling into group (b), and contributing to the term  $(\phi, \psi)_2^{(3)}$ , will effectively contain only *two* collisions. Finally, it is clear from the definitions of groups (b) and (c) that the sequences contributing to the terms  $(\phi, \psi)_3^{(3)}$  and  $(\phi, \psi)_4^{(3)}$  will contain *three* and *four* collisions, respectively. Thus, we have in (4-16) an expansion in the effective number k of collisions; moreover, the expansion evidently proceeds from high to low spatial correlation, and from low to high velocity correlation. These features of (4-16) will become clearer as we derive the specific diagrams relative to which these terms are defined.

In resumming the  $v$ -diagrams, we shall make use of three *invariance properties* of (4-14):

First, we shall frequently invoke the fact that the six integrals in (4-14) are each invariant under all permutations of the molecule labels. This is a consequence of the symmetry of  $I_3$ , which was mentioned in the first paragraph of Sec. 4.1.

Secondly, we shall use the fact that the six integrals in (4-14) are each invariant under a sign reversal of all velocities. To prove this, we begin by observing that the Jacobian of the transformation  $(\vec{V}_1, \vec{V}_2, \vec{V}_3) \rightarrow (-\vec{V}_1, -\vec{V}_2, -\vec{V}_3)$  is unity, so that the differentials in (4-14) are unaffected if the sign of each  $\vec{V}_i(0_v)$  variable is changed. Furthermore, the factor  $|\vec{V}_{21}(0_v) \cdot \hat{k}_{21}|$  is unaffected by a sign change because of the absolute value operation, while the Maxwell-Boltzmann factors depend only on the magnitudes of the velocities and not their directions. Finally, the invariance of the quantity in braces follows from the facts that a reversal of velocities in region  $0_v$  induces a velocity reversal in every region, while the functions  $\phi$  and  $\psi$  (and hence  $\phi$  and  $\psi$ ) are always of the same parity in the velocities [cf. the expressions in (2-24) and (2-25) for  $\vec{A}_N$  and  $\vec{B}_N$ ].

The third invariance property of (4-14) which we shall use says that the volume element

$$d\Omega_v = d\vec{V}_i d\vec{V}_j d\vec{V}_k d\hat{k}_{ji} d\vec{r}_{ki} |\vec{V}_{ji} \cdot \hat{k}_{ki}| \quad (4-17)$$

which in (4-14) refers to the phases of the three molecules *just before the first collision* in diagram  $v$ , may in fact be evaluated *just before or just after any collision* in the dynamical history of diagram  $v$ . We shall indicate the proof of this invariance property by first showing that we can transform  $d\Omega_v$  invariantly from above the first collision to below the first collision, and next that we can transform  $d\Omega_v$  invariantly from below the first collision to above the second collision. (Essentially, the invariance of  $d\Omega_v$  follows from Liouville's Theorem, which states that the volume element in phase space is invariant under transformations generated by the natural motion of the system.)

The transformation from above to below the first collision is (dropping the subscript  $v$ ):

$$\begin{aligned}\vec{V}_1(1) &= \vec{V}_1(0) + \vec{V}_{21}(0) \cdot \hat{k}_{21} \hat{k}_{21} \\ \vec{V}_2(1) &= \vec{V}_2(0) - \vec{V}_{21}(0) \cdot \hat{k}_{21} \hat{k}_{21} \\ \vec{V}_3(1) &= \vec{V}_3(0)\end{aligned}\tag{4-18}$$

From this it can be shown, with some algebra, that

$$d\vec{V}_1(1)d\vec{V}_2(1)d\vec{V}_3(1) = d\vec{V}_1(0)d\vec{V}_2(0)d\vec{V}_3(0)\tag{4-19a}$$

$$\vec{V}_{21}(1) \cdot \hat{k}_{21} = -\vec{V}_{21}(0) \cdot \hat{k}_{21}\tag{4-19b}$$

$$V_1^2(1) + V_2^2(1) + V_3^2(1) = V_1^2(0) + V_2^2(0) + V_3^2(0)\tag{4-19c}$$

Clearly, then, the velocity variables in (4-17) outside the braces can refer either to region 0 or to region 1. We remark that (4-19c) has already been invoked in obtaining (4-14), when

in (4-12) we dropped the velocity region designations from the Maxwell-Boltzmann factors; for we see from (2-5) that the product of these three Maxwell-Boltzmann factors depends only on the sum of the squares of the velocities. We see, then, that all velocities in (4-14) outside the braces can be changed from region  $0_v$  to region  $1_v$  if desired.

We shall next prove that the volume element  $d\Omega_v$  can be transformed invariantly from just below the first collision to just above the second collision in any  $v$ -diagram. The second collision is a 1-3 collision, so we let  $\hat{k}_{31}$  and  $\vec{r}_{21}$  be the relative position vectors at the instant of the second collision. The velocities just before the second collision are of course identical with the velocities just after the first collision, so the desired invariance property will be proved if we can show that

$$d\hat{k}_{31}d\vec{r}_{21}|\vec{v}_{31}(1) \cdot \hat{k}_{31}| = d\hat{k}_{21}d\vec{r}_{31}|\vec{v}_{21}(1) \cdot \hat{k}_{21}| \quad (4-20)$$

To prove (4-20), we let  $\tau$  be the time between the first and second collisions, and we note from Fig. 11 that

$$\vec{r}_{21} = -\hat{k}_{21} + \vec{v}_{21}(1)\tau \quad (4-21a)$$

$$-\hat{k}_{31} = \vec{r}_{31} + \vec{v}_{31}(1)\tau \quad (4-21b)$$

If we now regard (4-21a) as representing the transformation  $(\hat{k}_{21}, \tau) \rightarrow \vec{r}_{21}$ , then it is fairly straightforward to show that the Jacobian of this transformation is

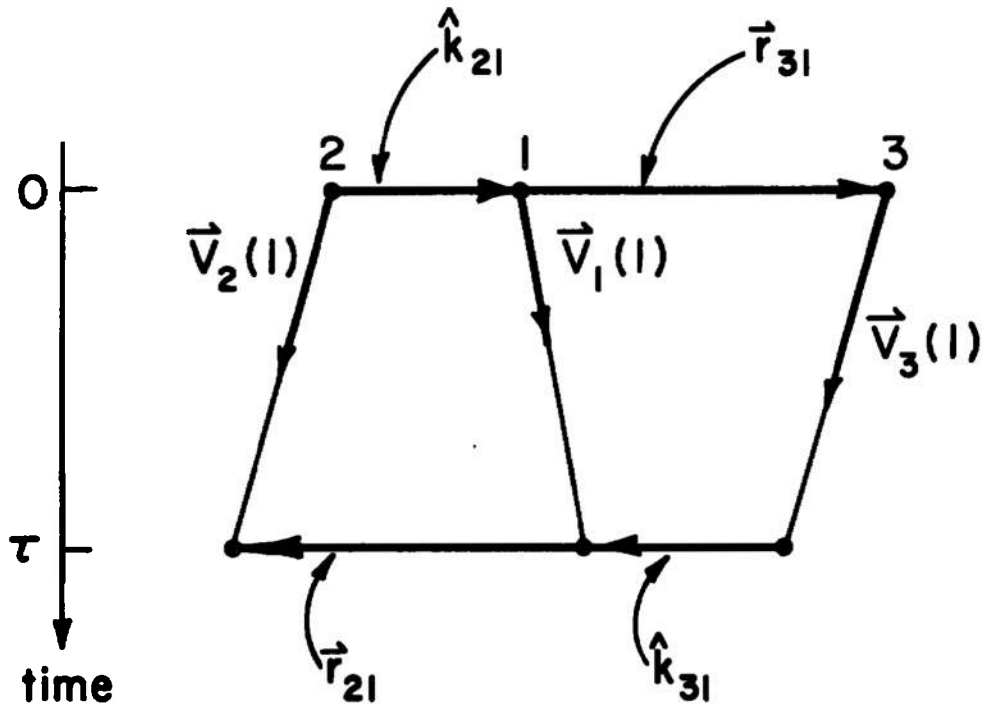


Figure 11. Illustrating the relation between the variables at the first and second collisions.

$$\frac{d\vec{r}_{21}}{dk_{21}d\tau} = |\vec{V}_{21}(1) \cdot \hat{k}_{21}| \tag{4-22a}$$

Similarly, from (4-21b) we deduce that

$$\frac{d\vec{r}_{31}}{dk_{31}d\tau} = |\vec{V}_{31}(1) \cdot \hat{k}_{31}| \tag{4-22b}$$

Using equations (4-22), we therefore have

$$\begin{aligned} d\hat{k}_{31}d\vec{r}_{21}|\vec{V}_{31}(1) \cdot \hat{k}_{31}| &= d\hat{k}_{31} \left[ d\hat{k}_{21}d\tau |\vec{V}_{21}(1) \cdot \hat{k}_{21}| \right] |\vec{V}_{31}(1) \cdot \hat{k}_{31}| \\ &= d\hat{k}_{21} \left[ d\hat{k}_{31}d\tau |\vec{V}_{31}(1) \cdot \hat{k}_{31}| \right] |\vec{V}_{21}(1) \cdot \hat{k}_{21}| \\ &= d\hat{k}_{21}d\vec{r}_{31}|\vec{V}_{21}(1) \cdot \hat{k}_{21}| \end{aligned}$$

which is the desired result (4-20). Note also that, since at the second collision  $\vec{r}_{23} = \hat{k}_{31} + \vec{r}_{21}$ , then

$$d\hat{k}_{31}d\vec{r}_{21} = d\hat{k}_{31}d\vec{r}_{23} \quad (4-23)$$

This means that  $\vec{r}_{21}$  on the right side of (4-20) may be replaced by  $\vec{r}_{23}$  if desired; i.e., it makes no difference whether we locate 2 relative to 1 or 3.

The arguments in the preceding two paragraphs can be repeated to show that the volume element  $d\Omega_v$  in (4-17) can refer to just before or just after any collision in the history of diagram  $v$ .

The foregoing invariance properties of (4-14) allow us to write the equation in the more general form

$$(\phi, \psi)^{(3)} = -\sigma^5 \sum_v \int_{\Omega_v} d\vec{v}_1 d\vec{v}_2 d\vec{v}_3 d\hat{k}_{21} d\vec{r}_{31} \quad (4-24)$$

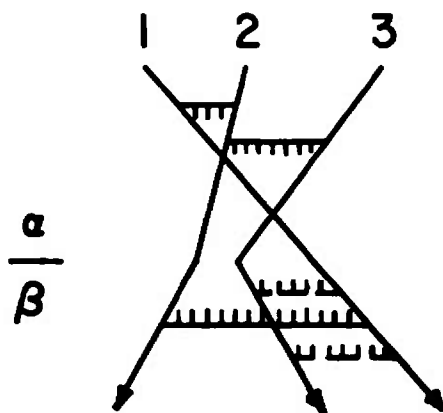
$$|\vec{v}_{21} \cdot \hat{k}_{21}| f_0(v_1) f_0(v_2) f_0(v_3) \{ (-1)^{\nu} \phi(0_v) * [\Psi(\vec{3}_v) - \Psi(2_v)] \}$$

Here, the velocity variables outside the braces refer to the velocities of the molecules either immediately before or immediately after any collision in the history of diagram  $v$ , in either the direct or reversed time sense, with the molecules labeled so that their positions are in accord with (4-1) at the chosen collision time.

We now turn to the task of using this more flexible form for  $(\phi, \psi)^{(3)}$ , together with the lemmas and theorems of Sec. 3.2, to effect the decomposition in (4-15) and (4-16).

Consider first groups (a) and (b) in (4-15). For these, we must evidently extract from the six  $v$ -diagrams in Fig. 10 all collision sequences containing *overlap collisions*. Now Theorem I [cf. Sec. 3.2 and Appendix A] tells us that any collision sequence containing a single-overlap collision (and hence *a fortiori* any sequence containing a double-overlap collision) cannot contain more than three complete collisions. This fact greatly simplifies our task of finding all the  $v$ -sequences containing double- or single-overlap collisions: it means that we need not worry about any collisions not explicitly indicated in the  $v$ -diagrams, save only those separating collisions which are concomittant with the required penetrating collisions.

Since a double-overlap collision requires at least two complete non-interacting collisions, it is clear from Fig. 10 that only diagram H2 is a possible source of collision sequences containing a double-overlap collision. Indeed, if in H2 pairs 1-2 and 1-3 both separate after (below) the 2-3 interacting collision, then the 2-3 collision will be a double-overlap collision. Moreover, since we do not care in which order the 1-2 and 1-3 separating collisions follow the 2-3 interacting collision, we obtain a total of *two*  $v$ -collision sequences containing at least one double-overlap collision. These two double-overlap sequences are shown in Fig. 12. In this figure we have used



$$\underline{H2}: \Phi(\alpha) * [\Psi(\beta) - \Psi(\alpha)]$$

Figure 12. All v-diagrams containing at least one double-overlap collision.

dashed lines in order to represent two distinct collision sequences by means of only one diagram; i.e., Fig. 12 represents one collision sequence in which 1 and 3 separate *before* 1 and 2, and another collision sequence in which 1 and 3 separate *after* 1 and 2. We label the *distinct* velocity regions in the diagram by small Greek letters, and we indicate below the diagram the form assumed by the quantity in braces in (4-24). Note that, since H2 has an even number of collisions, then  $(-1)^V = +1$  for this term.

A single-overlap collision requires the presence of at least one non-interacting collision, so it is clear from Fig. 10 that diagrams R1 and C1 cannot contribute any sequences containing a single-overlap collision. Furthermore, diagram R2 cannot either; for the Recollision Rule requires 1 and 2 to separate in R2 before 1 and 3 interact if 1 and 2 are to subsequently recollide. Thus, the only possible sources of  $v$ -sequences containing at least one single-overlap collision are diagrams C2, H1 and H2. An examination of these diagrams reveals that there are *five* single-overlap sequences in H2 (shown in Figs. 13a, 13b and 13c), *one* single-overlap sequence in H1 (shown in Fig. 13d), and *two* single-overlap sequences in C2 (shown in Fig. 13e). [Note that Figs. 13b, 13c and 13e each stand for two separate sequences.] We again label the *distinct* velocity regions by small Greek letters, and we indicate below each diagram the corresponding form of the integrand in equation (4-24), including the  $(-1)^{\nu}$  factor. It must be emphasized that the velocity region labels in each diagram in Fig. 13 refer only to the integrand appearing just below that diagram; that is, no connection is as yet implied or assumed between like-labelled velocity regions in different diagrams. (Actually, our particular choice of labels for the velocity regions in the diagrams of Fig. 13 was made with hindsight, for we shall find presently that like-labelled velocity regions in these single-overlap diagrams are in fact dynamically equivalent regions.)

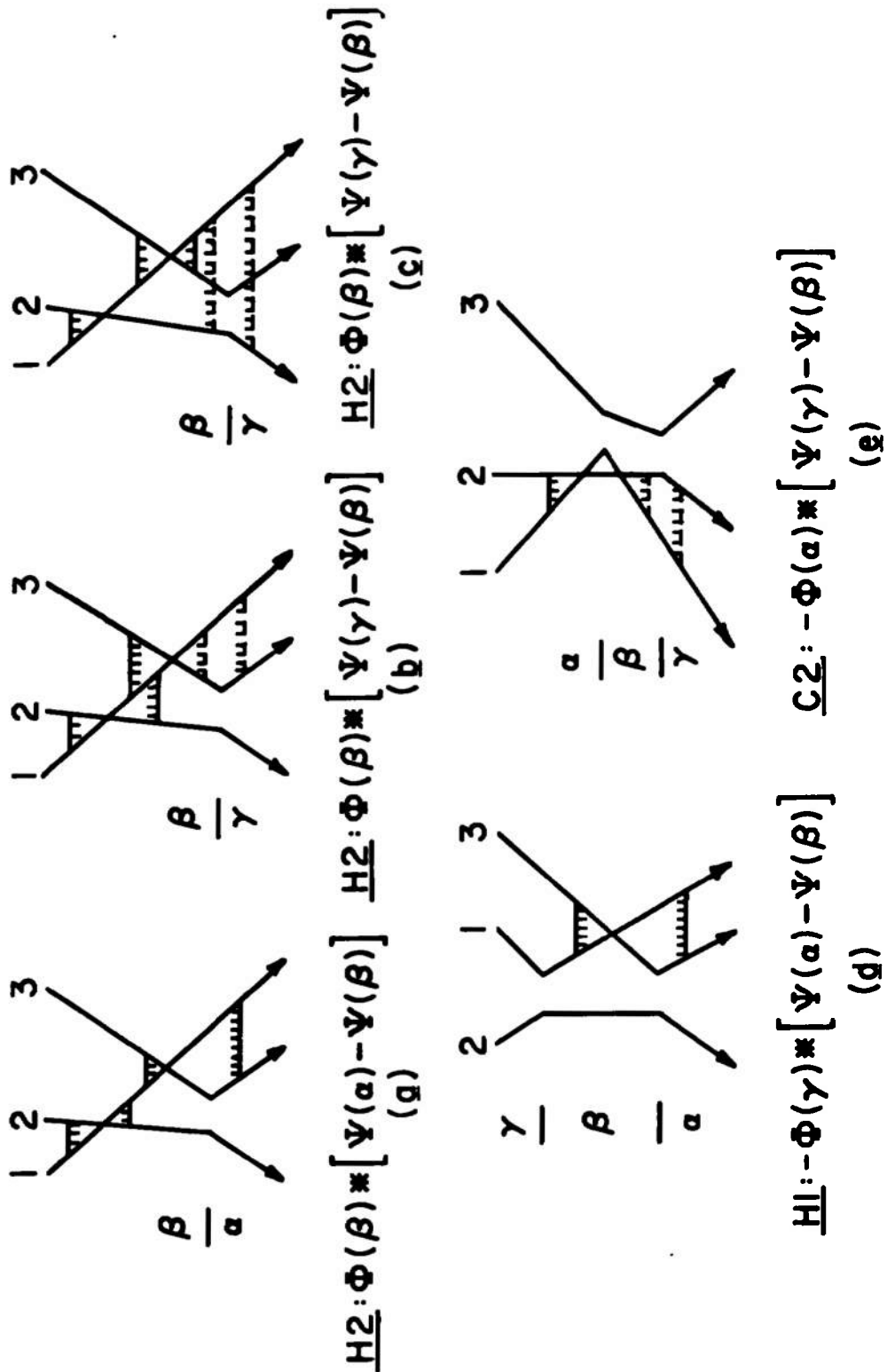


Figure 13. All v-diagrams containing at least one single-overlap collision.

Having thus extracted all the double-overlap  $v$ -sequences (Fig. 12) and all the single-overlap  $v$ -sequences (Fig. 13), let us now examine the *combined contributions* of these classes of diagrams, as represented respectively by the terms  $(\phi, \psi)_1^{(3)}$  and  $(\phi, \psi)_2^{(3)}$  in (4-16).

Consider first the double-overlap contributions ( $k=1$ ). Using the overlap notation in Fig. 3d, we can evidently represent the sum of the two double-overlap diagrams in Fig. 12 by the diagram in Fig. 14a; this diagram shows explicitly that 1 overlaps with both 2 and 3 at the instant of the 2-3 collision, and it is non-specific about the order in which the subsequent 1-2 and 1-3 separating collisions occur. If we interchange labels 2 and 3, we obtain the equivalent representation of the double-overlap term shown in Fig. 14b. Now diagrams 14a and 14b differ only in the ordering of the initial penetrating collisions; thus, the sum of these two diagrams (which is exactly twice the double-overlap contribution) gives a diagram in which the order of the 1-2 and 1-3 penetrating collisions is also not specified. Interchanging in this diagram labels 1 and 3, we thus obtain the diagram in Fig. 15 and the corresponding "double-overlap part" of the triple collision inner product,

$$(\phi, \psi)_1^{(3)} = -\sigma^5 \int_{\Omega_1} d\vec{V}_1 d\vec{V}_2 d\vec{V}_3 d\hat{k}_{21} d\vec{r}_{31} |\vec{V}_{21} \cdot \hat{k}_{21}| \prod_{i=1}^3 f_0(V_i) \{ \frac{1}{2} \phi(\alpha) * [\Psi(\beta) - \Psi(\alpha)] \} \tag{4-25}$$

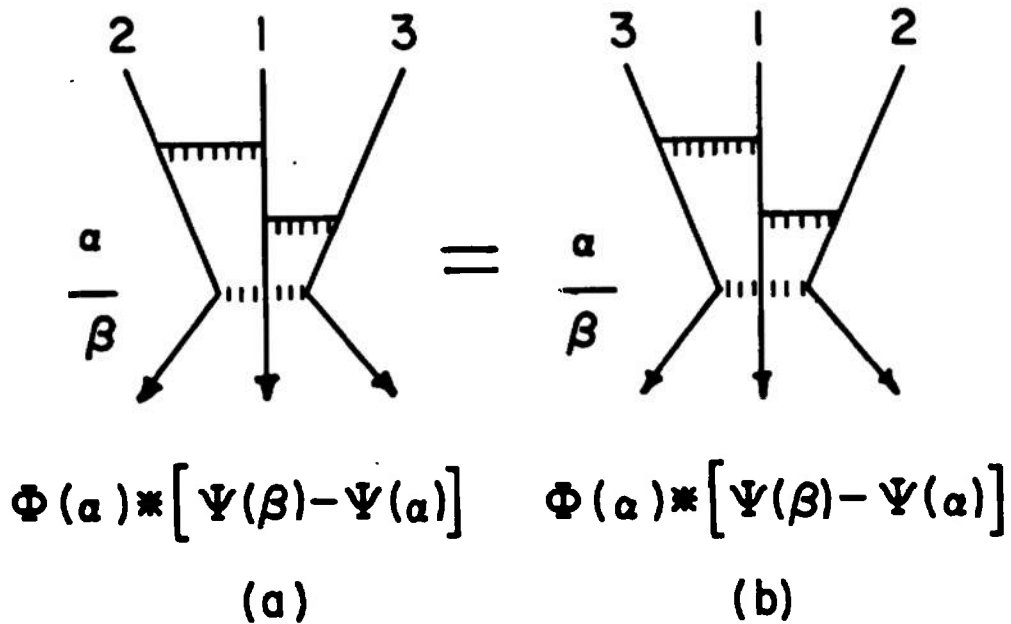


Figure 14. Equivalent double-overlap diagrams.

In this expression, the velocity variables outside the braces are most conveniently taken to be the  $\alpha$ -region velocities, and  $\Omega_1$  is that region in the space of points  $(\vec{V}_1 \equiv \vec{V}_1(\alpha), \hat{k}_{21}, \vec{r}_{31})$  which corresponds to a realization of the collision sequence depicted in Fig. 15. [Specifically, the points in  $\Omega_1$  satisfy the three conditions  $\vec{V}_{21} \cdot \hat{k}_{21} > 0$ ,  $|\vec{r}_{31}| < 1$  and  $|\vec{r}_{31} + \hat{k}_{21}| < 1$ .] The factor of 1/2 in the integrand of (4-25) arises because the diagram of Fig. 15 is the sum of the two diagrams in Fig. 14, each of which separately gives  $(\phi, \psi)_1^{(3)}$ . The reason we prefer the diagram in Fig. 15 over either of the diagrams in Fig. 14 is that the integrating volume associated with Fig. 15 is easier to specify analytically: we do not have to worry about the

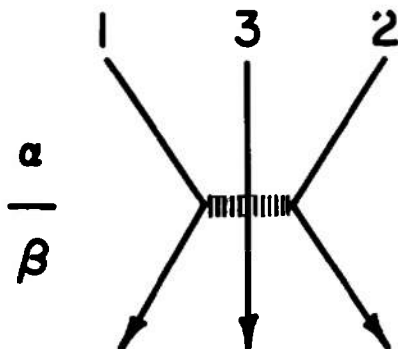


Figure 15. Diagram for  $(\phi, \psi)_1^{(3)}$ .

order of the penetrating collisions in Fig. 15. We remark that the dependence of equation (4-25) upon the diagram in Fig. 15 exactly parallels the dependence of equation (4-24) on the  $v$ -diagrams in Fig. 10; that is, the diagram in Fig. 15 specifies the integrating volume  $\Omega_1$  as well as the functional dependence of the  $\beta$ -region velocities upon the integrating variables.

It will be observed that the diagram in Fig. 15 is "symmetric" in the sense that a reversal of all velocities is equivalent to simply interchanging the velocity region

labels  $\alpha$  and  $\beta$ . Therefore, since (4-25) is unaffected by a reversal of all velocities, then it is also unaffected by an interchange of the labels  $\alpha$  and  $\beta$ . If such an interchange is made, and if the resulting expression is added to (4-25) and the sum divided by 2, we obtain an expression for  $(\phi, \psi)_1^{(3)}$  which is identical to (4-25) except that the quantity in braces is replaced by

$$\{-1/4 [\phi(\beta) - \phi(\alpha)] * [\Psi(\beta) - \Psi(\alpha)]\}$$

Since this is symmetric with respect to an interchange of  $\phi$  and  $\Psi$ , we deduce that  $(\phi, \psi)_1^{(3)}$  is symmetric in  $\phi$  and  $\psi$ :

$$(\phi, \psi)_1^{(3)} = (\psi, \phi)_1^{(3)} \quad (4-26)$$

In Sec. 5.1 we shall prove that  $(\phi, \psi)_1^{(3)}$  coincides with the Enskog inner product  $(\phi, \psi)_E^{(3)}$ . For now, though, we turn to consider the single-overlap term,  $(\phi, \psi)_2^{(3)}$ .

By definition,  $(\phi, \psi)_2^{(3)}$  is the sum of all the diagrams in Fig. 13. This summation is carried out in four steps, as is shown in Fig. 16: First, to diagram 13b we add diagram 13c (with 2 and 3 interchanged). Second, to the sum of diagrams 13b and 13c we add diagram 13e (with 2 and 3 interchanged). Third, to diagram 13a (with 2 and 3 interchanged) we add diagram 13d (with 2 and 3 interchanged). Finally, to the sum of diagrams 13a and 13d (with velocities reversed), we add the sum of diagrams 13b, 13c and 13e (with 1 and 2 interchanged). In this last operation -- the fourth "line" in Fig. 16 --

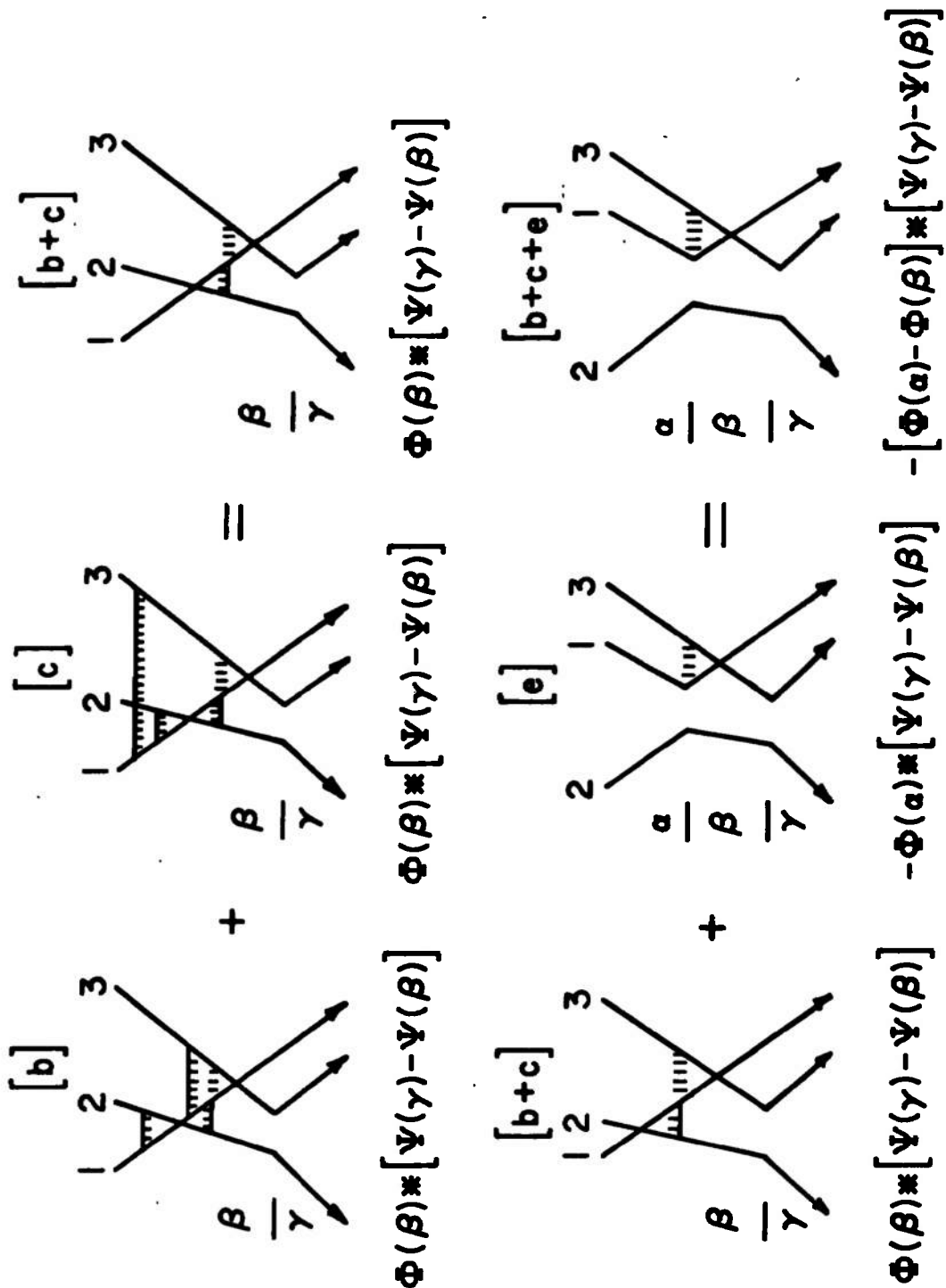


Figure 16. Summation of the single-overlap diagrams.



we observe that the [a+d] diagram requires 2 and 3 to separate *before* 1 and 3 interact, whereas the [b+c+e] diagram is non-committal about the order of the 2-3 separating collision and the 1-3 interacting collision. Consequently, the [a+d] integrand can be referred to the [b+c+e] diagram only if the [a+d] integrand is multiplied by a quantity  $\theta$ , which is unity if 2 and 3 separate before 1 and 3 collide and zero otherwise. Thus, we obtain for the "single-overlap inner product" the expression

$$\begin{aligned}
 (\phi, \psi)_2^{(3)} = & -\sigma^5 \int_{\Omega_2} d\vec{V}_1 d\vec{V}_2 d\vec{V}_3 d\hat{k}_{21} d\vec{r}_{31} |\vec{V}_{21} \cdot \hat{k}_{21}| \prod_{i=1}^3 f_0(V_i) \\
 & \{ -[\Phi(\alpha) - \Phi(\beta)] * [\Psi(\gamma) - \Psi(\beta)] \\
 & - \theta [\Psi(\alpha) - \Psi(\beta)] * [\Phi(\gamma) - \Phi(\beta)] \} \quad (4-27)
 \end{aligned}$$

where the integration volume  $\Omega_2$  and the velocity regions  $\alpha, \beta, \gamma$  are defined relative to the diagram in Fig. 17. The quantity  $\theta$  is also defined relative to this diagram, in the following way: if  $\tau_1$  is the time interval between the 1-2 collision and the 1-3 collision, and  $\tau_2$  the time interval between 1-2 collision and the 2-3 separating collision then

$$\theta \equiv \theta(\tau_1 - \tau_2) \equiv \begin{cases} 1, & \text{for } \tau_1 > \tau_2 \\ 0, & \text{for } \tau_1 < \tau_2 \end{cases} \quad (4-28)$$

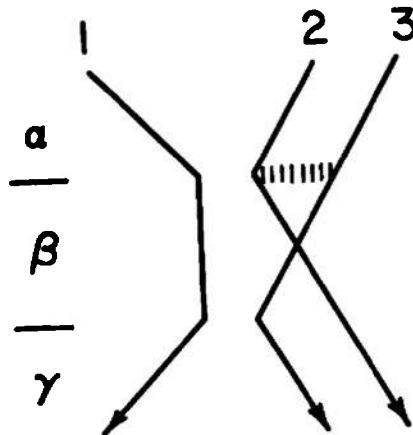


Figure 17. Diagram for  $(\phi, \psi)_2^{(3)}$ .

In words, the second term in the integrand in (4-27) contributes only when molecules 2 and 3 separate before molecules 1 and 3 collide.

In order to prove that  $(\phi, \psi)_2^{(3)}$  is symmetric, we imagine the integrating volume  $\Omega_2$  to be divided into two regions,  $\Omega_2(1)$  and  $\Omega_2(0)$ , where  $\theta=1$  and  $\theta=0$  respectively. In  $\Omega_2(1)$  the integrand is obviously symmetric in  $\phi$  and  $\psi$ . In  $\Omega_2(0)$  the integrand consists of only the first term, and hence is not symmetric. Here, however, the diagram in Fig. 17 must be modified to indicate that the 2-3 overlap definitely persists to the 1-3 collision. The resulting diagram is identical to

the one shown in Fig. 5b, and is evidently symmetric in the sense that a reversal of all velocities is equivalent to an interchange of velocity regions  $\alpha$  and  $\gamma$ . Thus, the integrand in  $\Omega_2(0)$  is invariant to an interchange of the regions  $\alpha$  and  $\gamma$ . But such an interchange in the first term of the integrand in (4-27) is evidently equivalent to an interchange of  $\phi$  and  $\psi$ . Thus, the integral in (4-27) is symmetric in  $\phi$  and  $\psi$  over regions  $\Omega_2(1)$  and  $\Omega_2(0)$  *separately*, so it follows that

$$(\phi, \psi)_2^{(3)} = (\psi, \phi)_2^{(3)} \quad (4-29)$$

We shall consider the problem of *numerically evaluating*  $(\phi, \psi)_2^{(3)}$  in Sec. 5.2.

Having now disposed of the "excluded volume" contributions to  $(\phi, \psi)^{(3)}$  -- i.e., contributions from collision sequences containing some sort of overlap collision -- we now turn to examine the effects on  $(\phi, \psi)^{(3)}$  due solely to deviations from "molecular chaos" -- i.e., contributions from collision sequences containing no overlap collisions. To obtain these non-overlap sequences, we return to the  $v$ -diagrams in Fig. 10 and we insert the concomittant separating collision after each required penetrating collision but *before* the next required collision, thus assuring the absence of overlap collisions. The resulting non-overlap collision sequences are shown in Fig. 18. We again indicate the distinct velocity regions in each diagram by small Greek letters, and we display below each diagram the corresponding integrand [i.e., the quantity in braces in (4-24)]. It must be emphasized

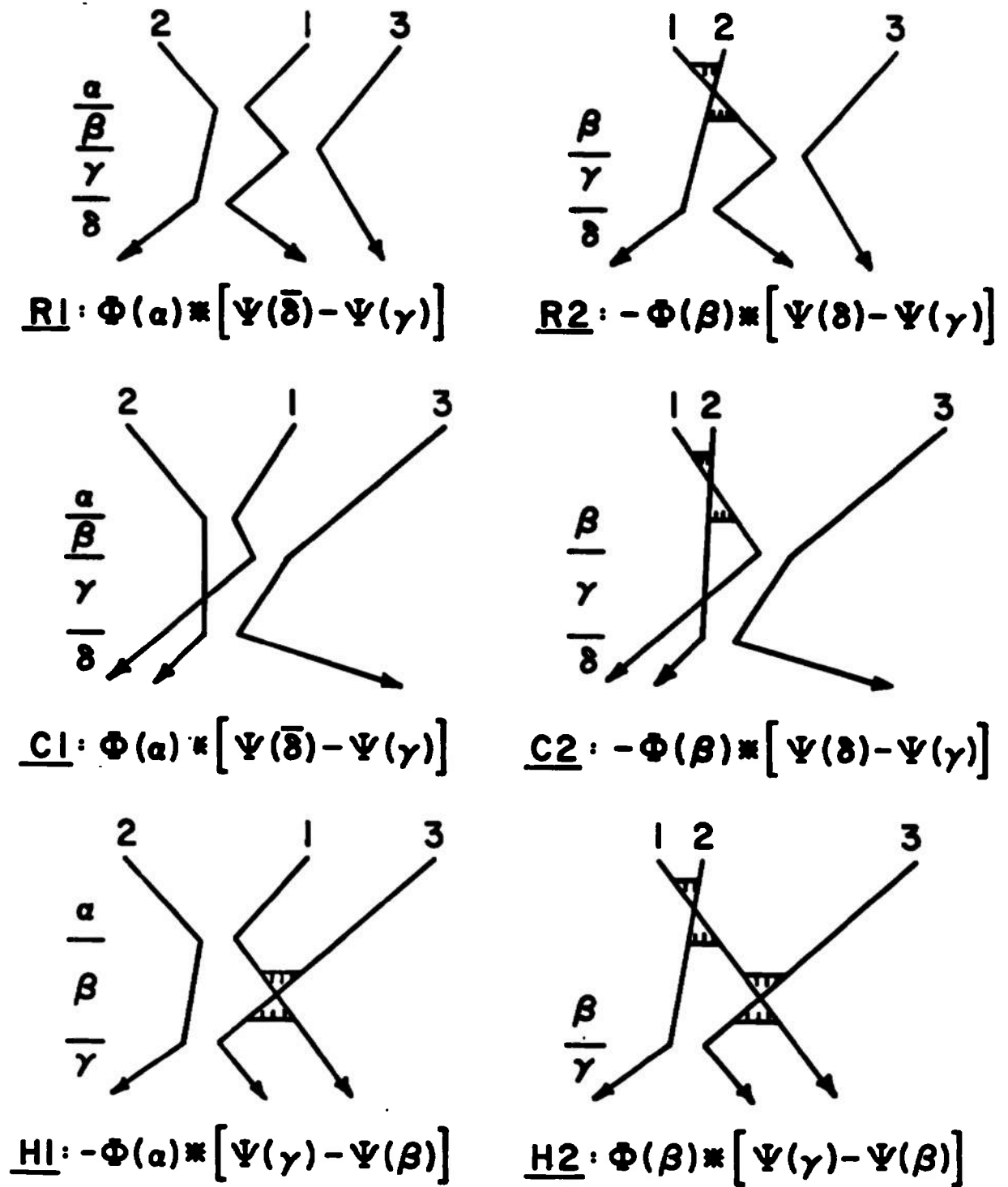


Figure 18. All v-diagrams not containing an overlap collision. [Note that these diagrams are subject to the restrictions stated in the text.]

that the diagrams in Fig. 18 are still subject to the First Collision Restriction (no collisions permitted above the "first" collision in any diagram) and the Real Collision Restriction (no additional collisions permitted between the "first" and "third" collisions in R1 and C1). In addition, we note that the integrands for R1 and C1 refer to region  $\bar{\delta}$ , which corresponds to the velocities after *all possible* interaction collisions have been allowed to occur [cf. (4-10)].

We now define the contribution to  $(\phi, \psi)^{(3)}$  from the diagrams of (4-15c) -- i.e., the  $k=3$  term in (4-16) -- to be that calculated from the non-overlap diagrams in Fig. 18 *ignoring*

- (i) the First Collision Restriction;
- (ii) the Real Collision Restriction;
- (iii) the distinction between velocity regions  $\bar{\delta}$  and  $\delta$  in diagrams R1 and C1.

When these three points are ignored, it becomes possible to combine each type 2 diagram in Fig. 18 with its type 1 counterpart. For example, in the absence of the above externally imposed conditions, the velocity regions  $\beta$ ,  $\gamma$  and  $\delta$  in R2 are seen to be equivalent to the like-labelled velocity regions in R1; we may therefore refer the R2 integrand directly to the R1 diagram. We similarly combine C2 with C1 and H2 with H1. Thus we find

$$\begin{aligned}
 (\phi, \psi)_3^{(3)} = & -\sigma^5 \sum_{\ell=1}^3 \int_{\Omega_{3\ell}} d\vec{V}_1 d\vec{V}_2 d\vec{V}_3 d\hat{k}_{21} d\vec{r}_{31} |\vec{V}_{21} \cdot \hat{k}_{21}| \prod_{i=1}^3 f_0(V_i) \\
 & \{ (-1)^{\ell-1} [\Phi(\alpha_\ell) - \Phi(\beta_\ell)] * [\Psi(\delta_\ell) - \Psi(\gamma_\ell)] \} \quad (4-30)
 \end{aligned}$$

where the integration volumes  $\Omega_{3\ell}$  and the velocity regions  $\alpha_\ell, \beta_\ell, \gamma_\ell, \delta_\ell$  are defined relative to the three diagrams in Fig. 19. We emphasize that these diagrams are not subject to any externally imposed restrictions, as are the diagrams in Fig. 10.

If, in the diagrams of Fig. 19, we reverse all velocities, and if we also interchange molecule labels 1 and 3, on the  $\ell=2$  and  $\ell=3$  diagrams, we see that the net effect is to interchange the velocity regions according to  $\alpha_\ell \leftrightarrow \delta_\ell, \beta_\ell \leftrightarrow \gamma_\ell$ . But such an interchange of velocity regions in (4-30) is evidently equivalent to interchanging  $\Phi$  and  $\Psi$ . Therefore, since (4-30) is invariant under velocity reversal and label permutations, we conclude that

$$(\phi, \psi)_3^{(3)} = (\psi, \phi)_3^{(3)} \quad (4-31)$$

Now,  $(\phi, \psi)_3^{(3)}$  evidently differs from the true non-overlap part of  $(\phi, \psi)^{(3)}$  in three respects: Firstly,  $(\phi, \psi)_3^{(3)}$  includes contributions from diagrams which violate the First Collision Restriction; these diagrams must be found and their contributions subtracted. Secondly,  $(\phi, \psi)_3^{(3)}$  includes contributions from R1-like and C1-like diagrams which violate the Real Collision Restriction; these diagrams too must be found and their contributions subtracted. Thirdly, for those R1 and C1

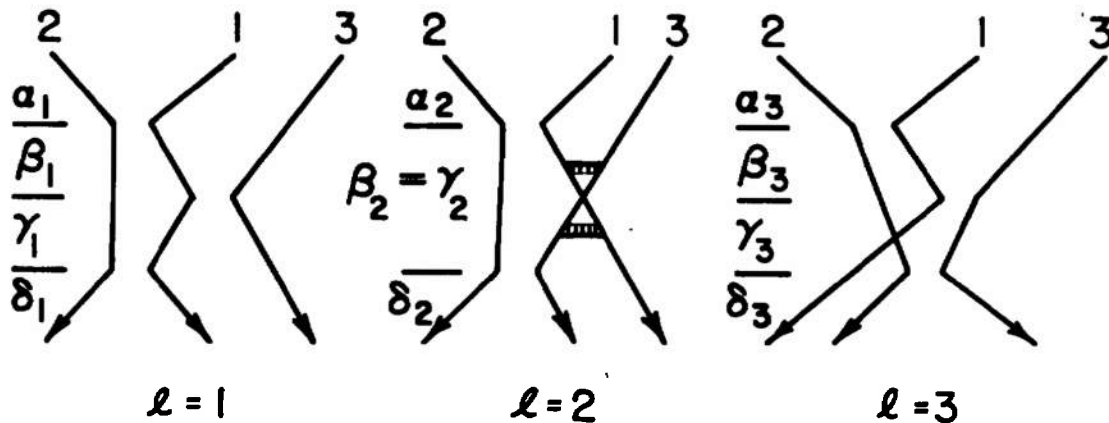


Figure 19. Diagrams for  $(\phi, \psi)_3^{(3)}$ .

collisions sequences that are succeeded by a fourth collision,  $(\phi, \psi)_3^{(3)}$  incorrectly uses for  $V_i(\bar{\delta})$  the velocities after the *third* collision instead of the velocities after the *last* collision; these diagrams must be found, their incorrect contributions subtracted, and their correct contributions added. Evidently, all these diagrams will contain *more* than three complete collisions. But here our task is greatly simplified by Theorem II [cf. Sec. 3.2 and Appendix A], which tells us that we need concern ourselves *only* with finding those diagrams in the above categories which contain *four* complete collisions. The appropriately signed contributions from these four-collision

sequences will, of course, constitute the fourth and final term in our expansion (4-16).

Evidently, the diagrams contributing to  $(\phi, \psi)^{(3)}$  fall into three classes, and so we discuss these three classes of diagrams in turn. The class (i) diagrams consist of all those sequences in Fig. 18 which have an additional non-interacting collision before (above) the "first" collision. The Recollision Rule tells us that diagrams R1, C1 and H1 may be preceded only by a 1-3 or a 2-3 collision, and diagrams R2 and C2 only by a 2-3 collision, while diagram H2 cannot be preceded by a collision between any pair. This yields a total of eight diagrams. However, half of these diagrams are not dynamically possible: Lemma 2 forbids R1 from having a prior 1-3 collision, and also C1 from having a prior 2-3 collision, while Lemma 1 forbids both H1 and C2 from having prior 2-3 collisions. The remaining four diagrams in class (i) are dynamically possible, and they are shown in Fig. 20. In these class (i) diagrams, we have changed the labelling of the velocity regions from Fig. 18 for later convenience. We have also incorporated into the integrands an additional factor of  $(-1)$ , reflecting the fact that these diagrams contribute in a "subtractive" sense.

The class (ii) diagrams consist of all those R1-like and C1-like sequences which have an additional non-interacting collision between the first and second collisions or between the second and third collisions. The Recollision Rule admits four possibilities: R1 can have a 2-3 non-interacting collision

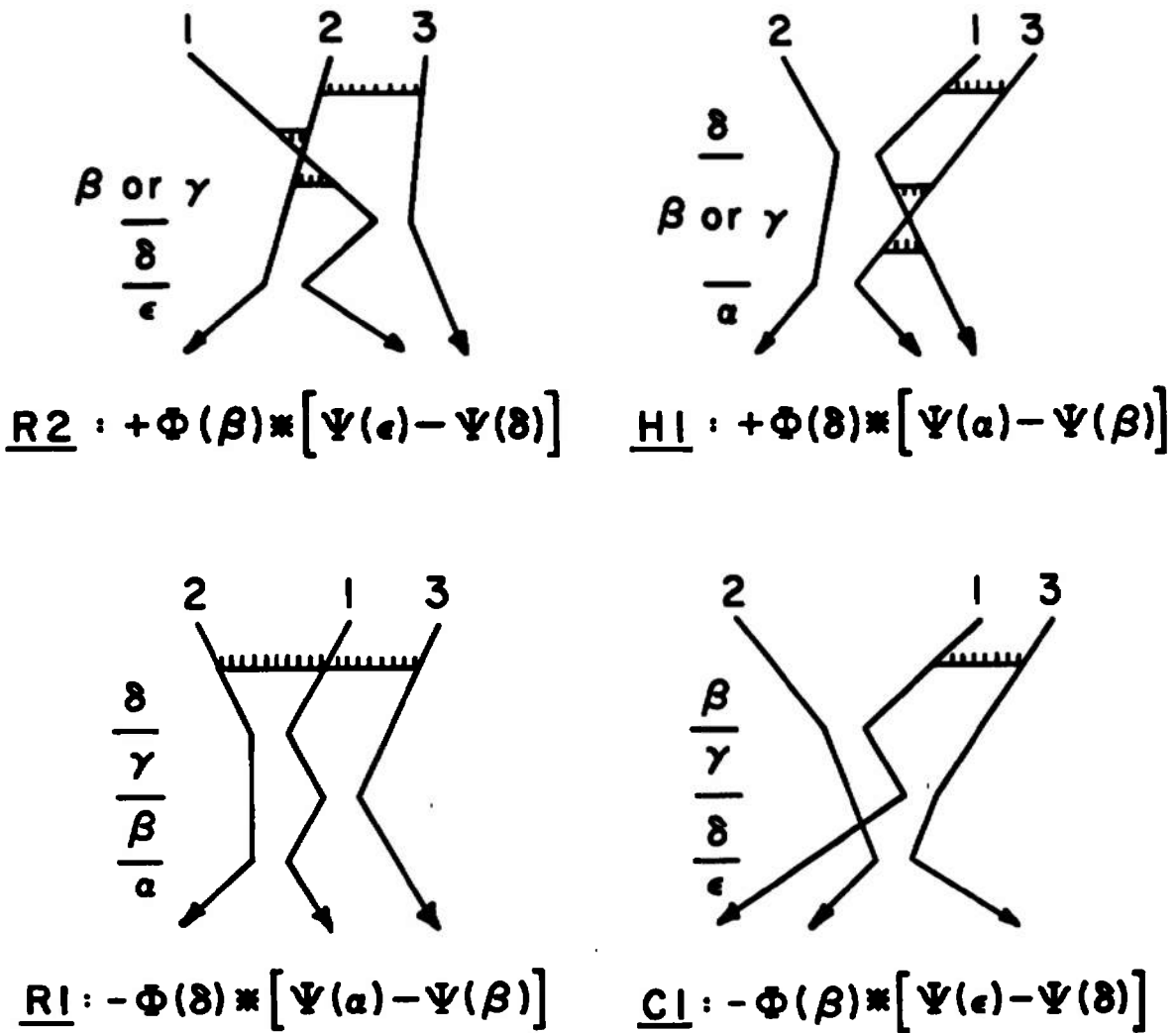


Figure 20. Four-collision diagrams: class (i).

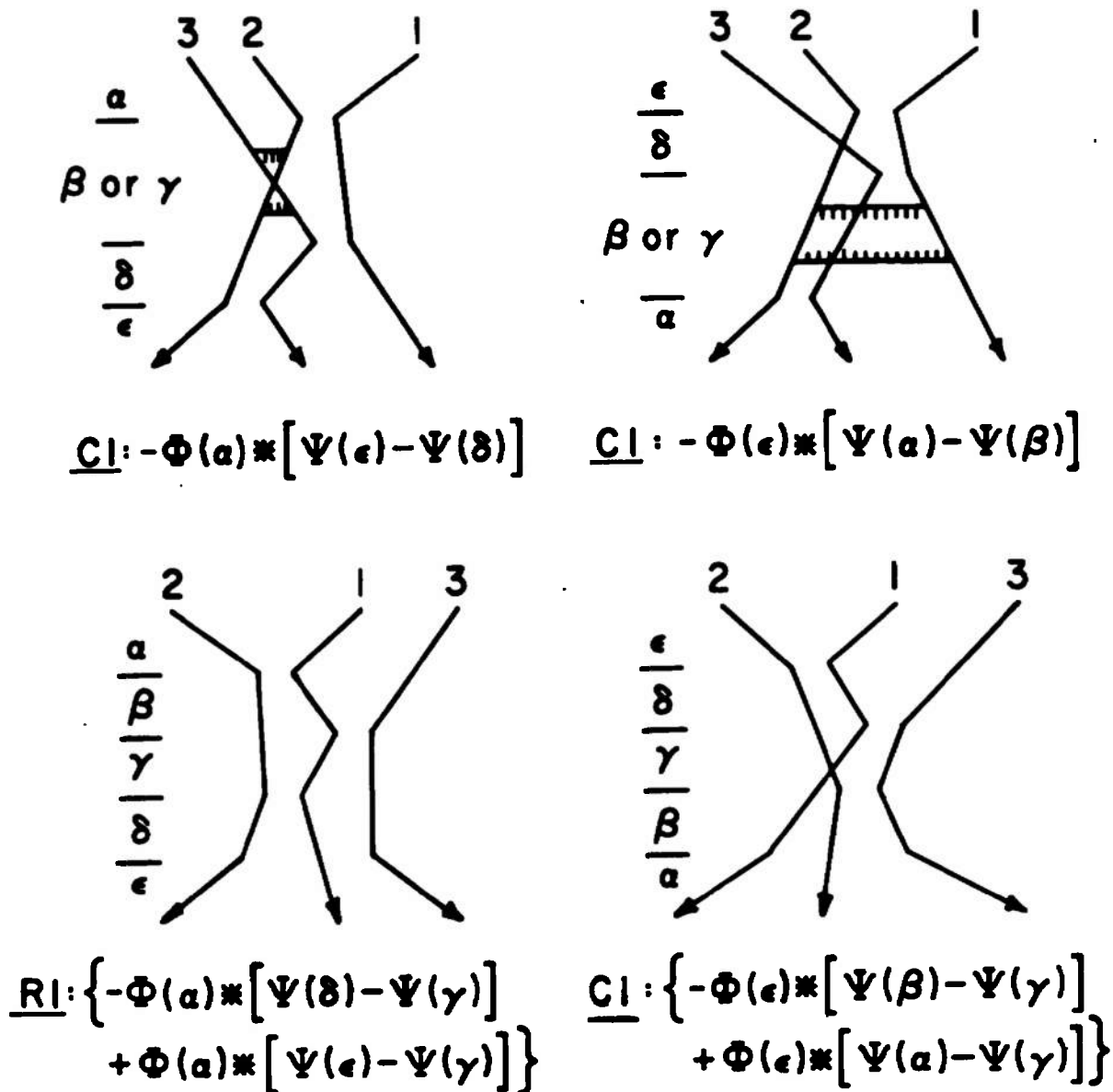


Figure 21. Four-collision diagrams: top row, class (ii); bottom row, class (iii).

between the first and second collisions *or* between the second and third collisions; and C1 can have a 2-3 non-interacting collision between the first and second collisions *or* a 1-2 non-interacting collision between the second and third collisions. Lemma 1 rules out the two R1 sequences. The two C1 sequences are possible, though, and we show them in the top row of Fig. 21. Again, we have relabelled the velocity regions, and we have incorporated an additional factor of (-1) into the integrands, reflecting their subtractive nature.

Finally, the class (iii) diagrams consist of all those R1 and C1 diagrams that can have a fourth interacting collision. By the Recollision Rule, this fourth collision can be either a 1-3 or a 2-3 collision for R1, and either a 1-3 or a 1-2 collision for C1. However, Lemma 2 rules out a fourth 1-3 collision for R1, as well as a fourth 1-2 collision for C1. The remaining two diagrams are dynamically possible, and are shown in the bottom row of Fig. 21. Again, for later convenience, we have relabelled the velocity regions in these diagrams. In determining the integrands for these class (iii) diagrams, we recall that they arise here because, in  $(\phi, \psi)_3^{(3)}$ , we incorrectly wrote  $\Psi(\delta)$  instead of  $\Psi(\bar{\delta})$  for these diagrams. Therefore, the integrand for each diagram contains a "subtractive term", corresponding to  $\Psi(\delta)$ , and an "additive term", corresponding to  $\Psi(\bar{\delta})$ .

To obtain  $(\phi, \psi)_4^{(3)}$ , we have now to add the contributions from the eight diagrams in Figs. 20 and 21. To this end, we first

reverse all velocities (where necessary) so that the velocity regions are encountered in the order  $\alpha, \beta, \gamma, \delta, \epsilon$ ; next, we renumber the molecules (where necessary) in such a way that the first collision in each diagram is a 1-2 collision and the second collision a 1-3 collision. With these changes, we find that like-labelled velocity regions in the four diagrams in the *top rows* of Figs. 20 and 21 are all equivalent and that the corresponding integrands can all be referred to the  $\ell=1$  diagram in Fig. 22. Similarly, like-labelled velocity regions in the four diagrams in the *bottom rows* of Figs. 20 and 21 are all equivalent, and the corresponding integrands can all be referred to the  $\ell=2$  diagram in Fig. 22. The integrand for the  $\ell=1$  diagram in Fig. 22 will therefore be the sum of the integrands of the top-row diagrams in Figs. 20 and 21; likewise, the integrand for the  $\ell=2$  diagram in Fig. 22 will be the sum of the integrands of the bottom-row diagrams in Figs. 20 and 21. We thus obtain the comparatively simple result

$$\begin{aligned}
 (\phi, \psi)_4^{(3)} = & -\sigma^5 \sum_{\ell=1}^2 \int_{\Omega_{4\ell}} d\vec{V}_1 d\vec{V}_2 d\vec{V}_3 d\hat{k}_{21} d\vec{r}_{31} |\vec{V}_{21} \cdot \hat{k}_{21}| \prod_{i=1}^3 f_0(V_i) \\
 & (-1)^\ell \{ [\Phi(\alpha_\ell) - \Phi(\beta_\ell)] * [\Psi(\epsilon_\ell) - \Psi(\delta_\ell)] \\
 & + [\Psi(\alpha_\ell) - \Psi(\beta_\ell)] * [\Phi(\epsilon_\ell) - \Phi(\delta_\ell)] \} \quad (4-32)
 \end{aligned}$$

where the integration volumes  $\Omega_{4\ell}$  and the velocity regions  $\alpha_\ell, \beta_\ell, \gamma_\ell, \delta_\ell, \epsilon_\ell$  are defined relative to the two diagrams in

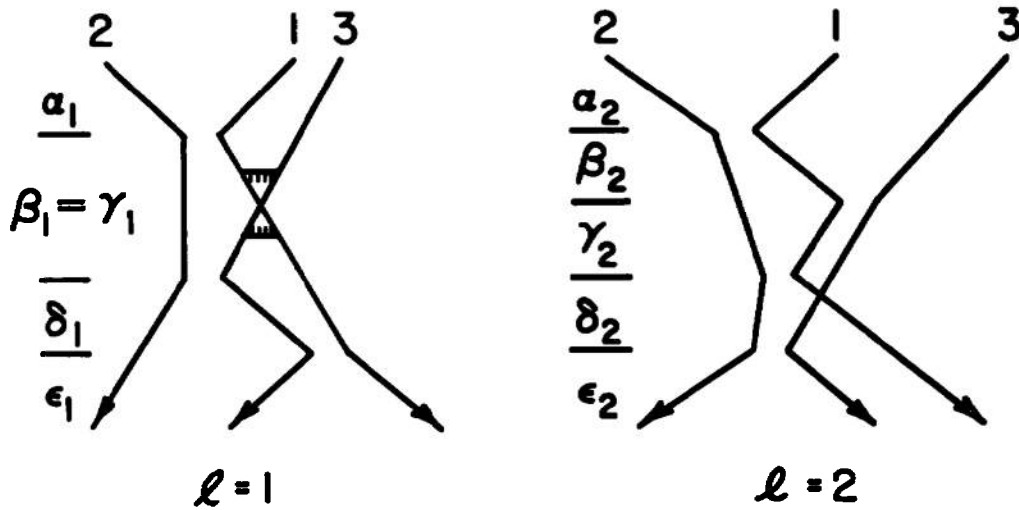


Figure 22. Diagrams for  $(\phi, \psi)_4^{(3)}$ .

Fig. 22. We observe that (4-32) is symmetric in  $\phi$  and  $\psi$ , so that

$$(\phi, \psi)_4^{(3)} = (\psi, \phi)_4^{(3)} \tag{4-33}$$

This completes our derivation of the terms appearing in the re-summed form of the triple collision inner product in (4-16). We have essentially replaced the  $v$ -diagrams in Fig. 10 with the diagrams in Figs. 15, 17, 19 and 22. We emphasize that, unlike the  $v$ -diagrams, our new diagrams are not subject to extra conditions or restrictions. We have proved that each term in (4-16) has the attractive property of being symmetric in  $\phi$  and  $\psi$ , a property that did not hold for the individual terms in

(4-24). Indeed, our work here constitutes an independent proof of the fact that [18]

$$(\phi, \psi)^{(3)} = (\psi, \phi)^{(3)} \quad (4-34)$$

Further attractive features of our new expansion will emerge in the next chapter.

### 4.3 Consequences for the Transport Coefficients

In (2-41) and (2-42) we found that the triple collision contributions to the transport coefficients,  $\lambda_1$  and  $\eta_1$ , are proportional to certain triple collision inner products. Therefore, the fact that the general triple collision inner product can be decomposed in the manner of (4-16) implies corresponding decompositions for  $\lambda_1$  and  $\eta_1$ . Thus, we write

$$\lambda_1 = \lambda_{11} + \lambda_{12} + \lambda_{13} + \lambda_{14} \quad (4-35)$$

$$\eta_1 = \eta_{11} + \eta_{12} + \eta_{13} + \eta_{14} \quad (4-36)$$

where

$$n\lambda_{1i} \equiv -\frac{k}{3} (\vec{A}, \vec{A})_i^{(3)} \quad (4-37)$$

$$n\eta_{1i} \equiv -\frac{kT}{10} (\vec{B}, \vec{B})_i^{(3)} \quad (4-38)$$

Here,  $\vec{A}$  and  $\vec{B}$  are, as before, the solutions to the linearized Boltzmann equations (2-6) and (2-7); the  $N^{\text{th}}$  Sonine approximations to  $\vec{A}$  and  $\vec{B}$  were given in (2-24) and (2-25) [cf. also Tables I and II].

The quantities  $\lambda_{11}$  and  $\eta_{11}$  are calculated by means of formula (4-25) and the collision sequence diagram in Fig. 15. This "double-overlap" diagram contains the dynamics of only *one* collision, and gives rise to purely "excluded volume" contributions to  $\lambda_1$  and  $\eta_1$ .

The quantities  $\lambda_{12}$  and  $\eta_{12}$  are calculated by means of formula (4-27) and the collision sequence diagram in Fig. 17. This "single-overlap" diagram contains the dynamics of *two* collisions, and gives contributions to  $\lambda_1$  and  $\eta_1$  which may be characterized as a mixture of excluded volume effects and effects due to deviations from molecular chaos in the velocity distribution.

The quantities  $\lambda_{13}$  and  $\eta_{13}$  are calculated by means of formula (4-30) and the collision sequence diagrams in Fig. 19. These no-overlap diagrams contain the dynamics of *three* collisions, and give rise to contributions due solely to deviations from molecular chaos in the velocity distribution.

Finally, the quantities  $\lambda_{14}$  and  $\eta_{14}$  are calculated by means of formula (4-32) and the collision sequence diagrams in Fig. 22. These no-overlap diagrams contain the dynamics of *four* collisions, and again give rise to contributions caused solely by deviations from molecular chaos in the velocity distribution.

The fact that the above expansion terminates at four collisions is worth emphasizing. Our previous investigations in I were based on collision integrals of the form (4-14), and it was

not clear just how many molecular collisions were actually involved. Of course, the theorems in Sec. 3.2, which prove that three-particle collision sequences cannot contain more than four complete collisions, have assumed "hard sphere" dynamics. However, it is a reasonable conjecture that contributions from five and more successive collisions among triplets of more realistic gas molecules will be negligibly small.

It is obvious from the formulae for the integrals  $(\phi, \psi)_i^{(3)}$  that the ease of computing  $\lambda_{1i}$  and  $\eta_{1i}$  increases considerably with decreasing  $i$ . This is because correlations among the *positions* of the molecules (which dominate in the lower  $i$  terms) are mathematically easier to express than correlations among their *velocities* (which dominate in the higher  $i$  terms). This will work to a practical advantage *if* it should turn out that the magnitudes of the successive terms in (4-35) and (4-36) decrease from left to right, in the manner of a "perturbation expansion". Present indications are that this is probably the case: As we shall see in the next chapter, the double-overlap terms,  $\lambda_{11}$  and  $\eta_{11}$ , coincide exactly with the Enskog quantities  $\lambda_{1E}$  and  $\eta_{1E}$ , respectively, while the single-overlap terms  $\lambda_{12}$  and  $\eta_{12}$  are on the order of roughly 3 to 6 percent of the Enskog terms (but of opposite sign). Recalling our preliminary findings, reported in I, that  $\lambda_1$  and  $\eta_1$  differ from  $\lambda_{1E}$  and  $\eta_{1E}$  by only a few percent, we are thus led to conjecture that the single-overlap terms  $\lambda_{12}$  and  $\eta_{12}$

alone constitute a reasonably accurate refinement of Enskog's approximate theory.

In the next chapter we shall analyze in detail the  $i=1$  and  $i=2$  terms in (4-35) and (4-36).

## CHAPTER V

NUMERICAL CALCULATIONS OF THE "EXCLUDED VOLUME"  
CONTRIBUTIONS TO THE TRANSPORT PROPERTIES

5.1 Equivalence of the "Double-Overlap" Con-  
tribution with Enskog's Approximation.

The formula for the leading term in our expansion (4-16) of the triple collision inner product -- the so-called "double-overlap" term -- is given in (4-25), and refers to the collision sequence diagram in Fig. 15. A more geometrical representation of this double-overlap collision sequence is shown in Fig. 23, which may be regarded as a "snapshot" of the molecules at the instant of the 1-2 interacting collision. We take the integrating variables in (4-25) to be the velocities and relative positions of the molecules instantaneously *before* the 1-2 collision (thus,  $\vec{V}_i = \vec{V}_i(\alpha)$ ). The integration volume  $\Omega_1$  is then determined by two conditions. First, that molecules 1 and 2 initially be converging:  $\vec{V}_{21} \cdot \hat{k}_{21} > 0$ . Second, that 3 be overlapping with both 1 and 2:  $|\vec{r}_{31}| < 1$  and  $|\hat{k}_{21} + \vec{r}_{31}| < 1$ . If we write  $\vec{V}'_i$  for the  $\beta$ -region velocities, then  $\vec{V}'_1$  and  $\vec{V}'_2$  will be given by (2-11), while  $\vec{V}'_3 = \vec{V}_3$ . Using the definitions of  $\Phi$  and  $\Psi$  in (4-3), we thus write (4-25) more explicitly as

$$(\phi, \psi)^{(3)} = -\frac{\sigma^5}{2} \int_{\substack{\vec{V}_{21} \cdot \hat{k}_{21} > 0 \\ |\vec{r}_{31}| < 1, |\hat{k}_{21} + \vec{r}_{31}| < 1}} d\vec{V}_1 d\vec{V}_2 d\vec{V}_3 d\hat{k}_{21} d\vec{r}_{31} |\vec{V}_{21} \cdot \hat{k}_{21}| \prod_{i=1}^3 f_0(V_i)$$

$$\sum_{m=1}^3 \sum_{n=1}^3 \phi(\vec{V}_m) * [\psi(\vec{V}_n) - \psi(\vec{V}'_n)] \quad (5-1)$$

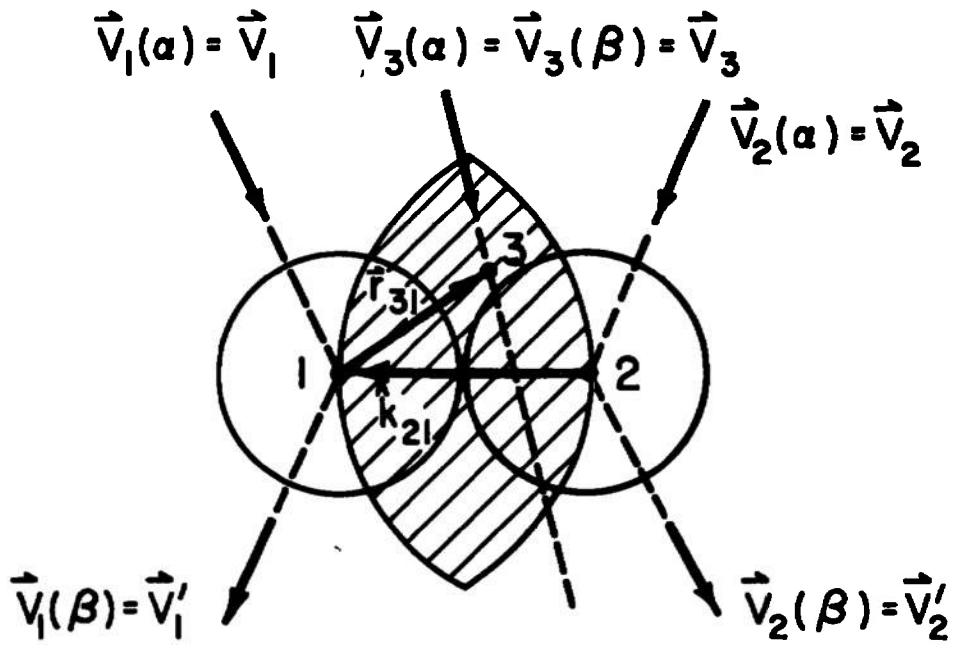


Figure 23. Integrating variables for  $(\phi, \psi)_I^{(3)}$ .

Since nothing in the integrand depends on the variable  $\vec{r}_{31}$ , we can perform this integration without difficulty. Noting that the integration region for  $\vec{r}_{31}$ , shown shaded in Fig. 13, is identical to the volume which determines the first density correction to  $g(\sigma)$  [cf. Fig. 2 and equation (2-46)], one easily finds  $\int d\vec{r}_{31} = 5\pi/12$ . Thus, (5-1) becomes

$$(\phi, \psi)_1^{(3)} = -\frac{5}{24}\pi\sigma^5 \int_{\vec{V}_{21} \cdot \hat{k}_{21} > 0} d\vec{V}_1 d\vec{V}_2 d\vec{V}_3 d\hat{k}_{21} |\vec{V}_{21} \cdot \hat{k}_{21}| \prod_{i=1}^3 f_0(V_i) \sum_{m=1}^3 \sum_{n=1}^3 \phi(\vec{V}_m) * [\phi(\vec{V}_n) - \psi(\vec{V}_n)] \quad (5-2)$$

Now, the  $n=3$  term here vanishes because  $\vec{V}'_3 = \vec{V}_3$ . Furthermore, the  $m=3$  contribution vanishes under the  $\vec{V}_3$  integration, since

$$\int d\vec{V}_3 f_0(V_3) \phi(\vec{V}_3) = 0$$

This is due to the fact that  $\phi(\vec{V}_3)$  is always proportional to either  $\vec{V}_3$  or  $\vec{V}_3^0 \vec{V}_3$  [cf. the expansions for  $\vec{A}$  and  $\vec{B}$  in (2-24) and (2-25)]; more generally, the vanishing above the above integral is a consequence of the normalization condition imposed on the distribution function (2-3) [cf. equation (2.1-14) of I]. Then since the quantities under the summation signs in (5-2) are independent of  $\vec{V}_3$ , the  $\vec{V}_3$  integration can be trivially done owing to the normalization of the Maxwell-Boltzmann function:

$$\int d\vec{V}_3 f_0(V_3) = n$$

Consequently, (5-2) reduces to

$$(\phi, \psi)_I^{(3)} = -\frac{5}{24} \pi \sigma^5 n \int_{\vec{V}_{21} \cdot \hat{k}_{21} > 0} d\vec{V}_1 d\vec{V}_2 d\hat{k}_{21} |\vec{V}_{21} \cdot \hat{k}_{21}| f_0(V_1) f_0(V_2)$$

$$\sum_{m=1}^2 \sum_{n=1}^2 \phi(\vec{V}_m) * [\psi(\vec{V}_n) - \psi(\vec{V}_n)] \tag{5-3}$$

A comparison of this last equation with equation (2-20), (2-23) and (2-48) reveals that

$$(\phi, \psi)_I^{(3)} = \frac{5}{12} \pi \sigma^3 n (\phi, \psi)^{(2)} \equiv (\phi, \psi)_E^{(3)} \tag{5-4}$$

Thus, the first term in the expansion (4-16) of the triple collision inner product coincides *exactly* with the Enskog approximation. The immediate consequence of (5-4) is that the first terms in the expansions (4-35) and (4-36) of  $\lambda_1$  and  $\eta_1$  coincide exactly with the Enskog predictions:

$$\lambda_{11} = \lambda_{1E} \equiv -\frac{5}{12} \pi \sigma^3 \lambda_0 \tag{5-5a}$$

$$\eta_{11} = \eta_{1E} \equiv -\frac{5}{12} \pi \sigma^3 \eta_0 \tag{5-5b}$$

With these results, our expressions for  $\lambda$  and  $\eta$  in (2-49) and (2-50) can be written

$$\lambda = \lambda_0 \left[ 1 + \frac{5}{12} \pi \sigma^3 n \left( \frac{48}{25} - 1 + \frac{\lambda_{12} + \lambda_{13} + \lambda_{14}}{|\lambda_{1E}|} \right) \right] \quad (5-6)$$

$$\eta = \eta_0 \left[ 1 + \frac{5}{12} \pi \sigma^3 n \left( \frac{32}{25} - 1 + \frac{\eta_{12} + \eta_{13} + \eta_{14}}{|\eta_{1E}|} \right) \right] \quad (5-7)$$

## 5.2 Evaluation of the "Single-Overlap" Contribution. Refinement of Enskog.

Equations (5-6) and (5-7) show clearly what must be done to effect a rigorous improvement of Enskog's approximation for the linear density dependence of the transport coefficients: we have to calculate the quantities  $(\lambda_{12} + \lambda_{13} + \lambda_{14}) / |\lambda_{1E}|$  and  $(\eta_{12} + \eta_{13} + \eta_{14}) / |\eta_{1E}|$ . These calculations can be made through equations (4-37) and (4-38), using the general formula for the inner products  $(\phi, \psi)_i^{(3)}$  derived in Sec. 4.2.

To the extent that our expansion of the triple collision inner product in (4-16) displays the terms in decreasing order of importance -- a conjecture which, although highly plausible, must ultimately be tested by direct numerical calculations -- we can obtain a "first correction" to Enskog's theory by evaluating only the quantities  $\lambda_{12} / |\lambda_{1E}|$  and  $\eta_{12} / |\eta_{1E}|$ . We shall, for the present, evaluate these quantities using the Sonine approximations for  $\vec{A}$  and  $\vec{B}$  in (2-24) and (2-25). The Nth Sonine approximation to (5-6) and (5-7) reads

$$\lambda(N) = \lambda_0(N) \left[ 1 + \frac{5}{12} \pi \sigma^3 n \left( \frac{48}{25} - 1 + \sum_{i=2}^4 \lambda_{1i}(N) / |\lambda_{1E}(N)| \right) \right] \quad (5-8)$$

$$\eta(N) = \eta_0(N) \left[ 1 + \frac{5}{12} \pi \sigma^3 n \left( \frac{32}{25} - 1 + \sum_{i=2}^4 \eta_{1i}(N) / |\eta_{1E}(N)| \right) \right] \quad (5-9)$$

The ratios under the summation signs can be read off from equations (2-53) and (2-54). In particular, the  $i=2$  ratios are

$$\frac{\lambda_{12}(N)}{|\lambda_{1E}(N)|} = \frac{-1}{a_1(N)} \sum_{k,\ell=1}^N a_k(N) a_\ell(N) \left[ S_{3/2}^{(k)}(W_1^2) \bar{W}_1^*, S_{3/2}^{(\ell)}(W_1^2) \bar{W}_1^* \right]_2^{(3)} \quad (5-10)$$

$$\frac{\eta_{12}(N)}{|\eta_{1E}(N)|} = \frac{-1}{b_0(N)} \sum_{k,\ell=0}^{N-1} b_k(N) b_\ell(N) \left[ S_{5/2}^{(k)}(W_1^2) \bar{W}_1^0 \bar{W}_1^*, S_{5/2}^{(\ell)}(W_1^2) \bar{W}_1^0 \bar{W}_1^* \right]_2^{(3)} \quad (5-11)$$

where the dimensionless triple-collision inner products  $[\phi, \psi]_2^{(3)}$  are given by (2-55):

$$[\phi, \psi]_2^{(3)} \equiv \frac{3}{10\pi} \sqrt{\frac{m}{\pi kT}} \frac{1}{n^3 \sigma^5} (\phi, \psi)_2^{(3)} \quad (5-12)$$

The formula for  $(\phi, \psi)_2^{(3)}$  which appears on the right side of the last equation is given in (4-27), and refers to the single-overlap collision sequence in Fig. 17. If we introduce into (4-27) the dimensionless velocity variables  $\bar{W}_i$  [cf. (2-26)] and the explicit forms of the Maxwell-Boltzmann functions [cf. (2-5)], and insert the resulting expression into (5-12), we obtain

$$\begin{aligned}
[\phi, \psi]_2^{(3)} = & \frac{3\sqrt{2}}{10\pi^6} \int_{\Omega_2} d\vec{W}_1 d\vec{W}_2 d\vec{W}_3 d\hat{k}_{21} d\vec{r}_{31} |\vec{W}_{21} \cdot \hat{k}_{21}| \exp(-W_1^2 - W_2^2 - W_3^2) \\
& \{ [\Phi(\alpha) - \Phi(\beta)] * [\Psi(\gamma) - \Psi(\beta)] \\
& + \Theta[\Psi(\alpha) - \Psi(\beta)] * [\Phi(\gamma) - \Phi(\beta)] \} \quad (5-13)
\end{aligned}$$

The integration volume  $\Omega_2$  and the velocity regions  $\alpha$ ,  $\beta$  and  $\gamma$  are still defined relative to the single-overlap diagram in Fig. 17, as is also the factor  $\Theta$  [cf. (4-28)]. We choose for our integrating variables the velocities and relative positions of the molecules instantaneously after the 1-2 collision in Fig. 17 (so that  $\vec{W}_i \equiv \vec{W}_i(\beta)$ ). In Fig. 24 we show the single-overlap collision sequence of Fig. 17 in more detail.

Our program now is as follows: Using Fig. 24, we must first express the  $\alpha$ - and  $\gamma$ -region velocities, and also the factor  $\Theta$ , as explicit functions of the integrating variables. Next, we must deduce from Fig. 24 an analytic expression for the integration region  $\Omega_2$ , so that (5-13) is brought into the form of an *iterated integral* with well-defined upper and lower integration limits. By these means, we transform the expression for  $[\phi, \psi]_2^{(3)}$  in (5-13) into a mathematically precise definite integral, defined without the use of any "physical" diagrams. We then proceed to evaluate this integral for those forms of  $\phi$  and  $\psi$  appearing on the right of (5-10) and (5-11), using the explicit formulae for the Sonine polynomials given in Table II. Finally using the  $a_K(N)$  and  $b_K(N)$  coefficients given in Table I, we evaluate the right sides of

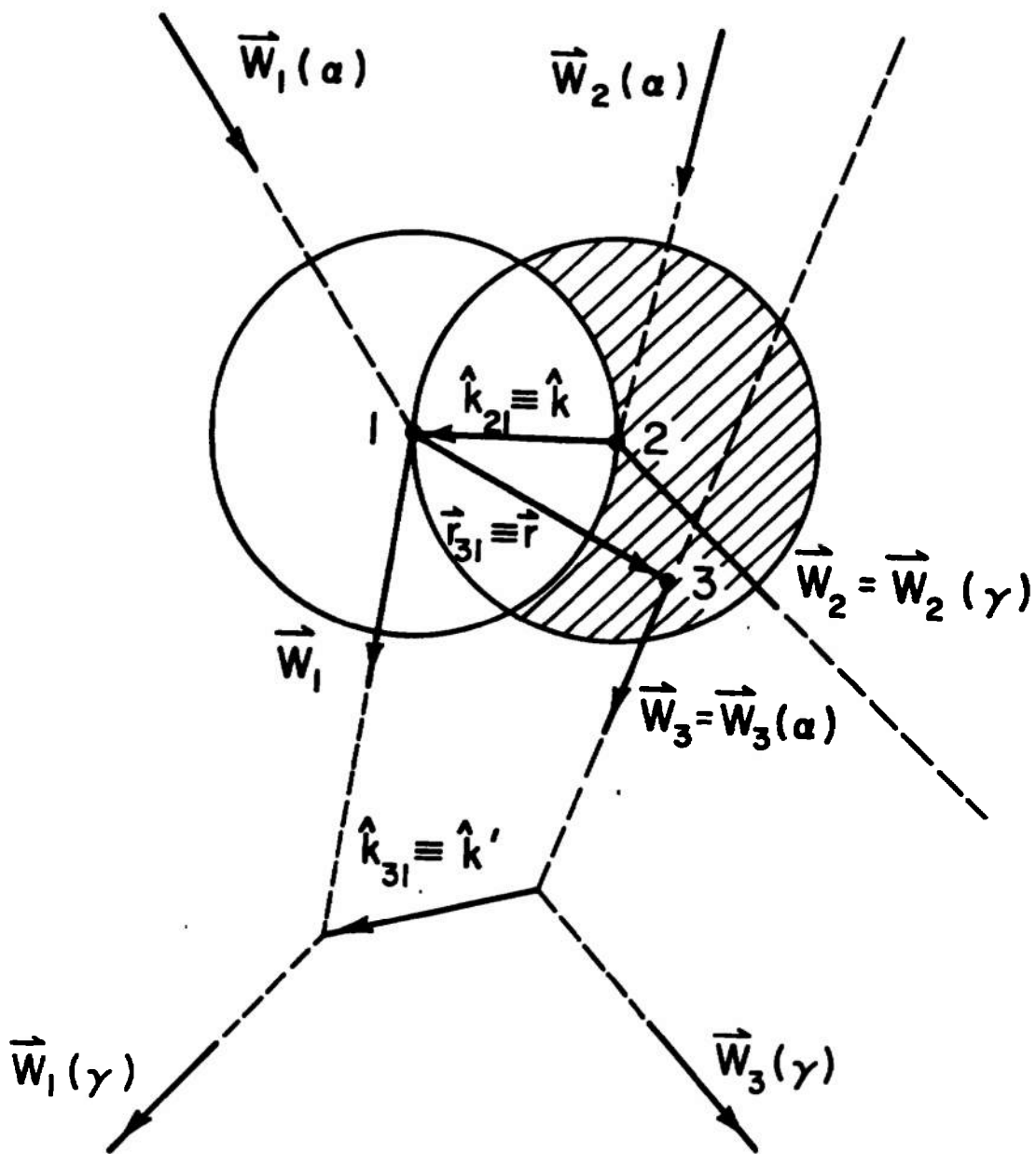


Figure 24. Integrating variables for  $(\phi, \psi)_2^{(3)}$ .

(5-10) and (5-11), and so obtain numerical values for the single-overlap contributions to (5-8) and (5-9). We shall perform the calculations for the first ( $N=1$ ) and second ( $N=2$ ) Sonine approximations.

The program just outlined entails an enormous amount of mathematical manipulations. In the first place, we find that in order to bring (5-13) into the form of an iterated integral with reasonable limits, the vector integrating variables must be defined in differently oriented frames; thus, rotation matrices must be introduced in order to find the components of these vectors in a common coordinate system. In the second place, (5-13) as it stands is a fourteen dimensional integral, and we perform seven of these integrations analytically; however, the performance of these seven integrations increases considerably the mathematical complexity of (5-13), particularly for the higher Sonine integrands. The remaining seven integrations must be done using Monte Carlo techniques. If a simple, straight forward Monte Carlo technique is applied, one does not obtain results of sufficient numerical accuracy; thus, we have taken considerable pains to develop a Monte Carlo method which is "tailored" to the specifics of our problem. Finally, we mention that calculations were made not only for the thermal conductivity and the viscosity, but also for the self-diffusion. Since we are working in the second Sonine approximation, we have to calculate three distinct integrals for each transport property;

therefore, we are evaluating here a total of *nine separate integrals* of the form (5-13).

It is simply not feasible to give here all or even most of the mathematical details involved in these calculations. Thus, we shall merely attempt to give the briefest possible sketch of the procedure, and then quote our numerical results.

We begin by making a transformation of variables from the velocities  $\vec{W}_1, \vec{W}_2, \vec{W}_3$  to

$$\begin{aligned}\vec{W}_0 &= \frac{1}{3}(\vec{W}_1 + \vec{W}_2 + \vec{W}_3) \\ \vec{W}_{21} &= \vec{W}_2 - \vec{W}_1 \\ \vec{W}_{31} &= \vec{W}_3 - \vec{W}_1\end{aligned}\tag{5-14}$$

It is also convenient to introduce the auxiliary variables  $\vec{W}_{10}, \vec{W}_{20}, \vec{W}_{30}$ :

$$\begin{aligned}\vec{W}_{10} &\equiv \vec{W}_1 - \vec{W}_0 = -\frac{1}{3}(\vec{W}_{21} + \vec{W}_{31}) \\ \vec{W}_{20} &\equiv \vec{W}_2 - \vec{W}_0 = -\frac{1}{3}(\vec{W}_{31} - 2\vec{W}_{21}) \\ \vec{W}_{30} &\equiv \vec{W}_3 - \vec{W}_0 = -\frac{1}{3}(\vec{W}_{21} - 2\vec{W}_{31})\end{aligned}\tag{5-15}$$

It is straightforward to show that the Jacobian of the transformation (5-14) is unity, and also that

$$\sum_{i=1}^3 W_i^2 = 3W_0^2 + E\tag{5-16a}$$

where the quantity E is defined by

$$E \equiv \sum_{i=1}^3 W_{i0}^2 = \frac{2}{3}(W_2^2 + W_3^2 - \vec{W}_{21} \cdot \vec{W}_{31}) \quad (5-16b)$$

For brevity, we shall also write

$$\hat{k}_{21} \equiv \hat{k}, \quad \vec{r}_{31} \equiv \vec{r}, \quad \hat{k}_{31} \equiv \hat{k}' \quad (5-17)$$

where  $\hat{k}_{31}$  is the collision vector for the 1-3 collision, as shown in Fig. 24. Equation (5-13) thus takes the form

$$\begin{aligned} [\phi, \psi]_2^{(g)} = & \frac{3\sqrt{2}}{10\pi^6} \int_{\Omega_2} d\vec{W}_0 d\vec{W}_{21} d\vec{W}_{31} d\hat{k} d\vec{r} |\vec{W}_{21} \cdot \hat{k}| \exp(-3W_0^2 - E) \\ & \{ [\Phi(\alpha) - \Phi(\beta)] * [\Psi(\gamma) - \Psi(\beta)] \\ & + \Theta[\Psi(\alpha) - \Psi(\beta)] * [\Phi(\gamma) - \Phi(\beta)] \} \end{aligned} \quad (5-18)$$

The  $\alpha$ - and  $\gamma$ -region velocities are given by equations of the form (2-11):

$$\begin{aligned} \vec{W}_1(\alpha) &= \vec{W}_1 + \vec{W}_{21} \cdot \hat{k} \hat{k} & \vec{W}_1(\gamma) &= \vec{W}_1 + \vec{W}_{31} \cdot \hat{k}' \hat{k}' \\ \vec{W}_2(\alpha) &= \vec{W}_2 - \vec{W}_{21} \cdot \hat{k} \hat{k} & \vec{W}_2(\gamma) &= \vec{W}_2 \\ \vec{W}_3(\alpha) &= \vec{W}_3 & \vec{W}_3(\gamma) &= \vec{W}_3 - \vec{W}_{31} \cdot \hat{k}' \hat{k}' \end{aligned} \quad (5-19)$$

If, in these equations, we replace each  $\vec{W}_i$  by  $\vec{W}_{i0}$ , we obtain the equations giving the values of the velocities  $\vec{W}_{i0}$  in the

$\alpha$  and  $\gamma$  regions. The corresponding equations for the velocities  $\vec{W}_0, \vec{W}_{21}, \vec{W}_{31}$  are easily found to be

$$\begin{aligned}
 \vec{W}_0(\alpha) &= \vec{W}_0 & \vec{W}_0(\gamma) &= \vec{W}_0 \\
 \vec{W}_{21}(\alpha) &= \vec{W}_{21} - 2\vec{W}_{21} \cdot \hat{k} \hat{k} & \vec{W}_{21}(\gamma) &= \vec{W}_{21} - \vec{W}_{31} \cdot \hat{k} \hat{k}' \\
 \vec{W}_{31}(\alpha) &= \vec{W}_{31} - \vec{W}_{21} \cdot \hat{k} \hat{k} & \vec{W}_{31}(\gamma) &= \vec{W}_{31} - 2\vec{W}_{31} \cdot \hat{k} \hat{k}'
 \end{aligned} \tag{5-20}$$

Evidently, (5-19) and (5-20) give the  $\alpha$ -region velocities in terms of the integrating variables; however, the formulae for the  $\gamma$ -region velocities contain the vector  $\hat{k}'$ , which itself is also a function of the integrating variables. In addition to determining  $\hat{k}'$ , we must also obtain expressions for the times  $\tau_1$  and  $\tau_2$  which enter into the factor  $\theta$ . By definition,  $\tau_1$  is the time between the 1-2 collision and the 1-3 collision, and  $\tau_2$  is the time between the 1-2 collision and the 2-3 separating collision. Therefore,  $\tau_1$  is the *smaller* root of the quadratic

$$|\vec{r} + \vec{W}_{31}\tau_1|^2 = 1 \tag{5-21a}$$

while  $\tau_2$  is the *positive* root of the quadratic

$$|(\vec{r} + \hat{k}) + (\vec{W}_{31} - \vec{W}_{21})\tau_2|^2 = 1 \tag{5-21b}$$

The collision vector  $\hat{k}'$  can then be obtained from  $\tau_1$  according to [cf. (4-21b)]

$$\hat{k}' = -\vec{r} - \vec{W}_{31}\tau_1 \quad (5-21c)$$

We shall defer giving the explicit expressions for  $\tau_1, \tau_2$  and  $\hat{k}'$  until we have reduced (5-18) to a definite integral.

In transforming (5-18) into an iterated integral with specific integration limits, we find it convenient to define three coordinate systems, I, II and III. All three coordinate systems are rest frames of  $l$ , but they are oriented differently:

Frame I:  $\vec{W}_1=0$ ; Z-axis points along  $\vec{W}_{21}$ , and X-axis is in the plane of  $\vec{W}_{21}$  and  $\hat{k}$  such that  $\hat{k}$  has a negative x-component.

Frame II:  $\vec{W}_1=0$ ; obtained by rotating Frame I about its Y-axis so that the Z-axis points along  $-\hat{k}$ .

Frame III:  $\vec{W}_1=0$ ; obtained by first rotating Frame II about its Z-axis until  $\vec{r}$  lies in the positive X half of the XZ-plane, and then rotating about the Y-axis until the Z-axis points along  $-\vec{r}$ .

The salient features of these frames are that they are all rest frames of  $l$  (in the  $\beta$ -region), and their Z-axes satisfy

$$\hat{z}_I \propto \vec{W}_{21} \quad (5-22a)$$

$$\hat{z}_{II} \propto -\hat{k} \quad (5-22b)$$

$$\hat{z}_{III} \propto -\vec{r} \quad (5-22c)$$

We now consider the integrating variables in (5-18) in the order  $\vec{W}_0, \vec{W}_{21}, \hat{k}, \vec{r}, \vec{W}_{31}$ .

•  $\vec{W}_0$ : This variable is proportional to the total center-of-mass velocity, and Fig. 24 imposes no restrictions on this quantity. Therefore,  $\vec{W}_0$  is to be integrated over all possible values:

$$\iiint_{\infty} d^3\vec{W}_0 \quad (5-22)$$

When  $\phi$  and  $\psi$  are Sonine polynomials, it turns out to be possible to factor out the  $\vec{W}_0$ -dependence from the integrand in (5-18) in a term-by-term manner, and to then perform the  $\vec{W}_0$ -integration analytically.

•  $\vec{W}_{21}$ : We specify this variable relative to Frame I. Since, by (5-22a), Frame I has its Z-axis along  $\vec{W}_{21}$ , then the angular integrations on  $\vec{W}_{21}$  are taken account of by a factor of  $4\pi$ . Consequently, the  $\vec{W}_{21}$ -integration has the form

$$4\pi \int_0^{\infty} W_{21}^2 dW_{21} \quad (5-23)$$

•  $\hat{k}$ : We specify this variable with respect to Frame I also. However, Frame I is defined so that its XZ-plane contains  $\hat{k}$ ; thus, the azimuthal integration on  $\hat{k}$  is taken account of by a factor of  $2\pi$ . We let  $\theta$  denote the polar angle of  $\hat{k}$  in Frame I, as shown in Fig. 25. The dynamics of the collision sequence in Fig. 24 requires that 1 and 2 be diverging just after their collision, so  $\hat{k}$  must be such that  $\vec{W}_{21} \cdot \hat{k} < 0$ . Therefore,  $\cos\theta$  is

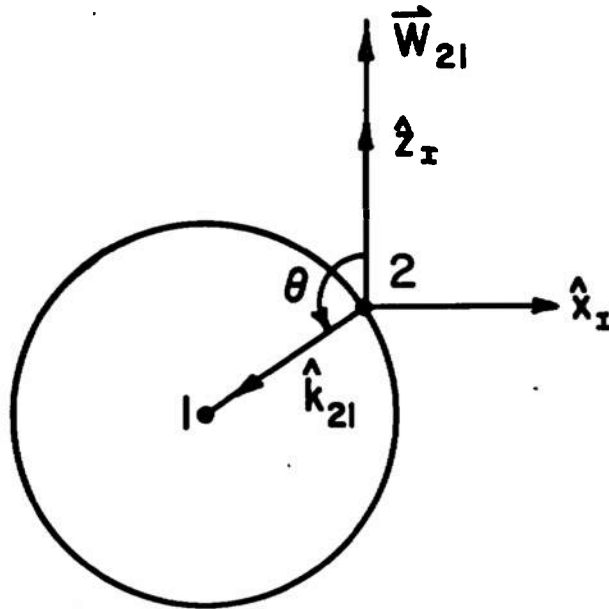


Figure 25. The variable  $\hat{k}_{21}$  in  $(\phi, \psi)^{(3)}$ .

restricted to the range  $(-1, 0)$ , and the  $\hat{k}$ -integration takes the form

$$2\pi \int_{-1}^0 d\cos\theta \quad (5-24)$$

• $\vec{r}$ : We specify this variable with respect to Frame II in polar coordinate form  $(r, \theta_r, \phi_r)$ . Since  $\vec{r}$  is restricted to lie in the shaded region of Fig. 24, we can deduce the limits on  $r, \theta_r$  and  $\phi_r$  from the diagram in Fig. 26:  $\phi_r$  can have any value between 0 and  $2\pi$ ,  $\cos\theta_r$  is restricted to values between  $1/2$  and 1, and  $r$  must lie between 1 and  $2\cos\theta_r$ . Thus, the

$\vec{r}$ -integration takes the form

$$\int_0^{2\pi} d\phi_r \int_{1/2}^1 d\cos\theta_r \int_1^{2\cos\theta_r} r^2 dr \quad (5-25)$$

•  $\vec{W}_{31}$ : We specify this last variable with respect to Frame III in polar coordinate form  $(W_{31}, \theta_w, \phi_w)$ . The dynamics of the collision sequence in Fig. 24 requires that 1 and 3 be aimed to collide in the future. The conditions which this requirement imposes on the  $\vec{W}_{31}$ -variables can be deduced from the diagram in Fig. 27: as long as  $\theta_w$  lies between 0 and a certain critical value  $\theta_0$ , then 1 and 3 will collide for any values of  $W_{31}$  and  $\phi_w$ . It is seen from Fig. 27, that  $\theta_0$  is such that  $\cos\theta_0 = \sqrt{r^2 - 1}/r = \sqrt{1 - r^{-2}}$ . Consequently, the  $\vec{W}_{31}$ -integration takes the form

$$\int_0^\infty W_{31}^2 dW_{31} \int_0^{2\pi} d\phi_w \int_{\sqrt{1-r^{-2}}}^1 d\cos\theta_w \quad (5-26)$$

Putting equations (5-22)-(5-26) into (5-18), and using the fact that

$$|\vec{W}_{21} \cdot \hat{k}| = -W_{21} \cos\theta$$

we thus obtain  $[\phi, \psi]_2^{(3)}$  as an *explicit eleven-fold iterated integral*:

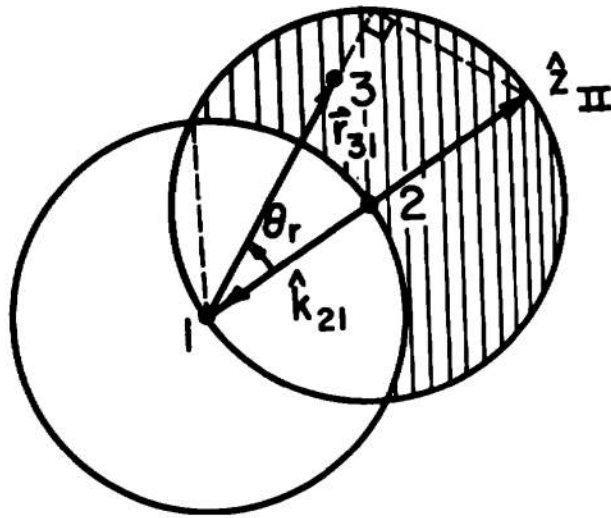


Figure 26. The variable  $\vec{r}_{31}$  in  $(\phi, \psi)^{(2)}$ .

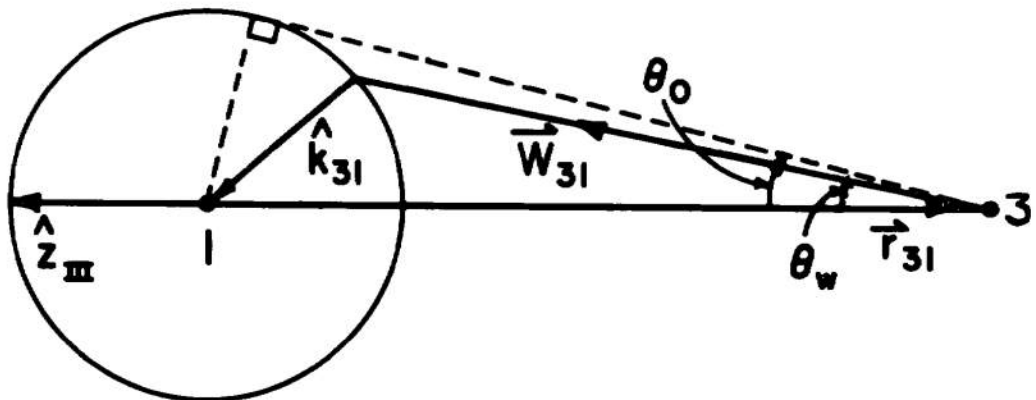


Figure 27. The variable  $\vec{W}_{31}$  in  $(\phi, \psi)^{(2)}$ .

$$\begin{aligned}
 [\phi, \psi]_2^{(3)} = & \frac{12\sqrt{2}}{5\pi^4} \iiint_{\infty} d^3\vec{W}_0 \int_0^{\infty} W_{21}^2 dW_{21} \int_{-1}^0 d\cos\theta \int_0^{2\pi} d\phi_r \int_{1/2}^1 d\cos\theta_r \\
 & \int_1^{2\cos\theta_r} r^2 dr \int_0^{2\pi} d\phi_w \int_0^{\infty} W_{31}^2 dW_{31} \int_{\sqrt{1-r^{-2}}}^1 d\cos\theta_w \\
 & (-W_{21}\cos\theta) \exp[-3W_0^2 - E] \\
 & \{ [\Phi(\alpha) - \Phi(\beta)] * [\Psi(\gamma) - \Psi(\beta)] \\
 & \quad + \theta [\Psi(\alpha) - \Psi(\beta)] * [\Phi(\gamma) - \Phi(\beta)] \}
 \end{aligned} \tag{5-27}$$

where

$$\Phi(\alpha) \equiv \sum_{i=1}^3 \phi(\vec{W}_i(\alpha)), \text{ etc.}; \quad \Psi(\alpha) \equiv \sum_{i=1}^3 \psi(\vec{W}_i(\alpha)), \text{ etc.} \tag{5-28}$$

$$\theta = \begin{cases} 1 & \text{if } \tau_1 > \tau_2 \\ 0 & \text{if } \tau_1 < \tau_2 \end{cases} \tag{5-29}$$

and where E and the  $\alpha$ - and  $\gamma$ -region velocities are given in (5-16b), (5-19) and (5-20). The evaluation of the integrand in (5-27) will evidently involve taking linear combinations and inner products of the vectors  $\vec{W}_{21}, \hat{k}, \vec{r}$  and  $\vec{W}_{31}$ ; consequently, it is necessary to find the Cartesian components of these vectors in some *common* coordinate system, expressing these coordinates in terms of the explicit integration variables in (5-27). It turns out to be simplest to use Frame III as this common coordinate system. The vector  $\vec{W}_{31}$  is already defined

relative to Frame III; however,  $\vec{w}_{21}$  and  $\hat{k}$  are defined relative to Frame I, while  $\vec{r}$  is defined relative to Frame II. We must therefore analyze the relationships between Frames I, II and III, construct the appropriate rotation matrices, and thereby bring the vectors  $\vec{w}_{21}$ ,  $\hat{k}$  and  $\vec{r}$  into Frame III. Having done this, we may then carry out the calculations indicated in equations (5-21) to obtain explicit expressions for  $\tau_1, \tau_2$  and  $\hat{k}'$  in terms of the integrating variables. Upon performing all these calculations, we find the formulae shown in Table III. By means of these formulae, along with equations (5-16b), (5-19), (5-20), (5-28) and (5-29), the integral in (5-27) can be evaluated for any given functions  $\phi$  and  $\psi$ . It is to be emphasized that this integral is now "mathematically self-contained", in that all the physical conditions imposed by the collision sequence diagram in Fig. 24 have now been incorporated into the integration limits and the formulae just mentioned.

We have now only to evaluate the integral (5-27) for those specific combinations of  $\phi$  and  $\psi$  functions that are required in (5-10) and (5-11) [cf. Table II]. Then, using the  $a_k(N)$  and  $b_k(N)$  values given in Table I, we immediately obtain the "single-overlap corrections" to the Enskog results--i.e., the  $i=2$  terms in (5-8) and (5-9). The evaluation of the required  $[\phi, \psi]_2^{(3)}$  integrals is an extremely lengthy calculation, and it does not seem feasible to reproduce it here. Consequently, we shall simply state in words what was done, remarking occasionally on certain interesting aspects of the calculations.

TABLE III

Dynamical quantities for the single-overlap collision sequence, expressed in terms of the integration variables in equation (5-27). [Note: Vector components are relative to Frame III.]

$$\vec{W}_{21} = W_{21} \begin{bmatrix} \sin\theta \cos\theta_r \cos\phi_r - \cos\theta \sin\theta_r \\ \sin\theta \sin\phi_r \\ \sin\theta \sin\theta_r \cos\phi_r + \cos\theta \cos\theta_r \end{bmatrix}$$

$$\vec{W}_{31} = W_{31} \begin{bmatrix} \sin\theta_w \cos\phi_w \\ \sin\theta_w \sin\phi_w \\ \cos\theta_w \end{bmatrix}$$

$$\hat{k} = \begin{bmatrix} -\sin\theta_r \\ 0 \\ \cos\theta_r \end{bmatrix} \quad \vec{r} = r \begin{bmatrix} 0 \\ 0 \\ -1 \end{bmatrix}$$

$$\hat{k}' = \begin{bmatrix} r(\epsilon-1) \cos\theta_w \sin\theta_w \cos\phi_w \\ r(\epsilon-1) \cos\theta_w \sin\theta_w \sin\phi_w \\ r(\epsilon-1) \cos^2\theta_w + r \end{bmatrix} \quad \text{where } \epsilon \equiv \sqrt{1 - \frac{1-r^{-2}}{\cos^2\theta_w}}$$

$$\tau_1 = \frac{1}{W_{31}} r(1-\epsilon) \cos\theta_w$$

$$\tau_2 = \frac{-\vec{r}_{32} \cdot \vec{W}_{32} + \sqrt{(\vec{r}_{32} \cdot \vec{W}_{32})^2 + W_{32}^2 (1-r_{32}^2)}}{W_{32}^2} \quad \text{where } \begin{cases} \vec{r}_{32} = \vec{r} + \hat{k} \\ \vec{W}_{32} = \vec{W}_{31} - \vec{W}_{21} \end{cases}$$

For those  $\phi$  and  $\psi$  functions required in (5-10) and (5-11), we first compute the corresponding  $\Phi$  and  $\Psi$  functions; we find it convenient to express these in terms of  $\vec{W}_0$  and the auxiliary variables  $\vec{W}_{10}, \vec{W}_{20}, \vec{W}_{30}$  [cf. (5-15)]. Next, the differences in  $\Phi$  and  $\Psi$  between the  $\alpha$  and  $\beta$  regions and between the  $\gamma$  and  $\beta$  regions are calculated as required in (5-27); the calculations of these differences is simplified somewhat by the fact that  $\vec{W}_0$  and the quantity  $E$  [cf. (5-16b)] are the same in all regions. We next take the scalar products of these differences in  $\Phi$  and  $\Psi$ , as indicated in (5-27); each scalar product is in the form of a sum of terms (from a few to very many depending on the particular  $\phi$  and  $\psi$  functions considered). Using various vector and tensor identities [cf. Chapter 1 of ref. 4], it is possible to reduce the  $\vec{W}_0$ -dependence in each term to a factor of  $|\vec{W}_0|^n$ , with the value of  $n$  usually being different for different terms. We can then carry out the  $\vec{W}_0$ -integration,

$$\iiint_{\infty} W_0^n \exp[-3W_0^2] d^3\vec{W}_0 \quad (5-30)$$

analytically on a term-by-term basis. This actually reduces the number of terms in the integrands considerably; for, only terms having an even power of  $W_0$  will survive, and of the surviving terms, several will differ only by numerical factors and can therefore be combined. After the  $\vec{W}_0$ -integration has been performed, the various  $[\phi, \psi]^{(3)}$  quantities are given as *eight-fold* iterated integrals.

The fact that  $\vec{W}_0$  could be integrated out with relative ease is a reflection of the fact that the dynamics of the collision sequence is independent of the velocity of the center-of-mass of the three molecules. Another variable which does not affect the collision dynamics for hard sphere molecules is the scale with respect to which all the velocities are measured (this is because the angle of deflection for two colliding hard sphere molecules is independent of their velocities). Suppose, in fact, we measure the two velocity variables  $\vec{W}_{21}$  and  $\vec{W}_{31}$  in (5-27) in units of  $W_{21}$ :

$$\left. \begin{aligned} \vec{W}_{21} &= W_{21} \hat{z} \\ \vec{W}_{31} &= W_{21} \vec{w} \end{aligned} \right\} \quad (5-31)$$

Essentially, this amounts to a change of variables of the form

$$(W_{21}, W_{31}) \rightarrow (W_{21}, w=W_{31}/W_{21}) \quad (5-32a)$$

with

$$dW_{21}dW_{31} = W_{21}dW_{31}dw \quad (5-32b)$$

The essential independence of the integrand with respect to the velocity scale manifests itself in the following fact: If relations (5-31) are introduced into the various integrands, then every term in these integrands is found to be homogenous in  $W_{21}$ ; that is, if  $F(\vec{W}_{21}, \vec{W}_{31})$  is a typical integrand term, then we discover that

$$F(\vec{W}_{21}, \vec{W}_{31}) = F(W_{21}\hat{z}, W_{21}\vec{w}) = W_{21}^n F(\hat{z}, \vec{w}) \quad (5-33)$$

with the value of  $n$  usually being different for different terms. In particular, we note that  $\hat{k}$  and  $\theta$  are homogeneous of degree zero, while  $E$  is homogeneous of degree two:

$$E = W_{21}^2 \left[ \frac{2}{3} (1 + w^2 - \hat{z} \cdot \vec{w}) \right] \equiv W_{21}^2 E^* \quad (5-34)$$

Therefore, if  $F(\vec{W}_{21}, \vec{W}_{31})$  in (5-33) is a typical term inside the braces of (5-27) (where we now assume  $\vec{W}_0$  has already been integrated out), then we can perform the  $W_{21}$ -integration,

$$\int_0^\infty (W_{21})^{2+3+1+n} \exp[-E^* W_{21}^2] F(\hat{z}, \vec{w}) dW_{21} \quad (5-35)$$

analytically on a term-by-term basis. We note that this integration removes the factor  $\exp[-E]$  and replaces it by the reciprocal of  $E^*$  raised to some half-odd-integer power.

Thus, by means of the  $\vec{W}_0$ -integration and the  $W_{21}$ -integration, we reduce (5-27) to the form of a *seven-fold iterated integral* with well-defined integration limits. However, the integrands are now very complicated functions of the integrating variables. Therefore, we proceed from this point using Monte Carlo techniques.

A fairly comprehensive review of general Monte Carlo methods has been given by Hammersley and Handscomb [24]. We shall outline briefly some of the essential points of the Monte Carlo approach which are pertinent to our work here.

Suppose it is desired to evaluate the integral of some function  $f(\vec{x})$ , where  $\vec{x}$  denotes an  $n$ -component variable, over some finite region  $\Omega$  in the space defined by the components of  $\vec{x}$ :

$$I = \int_{\Omega} f(\vec{x}) d\vec{x} \quad (5-36)$$

Letting  $|\Omega|$  denote the volume  $\Omega$ , we write this as

$$I = |\Omega| \int_{\Omega} f(\vec{x}) \left( \frac{1}{|\Omega|} \right) d\vec{x} \equiv |\Omega| \cdot \bar{f} \quad (5-37)$$

where  $\bar{f}$  is defined through the identity sign. If we now consider a distribution in the space of  $\vec{x}$  which is described by the *probability density function*

$$P(\vec{x}) = \begin{cases} 1/|\Omega|, & \text{for } \vec{x} \in \Omega \\ 0, & \text{for } \vec{x} \notin \Omega \end{cases} \quad (5-38)$$

then the quantity  $\bar{f}$  may be interpreted as the "mean value" of  $f$ , taken with respect to this distribution. [We note passing that the function  $P(\vec{x})$  defined in (5-38) is indeed a legitimate probability density function, since it satisfies the two requirements  $P(\vec{x}) \geq 0$  and  $\int P(\vec{x}) d\vec{x} = 1$ .] Now, if we had a set of points  $\{\vec{x}_1, \vec{x}_2, \dots, \vec{x}_N\}$  which were randomly distributed according to the density function in (5-38)--i.e., if we had a set of  $N$  points which were distributed *randomly and uniformly over*  $\Omega$ --then we could *estimate*  $\bar{f}$  by an ordinary averaging procedure:

$$\bar{f} \approx \frac{1}{N} \sum_{i=1}^N f(\vec{x}_i) \quad (5-39)$$

The *uncertainty* in so estimating  $\bar{f}$  would be given approximately by the root-mean-square deviation of the  $f(\vec{x}_i)$ -values, divided by the square root of the number of random points used.

The Monte Carlo method for evaluating the integral  $I$  in (5-36) therefore requires that one be able to:

- 1° Calculate, in some way, the volume  $|\Omega|$  of the integrating region  $\Omega$ ;
- 2° Devise a method for generating points  $\vec{x}_1, \vec{x}_2, \dots$  randomly and uniformly inside  $\Omega$ .

Then, normally using a high-speed digital computer, one *generates* the points  $\vec{x}_1, \vec{x}_2, \dots, \vec{x}_N$  in turn, *calculates* for these points the averages

$$\langle f \rangle \equiv \frac{1}{N} \sum_{i=1}^N f(\vec{x}_i), \quad \langle f^2 \rangle \equiv \frac{1}{N} \sum_{i=1}^N [f(\vec{x}_i)]^2 \quad (5-40)$$

and finally puts

$$I \approx |\Omega| \left[ \langle f \rangle \pm \frac{\sqrt{\langle f^2 \rangle - \langle f \rangle^2}}{\sqrt{N}} \right] \quad (5-41)$$

It is desired, of course, to make the "error" term in (5-41) as small as possible. Since the rms deviations of  $f$  is essentially fixed by the specifics of the problem, we must therefore take  $N$  as large as possible. The *maximum* value of  $N$  is essentially equal to the amount of computer time available,

divided by the amount of time the computer requires to generate one random point  $\vec{x}_i$  and calculate the corresponding value  $f(\vec{x}_i)$ . If, as frequently happens, the maximum value of  $N$  is not large enough to give a sufficiently accurate estimate of  $I$ , then one has two alternatives: either one must devise a more efficient means of generating the random points  $\{\vec{x}_i\}$ ; or, one must try to make a change of variables in (5-36),

$$\int_{\Omega} f(\vec{x}) d\vec{x} = \int_{\Omega'} f(\vec{x}) \left| \frac{\partial \vec{x}}{\partial \vec{x}'} \right| d\vec{x}' \equiv \int_{\Omega'} f'(\vec{x}') d\vec{x}' \quad (5-42)$$

in the hope that the new integrand  $f'$  will have a smaller rms deviation over the new region  $\Omega'$  than  $f$  had over  $\Omega$ .

There are many so-called "pseudo-random number" subroutines available by means of which a computer will generate on call a random value from a uniform distribution in the unit interval. In our work we use a subroutine written by Marsaglia and Bray [25]. We shall denote by  $\epsilon$  a random number from a uniform distribution in the unit interval, with the understanding that a *new* random number is implied each time  $\epsilon$  appears. We can generate a random value  $x$  from a uniform distribution in the interval  $[a,b]$  by means of the formula

$$x = a + (b-a)\epsilon \quad (5-43)$$

Thus, if the  $n$ -dimensional volume  $\Omega$  is a "box", with the  $i^{\text{th}}$  component of  $\vec{x}$  satisfying  $a_i < x^{(i)} < b_i$ , then we can generate a random point  $\vec{x}$  from a uniform distribution inside  $\Omega$  by putting

$$x^{(i)} = a_i + (b_i - a_i)r_i, \quad i=1, \dots, n \quad (5-44)$$

If  $\Omega$  is not a "box", then one has two options. On the one hand, one can surround  $\Omega$  by a "box"  $\Sigma$ , generate random points inside  $\Sigma$  in the manner of (5-44), and then keep only those points which happen to fall inside  $\Omega$ . On the other hand, one can construct a transformation of variables,  $\vec{x} \rightarrow \vec{x}'$  which is such that the transformed volume  $\Omega'$  is a "box". In the first method it is clear that only the fraction  $|\Omega|/|\Sigma|$  of the points initially generated in  $\Sigma$  will also lie in  $\Omega$ ; thus, if the shape of  $\Omega$  is such that it can only be enclosed in a "box"  $\Sigma$  with  $|\Sigma| \gg |\Omega|$ , then the first method is very inefficient. [We note in passing that one could extend the definition of  $f$  so that it is zero outside  $\Omega$ , thus making  $f$  defined everywhere inside  $\Sigma$ ; however, this approach can be shown to be completely equivalent to our first method, and thus cannot improve the situation any.] If a fairly simple transformation of variables can be found which transforms  $\Omega$  into a "box", then that is normally the method to use. It is always possible to write down transformations which carry  $\Omega$  into a "box" if the given integral can itself be written as an  $n$ -fold iterated integral with explicit integration limits; however, whether a sufficiently "simple" transformation can be written down is another question.

To these very general remarks about the Monte Carlo method for evaluating integrals, we should add one final comment. The uncertainty in the Monte Carlo estimate of an integral [cf. (5-41)] is inversely proportional to the square root of the number of points for which the integrand is evaluated, *regardless of the dimensionality of the integral*. This is in contrast to the situation with standard "classical" numerical methods (i.e., the trapezoid method, Simson's method, Gauss' method), where the number of points required for a given level of accuracy increases very rapidly with the dimensionality of the integral. It turns out that non-Monte Carlo methods are superior in four or less dimensions, while the Monte Carlo method is superior in five or more dimensions; indeed, for seven dimensional integrals, which are the kind we are faced with here, the Monte Carlo method is the only feasible one.

Returning now to the problem at hand, we have to evaluate integrals of the type (5-27), except that the  $\vec{W}_0$  and  $W_{2,1}$  integrations [the first four integrations in (5-27)] have already been performed analytically, and the  $W_{3,1}$ -integration has been replaced by an integration over the variable  $w$  [cf. (5-31) and (5-32)]. The quantities in braces in (5-27) now have a fairly complicated structure, as a result of having been expressed in terms of quantities more closely related to the integrating variables. However it found that, regardless of which Sonine polynomials are considered for  $\phi$  and  $\psi$ , the quantity in braces always contains the factor  $(\hat{z} \cdot \hat{k})(\vec{w} \cdot \hat{k}')$ .

The reason for this is that the factors  $[\phi(\alpha) - \phi(\beta)]$  and  $[\Psi(\alpha) - \Psi(\beta)]$  in (5-27) are always proportional to  $\vec{W}_{21} \cdot \hat{k}_{21}$  (which becomes  $\hat{z} \cdot \hat{k}$  after the  $W_{21}$ -integration), while the factors  $[\phi(\gamma) - \phi(\beta)]$  and  $[\Psi(\gamma) - \Psi(\beta)]$  in (5-27) are always proportional to  $\vec{W}_{31} \cdot \hat{k}'$  (which becomes  $\vec{w} \cdot \hat{k}'$  after the  $W_{21}$ -integration). Using the formula in Table III, it is easy to show that

$$\begin{aligned}\vec{W}_{21} \cdot \hat{k} &= W_{21} \cos \theta \\ \vec{W}_{31} \cdot \hat{k}' &= W_{31} r \epsilon \cos \theta_w\end{aligned}$$

so that the quantity in braces in (5-27) always contains the overall factor

$$(\hat{z} \cdot \hat{k})(\vec{w} \cdot \hat{k}') = w r \epsilon \cos \theta \cos \theta_w \quad (5-45)$$

If we extract the above factor from the quantity in braces in (5-27), then we obtain for  $[\phi, \psi]_2^{(3)}$  an expression of the general form

$$\begin{aligned}[\phi, \psi]_2^{(3)} &= \int_{-1}^0 d\cos \theta \int_0^{2\pi} d\phi_r \int_{1/2}^1 d\cos \theta_r \int_1^{2\cos \theta_r} \frac{r^2 dr}{r^2} \int_0^{2\pi} d\phi_w \\ &\int_0^\infty w^2 dw \int_{\sqrt{1-r^2}}^1 \frac{d\cos \theta_w}{\sqrt{1-r^2}} [(\cos \theta)(w r \epsilon \cos \theta \cos \theta_w)] \times F \quad (5-46a)\end{aligned}$$

where the extra factor of  $\cos \theta$  comes from the middle line in (5-27), and where the quantity  $F$  is some complicated function of *all* the integrating variables that accounts for "the rest"

of the integrand. Using simple differential formulae, it is easy to transform (5-46a) into

$$[\phi, \psi]_2^{(3)} = \frac{1}{24} \int_{-1}^0 d(\cos^3 \theta) \int_0^{2\pi} d\phi_r \int_0^{2\pi} d\phi_w \int_0^\infty w^3 dw$$

$$\int_{1/2}^1 d\cos \theta_r \int_1^{16\cos^4 \theta_r} \frac{d(r^4)}{d(r^4)} \int_{1-r^{-2}}^1 d(\cos^2 \theta_w) \times F \quad (5-46b)$$

Now, an integral of this type is not yet susceptible to Monte Carlo integration, because one of the variables, namely  $w$ , has an infinite range. It is therefore necessary to transform from  $w$  to some new variable  $u$ , such that: (i) the infinite range  $0 < w < \infty$  is transformed into a finite range  $a < u < b$ , and (ii) the quantity  $w^3 F |\partial u / \partial w|$  is a bounded function of  $u$  in the interval  $[a, b]$ . The particular transformation we have used is

$$u = \frac{1}{1 + w^4} \quad (5-47)$$

This transformation evidently maps the interval  $0 < w < \infty$  onto the interval  $0 < u < 1$ . The exponent of 4 was chosen after a careful study of the behavior of  $w^3 F |\partial u / \partial w|$  in the limits  $w \rightarrow 0$  and  $w \rightarrow \infty$ : it was determined that 4 was the largest exponent for which this quantity remained finite in these limits for all the required combinations of  $\phi$  and  $\psi$  functions. Consequently, all the inner product integrals which are to be calculated have the general form

$$[\phi, \psi]_2^{(3)} = \int_{-1}^0 d(\cos^3 \theta) \int_0^{2\pi} d\phi_r \int_0^{2\pi} d\phi_w \int_0^1 du$$

$$\int_{1/2}^1 d\cos \theta_r \int_1^{16\cos^4 \theta_r} d(r^4) \int_{1-r^2}^1 d(\cos^2 \theta_w) \times G \quad (5-48)$$

where  $G$  is a complicated but *bounded* function of all the integrating variables, the exact form of  $G$  depending on which Sonine polynomials are being considered. It is integrals of the form (5-48) which we must evaluate by a Monte Carlo procedure.

The integration volume  $\Omega$  for (5-48) consists of all points  $(\cos^3 \theta, \phi_r, \phi_w, u, \cos \theta_r, r^4, \cos^2 \theta_w)$  whose components lie between the corresponding integration limits in (5-48). If all these integration limits were constants, then  $\Omega$  would be a "box", and we could use the method described in (5-44) to generate points randomly and uniformly inside  $\Omega$ . However, we note that the limits on  $\cos^2 \theta_w$  depend on  $r^4$ , and the limits on  $r^4$  depend on  $\cos \theta_r$ . Thus, we shall have to devise a more sophisticated method for generating random points uniformly inside  $\Omega$ . The volume of  $\Omega$  is calculated by evaluating (5-48) with  $G=1$ , and is easily found to be

$$|\Omega| = \frac{16\pi^2}{3} \quad (5-49)$$

One way of proceeding here would be to enclose  $\Omega$  in a larger "box"  $\Sigma$ , generate random points inside  $\Sigma$  according to

the method (5-44), and then keep only those points which also fall inside  $\Omega$ . We find, though, that the smallest box enclosing  $\Omega$  has a volume about 5.6 times larger than  $\Omega$ , so our generating efficiency would be only about 18%. We have therefore chosen to adopt a different approach: Essentially, what we do is to express the composite n-variable probability density function  $P(\bar{X})$  in (5-38) as a product of n "conditional one-variable density functions". This allows us to generate points in such a way that the non-rectangular shape of  $\Omega$  is *automatically* accounted for, so that *every* point so generated is a "legitimate" point. (We remark that the problem is not so much to generate random points which simply lie inside  $\Omega$ , but rather to do it in such a way that the points cover  $\Omega$  *uniformly* to within normal statistical variations). For a discussion of the conditioning technique, we refer to Ref. 26 [esp. pp. 187-190]. When this technique is applied to our problem here, it yields the following set of formulae for generating points randomly and uniformly inside the integrating region  $\Omega$  of (5-48) :

$$\cos^3 \theta = -1 + \kappa_1 \quad (5-50a)$$

$$\phi_r = 2\pi\kappa_2 \quad (5-50b)$$

$$\phi_w = 2\pi\kappa_3 \quad (5-50c)$$

$$u = \kappa_4 \quad w \equiv [(1-u)/u]^{1/4} \quad (5-50d)$$

$$2\kappa_5 = 4\cos^3 \theta_r - 3\cos \theta_r + 1 \quad (5-50e)$$

$$r^4 = [1 + (4\cos^2 \theta_r - 1)\kappa_6]^2 \quad (5-50f)$$

$$\cos^2 \theta_w = (1-r^{-2}) + r^{-2}\kappa_7 \quad (5-50g)$$

In these formulae, the quantities  $\kappa_i$  represent random numbers drawn from a uniform distribution in the unit interval. We note that the first four formulae, (5-50a)-(5-50d), are precisely what we would expect on the basis of (5-48) and (5-44). The formulae for the last three variables are, however, different; this is because the limits for these variables are interrelated [cf.(5-48)]. These last three variables must be generated in the order given: Thus, we *first* draw a random number  $\kappa_5$  and compute  $\cos\theta_r$  from (5-50e); we note that (5-50e) must be inverted to calculate  $\cos\theta_r$ , but this can be easily done by the computer. With  $\cos\theta_r$  thus generated we *next* draw a random number  $\kappa_6$  and compute  $r^4$  according to (5-50f); we note that the value generated for  $r^4$  depends upon the value generated for  $\cos\theta_r$ . *Finally*, using the generated value of  $r^4$  along with a random number  $\kappa_7$ , we calculate a value for  $\cos^2\theta_w$  according to (5-50g).

It is, of course, *not* obvious that the generating formulae in (5-50) accomplish the desired goal of populating the seven-dimensional integrating region  $\Omega$  of (5-48) randomly and uniformly. To demonstrate the validity of these formulae and our use of them, let us regard them for the moment not as "generating formulae", but rather as equations specifying the *transformation of variables*

$$(\cos^3\theta, \phi_r, \phi_w, u, \cos\theta_r, r^4, \cos^2\theta_w) \rightarrow (\kappa_1, \dots, \kappa_7) \quad (5-51)$$

The reader can easily verify from (5-50) that this transformation maps  $\Omega$  onto the seven-dimensional unit cube ( $0 < \kappa_i < 1$ ,  $i=1, \dots, 7$ ), and, moreover, that the Jacobian of the transformation has the constant value  $|\Omega|$ :

$$\frac{\partial (\cos^3 \theta, \phi_r, \phi_w, u, \cos \theta_r, r^4, \cos^2 \theta_w)}{\partial (\kappa_1, \kappa_2, \kappa_3, \kappa_4, \kappa_5, \kappa_6, \kappa_7)} = \frac{16\pi^2}{3} = |\Omega| \quad (5-52)$$

Consequently, we can write (5-48) as

$$[\phi, \psi]_2^{(3)} = \int_0^1 d\kappa_1 \int_0^1 d\kappa_2 \cdots \int_0^1 d\kappa_7 \times |\Omega| G \quad (5-53)$$

where the dependence of  $G$  on the new integrating variables follows from its dependence on the old integrating variables via equations (5-50). Since the new integration region is the (seven-dimensional) unit cube, then the Monte Carlo estimate of the integral in (5-53) is

$$[\phi, \psi]_2^{(3)} = 1 \cdot \langle |\Omega| G \rangle \quad (5-54a)$$

where the average is taken with respect to a set of points  $(\kappa_1, \kappa_2, \dots, \kappa_7)$  generated randomly and uniformly inside the unit cube. Clearly this is equivalent to saying that

$$[\phi, \psi]_2^{(3)} = |\Omega| \cdot \langle G \rangle \quad (5-54b)$$

where the average is taken with respect to a set of points  $(\cos^3 \theta, \phi_r, \dots, \cos^2 \theta_w)$  generated according to (5-50). But (5-54b) also gives the Monte Carlo estimate of (5-48), provided

the indicated average is taken with respect to a set of points  $(\cos^3\theta, \phi_r, \dots, \cos^2\theta_w)$  generated *randomly and uniformly inside*  $\Omega$ . We conclude, then, that points generated according to (5-50) are indeed distributed randomly and uniformly over the integrating region of (5-48).

In summary, then, we can evaluate the integral (5-48) by generating  $N$  random "points" according to formulae (5-50), calculating the averages of  $G$  and  $G^2$  with respect to these points, and then putting

$$\boxed{[\phi, \psi]_2^{(3)} = \frac{16\pi^2}{3} \left[ \langle G \rangle \pm \frac{\sqrt{\langle G^2 \rangle - \langle G \rangle^2}}{\sqrt{N}} \right]} \quad (5-55)$$

Denoting, for the sake of brevity, the single-overlap triple collision inner products on the right hand sides of (5-10) and (5-11) by

$$a_{k\ell} \equiv \left[ s_{3/2}^{(k)}(w_1^2) \bar{w}_1, s_{3/2}^{(\ell)}(w_1^2) \bar{w}_1 \right]_2^{(3)} \quad (5-56a)$$

$$b_{k\ell} \equiv \left[ s_{5/2}^{(k)}(w_1^2) \bar{w}_1^0 \bar{w}_1, s_{5/2}^{(\ell)}(w_1^2) \bar{w}_1^0 \bar{w}_1 \right]_2^{(3)} \quad (5-56b)$$

and defining the "reduced" single-overlap parts of  $\lambda_1$  and  $\eta_1$  in the  $N^{\text{th}}$  Sonine approximation by

$$\lambda_{12}^*(N) \equiv \lambda_{12}(N) / |\lambda_{1E}(N)| \quad (5-57a)$$

$$\eta_{12}^*(N) \equiv \eta_{12}(N) / |\eta_{1E}(N)| \quad (5-57b)$$

we show the results of our Monte Carlo calculations in Column A of Table IV. These results were obtained by carrying out the computational procedure just described, using 50,000 random points; the calculations required approximately 9 minutes on a UNIVAC 1108 computer. Included in Table IV are the results of parallel calculations for the coefficient of self-diffusion,  $D$ . The values obtained for  $\lambda_{12}^*$  and  $\eta_{12}^*$  are calculated from (5-10) and (5-11), respectively, and represent "corrections" to the Enskog terms of -1 in equations (5-8) and (5-9). An equation analogous to (5-8) and (5-9) holds for the self-diffusion  $D$ , except that there is no additional "spatial inhomogeneity" term for  $D$  as there is for  $\lambda$  and  $\eta$ .

The  $\pm$  uncertainties quoted in column A of Table IV should be considered as "one standard deviation" uncertainties. An attempt was made to reduce these uncertainties *without* increasing the number of points used (and hence the amount of computer time used). To do this, we have resorted to a technique known as "importance sampling".

Importance sampling is roughly equivalent to making a change of integrating (or generating) variables which decreases the rms deviation of the integrand, thereby decreasing the uncertainty in the average value computed for this integrand. To illustrate the approach we have taken, consider again equation (5-53). Suppose we can find some function  $P(\nu_1)$  that satisfies

TABLE IV

Monte Carlo estimates of the single-overlap triple collision integrals, and the consequent fractional corrections to the Enskog values for  $\lambda_1, \eta_1$  and  $D_1$  in the first(1) and second(2) Sonine approximations.

Quantity	Column A (straight sampling)	Column B (importance sampling)
$a_{11}$	$-0.0311 \pm .0018$	$-0.0284 \pm .0008$
$a_{12}$	$0.0333 \pm .0007$	$0.0331 \pm .0004$
$a_{21}$	$0.0331 \pm .0007$	$0.0334 \pm .0004$
$a_{22}$	$0.0214 \pm .0034$	$0.0276 \pm .0014$
$b_{00}$	$-0.0628 \pm .0017$	$-0.0631 \pm .0008$
$b_{01}$	$0.0194 \pm .0008$	$0.0194 \pm .0004$
$b_{10}$	$0.0189 \pm .0007$	$0.0198 \pm .0004$
$b_{11}$	$-0.0709 \pm .0047$	$-0.0631 \pm .0018$
$c_{00}$	$-0.1186 \pm .0009$	$-0.1181 \pm .0008$
$c_{01}$	$0.0391 \pm .0009$	$0.0393 \pm .0006$
$c_{10}$	$0.0387 \pm .0009$	$0.0397 \pm .0005$
$c_{11}$	$0.0298 \pm .0025$	$0.0322 \pm .0015$
$\lambda_{12}^*(1)$	$0.0311 \pm .0018$	$0.0284 \pm .0008$
$\lambda_{12}^*(2)$	$0.0256 \pm .0018$	$0.0228 \pm .0008$
$\eta_{12}^*(1)$	$0.0628 \pm .0017$	$0.0631 \pm .0008$
$\eta_{12}^*(2)$	$0.0617 \pm .0017$	$0.0618 \pm .0008$
$D_{12}^*(1)$	$0.1186 \pm .0009$	$0.1181 \pm .0008$
$D_{12}^*(2)$	$0.1151 \pm .0009$	$0.1146 \pm .0008$

1°  $P(\kappa_1) > 0$  for  $0 \leq \kappa_1 \leq 1$ ,

$$2^\circ \int_0^1 P(\kappa_1) d\kappa_1 = 1$$

3°  $P(\kappa_1)$  "follows"  $G$  in  $0 \leq \kappa_1 \leq 1$  in the sense that  $P(\kappa_1)/G$  is more nearly a constant in this interval than  $G$  itself is, independently of the other variables  $\kappa_2, \dots, \kappa_7$ .

Items 1° and 2° tell us that  $P(\kappa_1)$  can be regarded as a probability density function for  $\kappa_1$  over the unit interval. If we now write (5-53) as

$$[\phi, \psi]_2^{(3)} = \int_0^1 P(\kappa_1) d\kappa_1 \int_0^1 d\kappa_2 \cdots \int_0^1 d\kappa_7 \times |\Omega| \left[ \frac{G}{P(\kappa_1)} \right] \quad (5-58)$$

then we see that this integral can also be evaluated in the following way: Generate the variables  $\kappa_2, \dots, \kappa_7$  uniformly inside the unit interval as before, but now generate  $\kappa_1$  according to the density function  $P(\kappa_1)$ . [Techniques for generating random numbers from a non-uniform distribution characterized by a non-constant probability density function are derived and discussed in detail in Ref. 26.] The above integral can now be calculated as the average value, with respect to the points so generated, of the new integrand,

$$|\Omega| \left[ \frac{G}{P(\kappa_1)} \right]$$

Since, by item 3°, this new integrand has a smaller variance than the old integrand,  $|\Omega|G$ , it follows that the numerator of the uncertainty term in (5-55) will be correspondingly reduced.

We can carry out the above procedure for each of the  $\kappa_i$ -variables in turn; however, we should *not* expect to be able to reduce the uncertainty to zero. This is because item 3° can usually not be strictly satisfied "independently of the other variables"; indeed, 3° could be *strictly* satisfied only if the  $\kappa_1$ -dependence in  $G$  could be exactly factored out.

By using a very empirical trial-and-error procedure, guided by a rough determination of the "average behavior" of a typical  $G$  as a function of each of the variables  $\kappa_i$  in (5-53), we settled on the following combination of density functions to use in our importance sampling procedure:

$$P(\kappa_1) \propto \exp[-3(1-\kappa_1)] \quad (5-59a)$$

$$P(\kappa_2) \propto 1 - 0.7\cos 2\pi\kappa_2 \quad (5-59b)$$

$$P(\kappa_3) \propto 1 + 0.7\cos 2\pi\kappa_3 \quad (5-59c)$$

$$P(\kappa_5) \propto \exp[-\kappa_5] \quad (5-59d)$$

The results are shown in column B of Table IV. On the average, the uncertainties in the thermal conductivity and the viscosity were reduced by a factor of 2, while the uncertainty in the self-diffusion was not much affected (but note that the self-diffusion uncertainties were comparatively small to begin

with). The computer run used to obtain the column B results took about nine and one-half minutes, as opposed to about nine minutes flat for the column A results. However, about *forty* minutes of computer time would have been required by the straight-sampling program to obtain results as accurate as those found in the importance-sampling run, since the number of points used must be increased by a factor of four in order to halve the uncertainty. Thus, our attempt at importance sampling may be regarded as fairly successful.

We take as our "best" results the column B figures for  $\lambda_{12}^*$ ,  $\eta_{12}^*$ , and  $D_{12}^*$ . It will be observed that the second Sonine approximation figures are smaller than the first Sonine approximation figures by 2% for the viscosity, 3% for the self-diffusion, and 20% for the thermal conductivity. The 20% difference for the thermal conductivity is both surprising and disappointing: *either* our calculations for the thermal conductivity are in error; *or* the Sonine approximation is not a rapidly convergent one, so far as the first density density correction to the thermal conductivity is concerned. Very careful checks of our derivations and computer coding have not turned up any errors, so we believe the second alternative is a very distinct possibility. However, until this question is definitely resolved, we have decided not to initiate a several-hour long computer run aimed at *further* reducing the quoted uncertainties.

We are presently preparing a Monte Carlo calculation based on the *eleven-dimensional* integral in (5-27), rather than the seven-dimensional integral of (5-48). If certain convergence problems can be worked out, we could thus bypass the lengthy calculations involved in proceeding analytically from (5-27) to (5-48). At present, we see this approach as the one most likely to resolve the difficulty with the thermal conductivity, as well as providing a fairly independent check of our other results. This approach might also enable us to investigate higher Sonine approximations, something which is quite out of the question using (5-48) because of the great algebraic complexity of the integrands for these higher Sonine terms.

CHAPTER VI  
DISCUSSION OF RESULTS

6.1 Summary of Accomplishments

In this report we have demonstrated that, up to terms linear in the density  $n$ , the thermal conductivity  $\lambda$ , the shear viscosity  $\eta$  and the coefficient of self diffusion  $D$  of a gas of hard sphere molecules can be represented by

$$\lambda = \lambda_0 \left\{ 1 + \frac{5}{12} \pi \sigma^3 n [1.92 + \lambda_{i1}^* + \lambda_{i2}^* + \lambda_{i3}^* + \lambda_{i4}^*] \right\} \quad (6-1)$$

$$\eta = \eta_0 \left\{ 1 + \frac{5}{12} \pi \sigma^3 n [1.28 + \eta_{i1}^* + \eta_{i2}^* + \eta_{i3}^* + \eta_{i4}^*] \right\} \quad (6-2)$$

$$D = D_0 \left\{ 1 + \frac{5}{12} \pi \sigma^3 n [D_{i1}^* + D_{i2}^* + D_{i3}^* + D_{i4}^*] \right\} \quad (6-3)$$

Here,  $\lambda_0$ ,  $\eta_0$  and  $D_0$  are the transport coefficients in the low pressure limit (derived from the linearized Boltzmann equation), and  $\sigma$  is the diameter of the hard sphere molecules. In these equations,  $\lambda_{ii}^*$ ,  $\eta_{ii}^*$  and  $D_{ii}^*$  represent reduced transport coefficients that account for correlations among the positions and the velocities of three molecules. They are given by expressions of the form

$$\lambda_{ii}^* = - \frac{1}{a_i(N)} \sum_{k=1}^N \sum_{\ell=1}^N a_k(N) a_\ell(N) [\phi_k, \phi_\ell]_i^{(3)} \quad (6-4)$$

$$\eta_{1i}^* = - \frac{1}{b_0(N)} \sum_{k=0}^{N-1} \sum_{\ell=0}^{N-1} b_k(N) b_\ell(N) [\psi_k, \psi_\ell]_i^{(3)} \quad (6-5)$$

where the coefficients  $a_k(N)$  and  $b_k(N)$  are given in Table I, and where the quantities  $[\phi_k, \phi_\ell]_i^{(3)}$  and  $[\psi_k, \psi_\ell]_i^{(3)}$  are "triple collision inner products" of various Sonine polynomials (or more simply, "triple collision integrals"). The coefficients  $D_{1i}^*$  are given by a similar expression. We have proved that the triple collision integrals are *symmetric* in the sense that

$$[\phi, \psi]_i^{(3)} = [\psi, \phi]_i^{(3)} \quad (6-6)$$

The expansions (6-1), (6-2) and (6-3) correspond to an expansion of the triple collision integrals,

$$[\phi, \psi]^{(3)} = [\phi, \psi]_1^{(3)} + [\phi, \psi]_2^{(3)} + [\phi, \psi]_3^{(3)} + [\phi, \psi]_4^{(3)} \quad (6-7)$$

in which we take into account, in turn, the effects of one, two, three and four successive binary collisions among three gas molecules. The major features of this expansion are summarized in Table V. It was proved that the expansion terminates after four collisions among three (hard sphere) gas molecules.

The leading terms,  $\lambda_{1i}^*$ ,  $\eta_{1i}^*$  and  $D_{1i}^*$ , are due to collision sequences in which the positions of the three molecules are highly correlated. Specifically, the phases are constrained by the "excluded volume" condition that two pairs of

TABLE V

Expansion of the triple collision integrals.

$$[\phi, \psi]^{(3)} = [\phi, \psi]_1^{(3)} + [\phi, \psi]_2^{(3)} + [\phi, \psi]_3^{(3)} + [\phi, \psi]_4^{(3)}$$



- increasing number of collisions.
- decreasing correlations in the position variables; i.e., "decreasing excluded volume effects".
- increasing correlations in the velocity variables; i.e., "increasing deviations from molecular chaos".
- increasing range of correlations.
- increasing difficulty of computation.
- decreasing magnitude.

TABLE VI

Numerical results for the single-overlap terms.

	First Sonine Approx.	Second Sonine Approx.
$\lambda_{12}^*$	0.0284 ± .0008	0.0228 ± .0008
$\eta_{12}^*$	0.0631 ± .0008	0.0618 ± .0008
$D_{12}^*$	0.1181 ± .0008	0.1146 ± .0008

molecules be overlapping while the third pair is colliding. Such "double-overlap" collision sequences involve the dynamics of only *one* binary collision. It was shown that these leading terms coincide with the predictions of the Enskog theory:

$$\lambda_{11}^* = \eta_{11}^* = D_{11}^* = -1 \quad (6-8)$$

The second terms,  $\lambda_{12}^*$ ,  $\eta_{12}^*$  and  $D_{12}^*$ , are due to collision sequences in which only one pair of molecules is overlapping while another pair is colliding. These "single-overlap" collision sequences involve the dynamics of *two* successive binary collisions, and thus give rise not only to an excluded volume effect, but also to a departure from strict molecular chaos. We have derived explicit integral expressions for these single-overlap terms, and we have evaluated these integrals numerically. The results are summarized in Table VI.

We see that these single-overlap terms change the Enskog estimates for the thermal conductivity and the viscosity by approximately 2% and 6%, respectively. The contribution to the coefficient of self diffusion is more significant and amounts to approximately 11%.

Our formulation of the triple collision contributions to the transport coefficients makes use of the solutions of the well-known linearized Boltzmann equation. These solutions are traditionally obtained by a procedure which *approximates* them as finite sums of Sonine polynomials [4,5]. These Sonine expansions

produce rapidly converging expressions for the *dilute limit* coefficients  $\lambda_0, \eta_0$  and  $D_0$ , in the sense that the values for these quantities calculated using the first *two* Sonine terms differ from the values calculated using the first Sonine term *alone* by only about 2%. We find [cf. Table VI] that the values for  $\eta_{12}^*$  and  $D_{12}^*$  are likewise fairly insensitive to the order of the Sonine approximation: the second Sonine approximation lowers  $\eta_{12}^*$  by about 2% and  $D_{12}^*$  by about 3%, from the corresponding values found in the first Sonine approximation. However, the second Sonine approximation value for  $\lambda_{12}^*$  is about 20% lower than the first Sonine approximation value. So far, we have been unable to locate any errors in our calculations. Thus, it seems that a rapid convergence of the Sonine expansion procedure can *not* be taken completely for granted, and further research on this point is required.

We conjecture that the *excluded volume* terms represent the *dominant* contributions to the density dependence of the transport coefficients. This conjecture is based on a comparison of our present results for the single-overlap and double-overlap terms with the previous results reported in I. Unfortunately, our previous results are not accurate enough to allow a definite conclusion to be drawn in this regard. We recall that in I we considered only the thermal conductivity and the viscosity, and these only in the first Sonine approximation; moreover, the formulation of the triple collision integrals in I permitted an accuracy of only about one-tenth that available

by our present method. Consequently, the validity of the last point mentioned in Table V must ultimately be established by an explicit calculation of the integrals  $[\phi, \psi]_3^{(3)}$  and  $[\phi, \psi]_4^{(3)}$ . To the extent that our conjecture is correct, though, the figures quoted in the second column of Table VI should represent the most accurate numerical refinement to date of the predictions of the Enskog theory.

We recall that the density dependence of the *thermodynamic* properties of a gas is completely determined by "excluded volume effects" representing correlations in the positions of the gas molecules, and is not affected at all by correlations in the velocities. Our present results indicate that, for the density dependence of the *transport* properties of a gas, velocity correlations do contribute somewhat, but it is again the excluded volume effects which play the dominant role.

## 6.2 Outlook

In the present report we have developed a physical expansion which accounts for the effects of sequences of binary collisions among three gas molecules upon the first density coefficients ( $\lambda_1$  and  $\tau_1$  in (1-2)) of the transport properties of a moderately dense gas. In this section we want to comment on how the insight gained in this research can be used to improve our capability of calculating transport coefficients.

We first note that the expansion procedure developed in this report can be extended to account for sequences of binary collisions among *more* than three molecules. Such sequences need to be considered in calculating the higher order density terms in the expansions (1-2). One would expect that the next terms in (1-2) would be proportional to  $\rho^2$ , with coefficients of proportionality being determined by four-particle collision integrals. However, as noted in I, the four-particle collision integrals turn out to be divergent; the reason is that the coefficients of  $\rho^2$  in (1-2) have the form

$$\lambda_2 + \lambda_2' \log \rho \quad \text{and} \quad \eta_2 + \eta_2' \log \rho$$

Nevertheless one could carry out a *partial* evaluation of the four-particle collision integrals with our procedure. Thus, a first approximation to  $\lambda_2$  and  $\eta_2$  would refer to a collision sequence involving four gas molecules in which one pair of molecules is colliding while all the other pairs are overlapping. This contribution is convergent and leads to terms proportional to  $\rho^2$  which are the same as those in the Enskog theory. Physically, we would again expect this to be the dominant effect. Thus, it might be advantageous to represent the transport coefficient as a sum of *two* series: one which is a power series in the density, and another which contains (among others) non-analytic terms such as  $\rho^2 \log \rho$ . The coefficients of the first series could then be evaluated in

successive approximations by our procedure: The first approximations would contain those n-particle collisions where one pair is colliding while all other pairs are overlapping; this would reproduce the coefficients in the power series predicted by the theory of Enskog. Molecular dynamics results confirm our suggestion that these coefficients provide a good first approximation [27]. A second approximation to the coefficients of the power series would be obtained by considering those n-particle collisions where one pair is colliding while all the other pairs *except one* are overlapping; for n=3 this would be our terms  $\lambda_{12}^*$  and  $\eta_{12}^*$  in (6-1), which were calculated in this report. Other terms could then be regrouped to give a *second* series with a non-analytic density dependence. However, the coefficient of the leading term,  $\rho^2 \log \rho$ , in this second series is determined by collision integrals that do not involve any pairs of molecules that overlap. Therefore, extrapolating by analogy our physical results for three-particle collisions, we would expect that the quantitative effects of this second series would be small. This conclusion is supported by an analysis of precise experimental viscosity data to be reported in a future technical report.

In the present report we have formulated the theory of predicting transport properties for a moderately dense gas of *hard spherical* molecules. However, the engineer requires methods for predicting transport properties of gases of molecules with a more realistic intermolecular interaction.

In conclusion, therefore, we indicate how the procedure developed in this report may be generalized to more realistic gases. We do *not* want to suggest that the problem of calculating transport properties of dense real gases is on the verge of being solved; indeed, calculating the effects of collisional transfer and of triple collisions involving bounded states poses a very difficult challenge for the future. Nevertheless, our analysis does suggest how to treat the effect of successive collisions among three gas molecules when the molecules interact via a potential with a hard core and a finite range.

For hard sphere molecules the leading term appeared to be obtained by a *partial* evaluation of the triple collision integrals, namely by restricting the integration region to the excluded volume configuration indicated in Fig. 2. These are precisely the same configurations as those which determine the third virial coefficient  $A_2$  in the virial expansion (1-1) of the *equilibrium* properties. For molecules with a finite interaction range, one could again consider a partial evaluation of the triple collision integrals by restricting the integration to those configurations that determine the corresponding third virial coefficient for the equilibrium virial series. Our results lead to the conjecture that such a partial evaluation may again be a very good approximation for predicting the transport properties. Thus, our analysis may open a way to extend the Enskog theory, which is so successful for hard sphere molecules, to molecules with a more realistic interaction potential.

## APPENDIX A

## THEOREMS ON THE DYNAMICS OF THREE HARD SPHERE MOLECULES

► *Lemma 1.* In the collision sequence defined by the diagram in Fig. 28, it is not possible for spheres 2 and 3 to collide or overlap in the time interval  $t_1 \leq t \leq t_5$ .

• *Proof.* If the three spheres have diameter  $\sigma$ , we must evidently prove that

$$r_{32}(t) > \sigma \quad \text{for} \quad t_1 \leq t \leq t_5 \quad (\text{A-1})$$

However, in view of the symmetry of the recollision sequence, it suffices to prove this inequality for  $t_3 \leq t \leq t_5$  only.

The theorem is most easily proved by examining the actual trajectories of the three particles in a particular reference frame. In this frame, the center of 1 is at rest at the

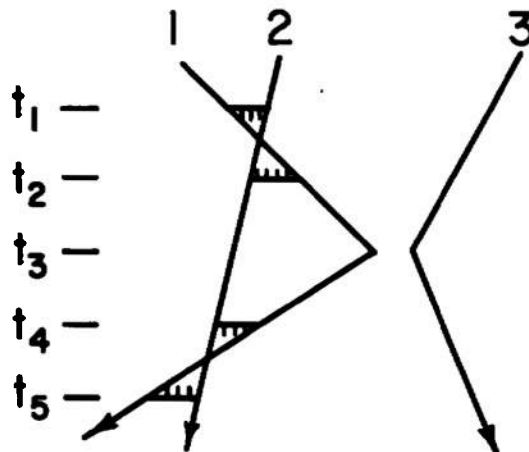


Figure 28. Diagram of Lemma 1.

origin 0 prior to the 1-3 collision ( $t < t_3$ ). The frame is oriented so that the center of 2 moves in the XZ plane in the positive Z direction. The situation is depicted in Fig. 29. Points A and B lie in the XZ plane, and denote the points where the center of 2 meets the action sphere of 1 at times  $t_1$  and  $t_2$  respectively. For times  $t > t_2$ , the center of 2 lies on the extension of vector  $\overline{AB}$ . Vector  $\overline{OB}$  has length  $\sigma$  and makes an angle  $\theta_1$  with the X axis, with

$$0 < \theta_1 < \frac{\pi}{2} \quad (\text{A-2})$$

We let C denote the point where the center of 3 strikes the action sphere of 1 at time  $t_3$ . In this interacting collision, 1 and 3 will exchange velocity components along  $\overline{OC}$ . As a consequence, 3 will be deflected so that, for  $t > t_3$ , its center moves in the plane perpendicular to  $\overline{OC}$  at C (plane P3), and 1 will be knocked so that for  $t > t_3$ , its center moves along the extension of vector  $\overline{CO}$ . We specify the location of point C on the surface of the action sphere of 1 by means of two angles,  $\theta_2$  and  $\phi$ :  $\phi$  is the angle that  $\overline{OC}$  makes with the XZ plane, and  $\theta_2$  is the angle that the positive Z axis makes with the plane containing  $\overline{OC}$  and the Y axis (plane P1). [Thus, in Fig. 29,  $\theta_2$  is measured in the XZ plane, even though  $\overline{OC}$  is not necessarily in this plane.]

We now examine the restrictions on the location of point C if it is required that there be a 1-2 collision at some time  $t_4 > t_3$ . Since, for  $t > t_3$ , the center of 2 is on line AB above B,

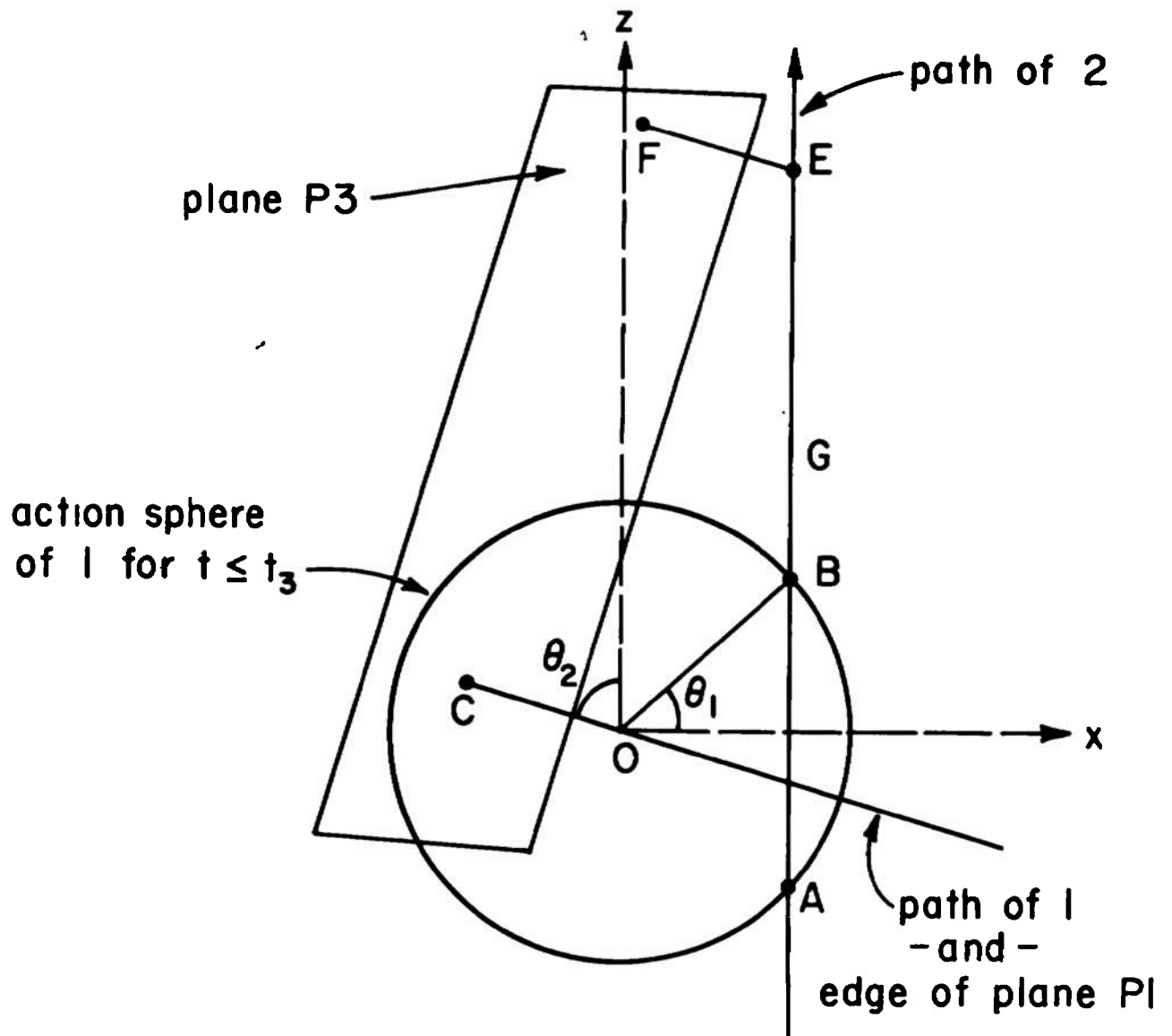


Figure 29. Diagram used in proof of Lemma 1.

then in order for 1 and 2 to collide, 3 must knock the action sphere of 1 across some portion of the line AB above B. This requires that in the  $t_3$  collision 1 be given a positive velocity component in the direction  $\vec{OB}$ . This in turn can happen only if  $\vec{CO} \cdot \vec{OB} > 0$ ; thus C *must lie in the hemisphere opposite B.*

If C lies in the hemisphere opposite B, then it follows that the distance from C to any point on the line AB above B is greater than  $\sigma$ . Thus,  $r_{32}(t_3) > \sigma$ . In order for  $r_{32}(t)$  to become equal to  $\sigma$  for some time  $t = t_6 > t_3$ , it is necessary for the plane of the path of 3 to intersect some portion of the line AB above B. For this to happen, C *must lie in the +Z hemisphere.*

If now we require *both* a 1-2 collision and a 3-2 collision for some times  $t_4 > t_3$  and  $t_6 > t_3$  respectively, then C must lie in the hemisphere opposite B *and* in the +Z hemisphere. This restricts C to the sector of the action sphere of 1 defined by

$$\theta_1 < \theta_2 < \frac{\pi}{2}$$

and

(A-3)

$$-\frac{\pi}{2} < \phi < \frac{\pi}{2}$$

Consider the distance between the path of 2 for  $t > t_3$  and the plane P3. Since these intersect, there are two points on the line AB above B whose distances to the plane

P3 are exactly  $\sigma$ . We denote as point E the position of 2 at the earlier time  $t_E$  when the distance  $|\overrightarrow{EF}| = \sigma$ . For all times  $t_3 \leq t < t_E$ ,  $r_{32}(t) > \sigma$ , so the time  $t_6$  of *first contact of pair 32* must be greater than or equal to  $t_E$ :

$$t_6 \geq t_E \quad (\text{A-4})$$

Next, consider the distance between the path of 2 for  $t > t_3$  and the plane P1. Since the distance from point B to this plane is  $\sigma \sin(\theta_1 + [\pi/2 - \theta_2]) < \sigma$ , then at some time  $t_G > t_2$  the center of 2 will be at a point G such that the distance from G to the plane P1 is exactly  $\sigma$ . The time  $t_5$  of the *last contact of pair 12* must clearly be less than or equal to  $t_G$ :

$$t_5 \leq t_G \quad (\text{A-5})$$

We now wish to compare the distance from G to the plane P1 with the distance from E to this same plane. The former is by definition  $\sigma$ . The latter is just the length  $|\overrightarrow{OE}|$ , inasmuch as  $\overrightarrow{OE}$  is seen to be perpendicular to  $\overrightarrow{CO}$  and hence perpendicular to the plane P1. Now from Fig. 29 it will be seen that  $\overrightarrow{OE}$  and  $\overrightarrow{OB}$  have equal projections on the X axis, so that

$$|\overrightarrow{OE}| \cos \theta_2 = |\overrightarrow{OB}| \cos \theta_1 = \sigma \cos \theta_1 \quad (\text{A-6})$$

By the first of equations (A-3) we deduce that  $\cos \theta_1 > \cos \theta_2$ , so that  $|\overrightarrow{OE}| > \sigma$ . Thus E is farther from the plane P1 than G is. Therefore,

$$t_E > t_G \quad (A-7)$$

Comparing (A-7) with (A-4) and (A-5), we conclude that

$$t_6 > t_5 \quad (A-8)$$

Thus 3 can collide with 2 *only after* 1 and 2 have separated at time  $t_5$ , which proves the lemma.

*Q.E.D.*

► **THEOREM I.** If a three-particle collision sequence contains at least one single-overlap collision, then it cannot contain more than three complete collisions.

• *Proof.* We shall first list all possible three-particle collision sequences which contain a single-overlap collision and a total of three complete collisions. Then we shall show that it is not possible to add a fourth complete collision to any of these sequences without violating Lemma 1 (or the Recollision Rule, as stated on p.39).

We suppose that at time  $t=0$  spheres 1 and 2 collide while spheres 1 and 3 overlap. This will constitute the "known" single-overlap collision; whether or not other overlap collisions occur for  $t>0$  or  $t<0$  is immaterial. Nevertheless, we must immediately allow for three cases, according to whether this single-overlap collision is (a) interacting, (b) penetrating, or (c) separating. [See top of Fig. 30]. Now, the very existence of this overlap collision already implies the existence of *two* complete

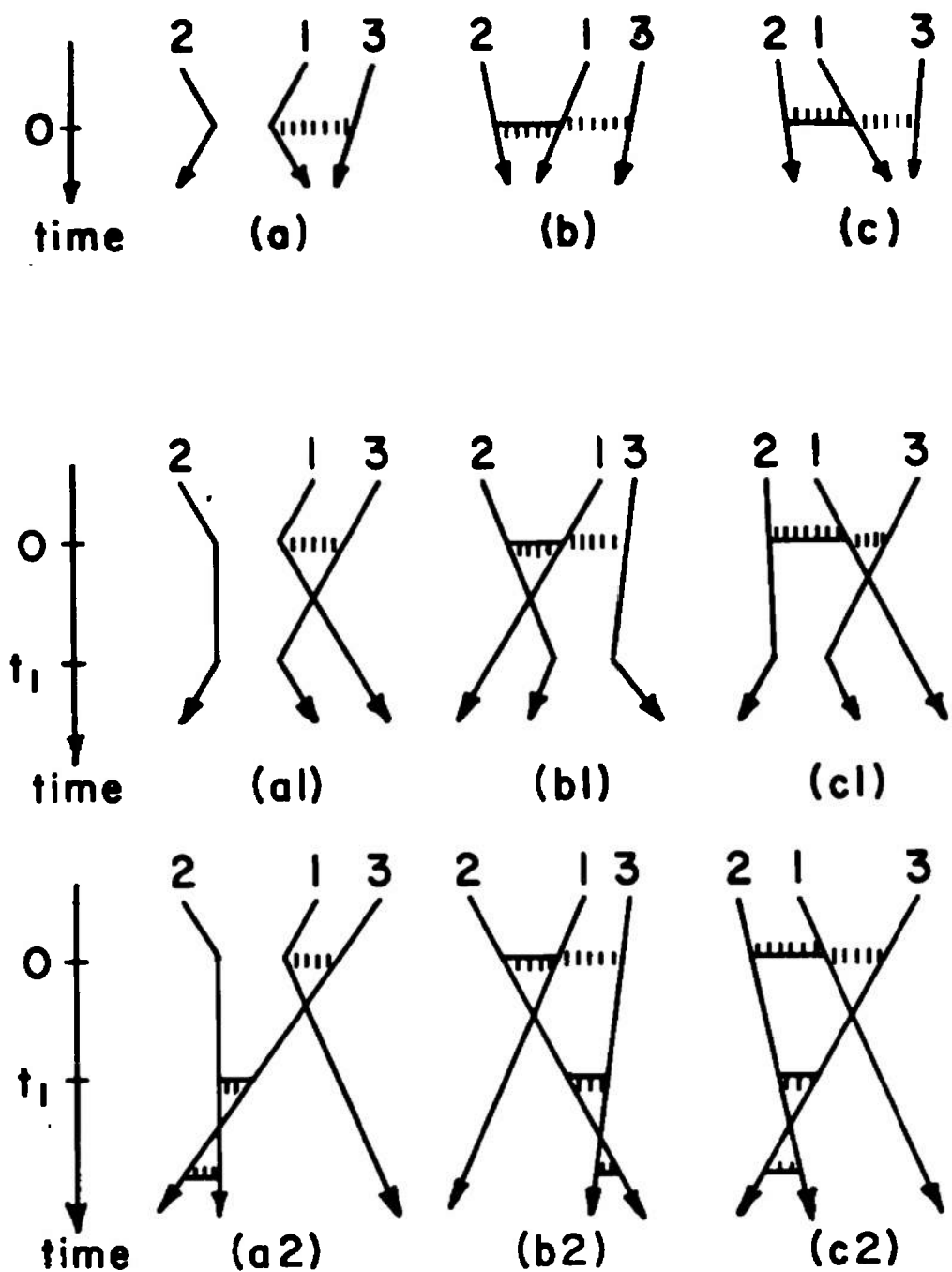


Figure 30. Diagram used in proof of Theorem I.

collisions -- namely, a 1-2 collision and a 1-3 collision. Therefore, we can obtain all possible sequences with three complete collisions by appending to (a), (b) and (c) in turn each possible third complete collision. This third collision may occur either in the past or in the future. However, we observe that any third collision in the past of (a) can be made a third collision in the future of (a) simply by reversing the sense of time; moreover, by this same device we can make any third collision in the past of (b) a third collision in the future of (c), and any third collision in the past of (c) a third collision in the future of (b). Therefore, it suffices to consider only the possible *future* third complete collisions for each of the cases (a), (b) and (c). An inspection of diagrams (a), (b) and (c) in Fig. 30 reveals that the next future complete collision cannot occur between 1 and 2 or between 1 and 3 since these pairs have already collided. [Note: 1 and 3 will of course undergo a separating collision in the future, but this is not *another complete* collision; likewise for 1 and 2 in case (b).] Consequently, the only candidate for the future third collision in each case is the pair 2 and 3.

If 2 and 3 are overlapping at  $t=0$ , in which case the 1-2 collision is actually a *double-overlap* collision, then this third complete collision has "already" occurred; moreover, it is clear that 2 and 3 cannot then recollide, this for the same reason that 1-2 and 1-3 cannot recollide. Thus, Theorem I holds trivially for a double-overlap collision. We therefore consider the non-trivial case in which 2 and 3 are not

overlapping at  $t=0$ , and are aimed to collide at some time  $t_1 > 0$ . Two cases can now be distinguished, corresponding to a 2-3 *interacting* collision (which we label "1") and a 2-3 *penetrating* collision (which we label "2"). Therefore we have six possible diagrams containing a single-overlap collision and a total of three complete collisions: (a1), (a2), (b1), (b2), (c1) and (c2). We show these diagrams in Fig. 30.

Our next task is to demonstrate that it is not possible to add another complete collision *either* in the past ( $t < 0$ ) *or* in the future ( $t > t_1$ ) of any of these six collision sequences.

If a fourth complete collision occurred at some  $t < 0$ , it would have to be a 2-3 collision. This follows by the same reasoning we used in establishing that the third collision at time  $t_1$  would have to be a 2-3 collision. On the other hand, if a fourth complete collision occurred at some  $t > t_1$  it would have to be other than a 2-3 collision, since 2 and 3 have just collided at time  $t_1$ . Thus, our theorem will be proved if we can establish that, for each of the six diagrams (a1) through (c2),

$\alpha$ : a 2-3 collision cannot occur for  $t < 0$

$\beta$ : a 1-2 collision cannot occur for  $t > t_1$

$\gamma$ : a 1-3 collision cannot occur for  $t > t_1$

Of the  $6 \times 3 = 18$  propositions to be proved, we can dispose of 10 of them rather easily by simply invoking the Recollision Rule (cf. p.39):

Diagrams (b2) and (c2) are composed of three non-interacting collisions involving the three pairs 1-2, 1-3, 2-3. Since there

are no interacting collisions present, all pairs will recede in the past and future, and no further collisions can occur.

Therefore

(b2) satisfies  $\alpha$ ,  $\beta$  and  $\gamma$

(c2) satisfies  $\alpha$ ,  $\beta$  and  $\gamma$

Diagrams (b1) and (b2) differ only in that the 2-3 collision at time  $t_1$  is interacting for (b1) and penetrating for (b2). For times  $t \leq t_1$  the diagrams are "dynamically equivalent"; i.e., for  $t \leq t_1$  the conditions on the phases of the three particles are identical, and are not affected by whether 2 and 3 bounce off each other or penetrate each other at the  $t_1$  collision. Therefore, from the fact that (b2) satisfies  $\alpha$  we may deduce

(b1) satisfies  $\alpha$

Similarly, (c1) and (c2) are dynamically equivalent for  $t \leq t_1$ , so from the fact that (c2) satisfies  $\alpha$  we may deduce

(c1) satisfies  $\alpha$

Finally, we observe that (a2) and (c2) are dynamically equivalent for  $t > 0$ , so since (c2) satisfies  $\beta$  and  $\gamma$ , then

(a2) satisfies  $\beta$  and  $\gamma$

We are now left with eight propositions to prove; these will require Lemma 1, which states that at no time during the recollision sequence (12)(13)<sup>i</sup>(12) is it possible for 2 and 3 to collide or overlap.

For times  $t \leq t_1$  diagrams (a1) and (a2) are dynamically equivalent, so we discuss proposition  $\alpha$  for these two diagrams together. Suppose  $\alpha$  were violated, and for some  $t' < 0$  a 2-3 collision occurred. Then reading from  $t'$  to  $t_1$  we would have

sequences of the form  $(23)(12)^i(23)$ , with 1 and 3 overlapping at  $t=0$ . But this violates Lemma 1, as can be seen by a trivial relabelling of the particles; thus, we conclude that

(a1) satisfies  $\alpha$

(a2) satisfies  $\alpha$

For times  $t \geq 0$  diagrams (a1) and (c1) are dynamically equivalent, so we discuss propositions  $\beta$  and  $\gamma$  for these two diagrams together. First, suppose  $\beta$  were violated, and for some time  $t' > t_1$  a 1-2 collision occurred. Then reading from time 0 to time  $t'$  we would have sequences of the form  $(12)(23)^i(12)$ , with 1 and 3 overlapping at  $t=0$ . This violates Lemma 1, as can be seen by a relabelling of the particles, and therefore

(a1) satisfies  $\beta$

(c1) satisfies  $\beta$

Next, suppose  $\gamma$  were violated in (a1) or (c1), so that for some time  $t' > t_1$  a 1-3 collision occurred. For this to happen, the 1-3 overlap condition which existed at  $t=0$  must have been terminated prior to time  $t_1$  (by the Recollision Rule), and so we let  $t''$  ( $0 < t'' < t_1$ ) be the time when the requisite separating collision occurred. Reading backwards in time from  $t'$  to  $t''$  we have sequences of the form  $(13)(23)^i(13)^n$ . The "last" collision,  $(13)^n$ , starts a time  $t''$  (still reading backwards), and is not yet completed at time 0 when 1 and 2 collide. This is a violation of Lemma 1, however, and therefore

(a1) satisfies  $\gamma$

(c1) satisfies  $\gamma$

It remains only to prove that diagram (b1) satisfies propositions  $\beta$  and  $\gamma$ . Now in this diagram, 1 overlaps with both 2 and 3 immediately after  $t=0$ . Let  $t' > 0$  and  $t'' > 0$  be the time when 1 and 2 separate and the time when 1 and 3 separate, respectively. If either  $t'$  or  $t''$  is greater than  $t_1$ , then the 2-3 collision at time  $t_1$  is an interacting overlap collision. But because of our disposal of the (a1) and (a2) diagrams, we know that a collision sequence containing an interacting overlap collision cannot violate the theorem. Thus, we restrict our attention to the cases where both  $t'$  and  $t''$  are less than  $t_1$ , and we distinguish two cases:  $t' < t''$  and  $t' > t''$ . For  $t' < t''$ , 1 and 2 separate while 1 and 3 are overlapping, and subsequently 2 and 3 interact; this is identical to diagram (c1), which diagram we have proved does not violate the theorem. For  $t' > t''$ , 1 and 3 separate while 1 and 2 are overlapping, and subsequently 2 and 3 interact; interchanging labels 2 and 3, we again obtain diagram (c1). We may conclude, then, that (b1) does not violate the theorem, and in particular that

(b1) satisfies  $\beta$  and  $\gamma$

We have thus shown that all six diagrams, (a1) through (c2), satisfy propositions  $\alpha$ ,  $\beta$  and  $\gamma$ , and our proof is complete.

*Q.E.D.*

► *THEOREM II.* If a three-particle collision sequence contains no single-overlap collision, then it cannot contain more than four complete collisions.

• *Proof.* Since by hypothesis no overlap collisions are allowed, then in between any concomittant pair of non-interacting penetrating and separating collisions, no third collision may occur. Thus, all *complete* collisions are disjoint, and we may unambiguously define a collision sequence by a left-to-right juxtaposition of  $(ab)$ -symbols, as defined in Sec. 3.2 [cf. (3-1)]. Our method of proof is to first list all possible collision sequences containing four complete collisions, and to then show that it is impossible to add a fifth complete collision without violating either the Recollision Rule or Lemmas 1, 2 or 3.

To obtain the four-collision sequences, let us assume the first collision is (12) and the second is (13). By the Recollision Rule the third collision can only be (12) or (23). If the third collision is (12), then the fourth collision can only be (13) or (23); if the third collision is (23), then the fourth collision can only be (12) or (13). Thus the candidates for the possible sequences containing four complete collisions are

(12) (13) (12) (13)

(12) (13) (12) (23)

(12) (13) (23) (12)

(12) (13) (23) (13)

We next display explicitly the interacting or non-interacting nature of the middle two collisions, at the same time indicating which sequences violate the Recollision Rule [RR] or Lemmas 1, 2 or 3 ([L1], [L2], [L3]).

$(12)(13)^i(12)^i(13)$ [L2]	$(12)(13)^n(12)^i(13)$ [RR]
$(12)(13)^i(12)^i(23)$	$(12)(13)^n(12)^i(23)$ [RR]
$(12)(13)^i(23)^i(12)$ [L2]	$(12)(13)^n(23)^i(12)$ [L1]
$(12)(13)^i(23)^i(13)$	$(12)(13)^n(23)^i(13)$
$(12)(13)^i(12)^n(13)$ [RR]	$(12)(13)^n(12)^n(13)$ [RR]
$(12)(13)^i(12)^n(23)$	$(12)(13)^n(12)^n(23)$ [RR]
$(12)(13)^i(23)^n(12)$ [L1]	$(12)(13)^n(23)^n(12)$ [RR]
$(12)(13)^i(23)^n(13)$ [RR]	$(12)(13)^n(23)^n(13)$ [RR]

We thus find that there are only four dynamically possible sequences of four complete collisions which do not involve an overlap. [We ignore for the moment the interacting or non-interacting nature of the first and fourth collisions.] It will be observed that two of these possible sequences are

$$(12)(13)^i(12)^i(23)$$

$$(12)(13)^i(12)^n(23)$$

while the other two sequences can be obtained from these by reversing time and renumbering the molecules. Hence, the above two sequences are the only "dynamically independent" sequences of four complete collisions [this observation justifies our remark in the text concerning (3-2)], and we may without loss of generality confine our further remarks to these two sequences.

The possible three-particle collision sequences containing *five* complete collisions and no single-overlap collision can evidently be obtained in two ways: *Either* we can add a (13)

or (23) collision *in front* of the two four-collision sequences (in which case we must pay attention to the interacting or non-interacting nature of the first collision); *or* we can add a (12) or (13) collision *in back* of the two four-collision sequences (in which case we must pay attention to the interacting or non-interacting nature of the last collision). We list below all these possibilities, and we indicate as before which sequences violate which restrictions. We use the fact, mentioned in the text, that sequences constructed by inserting additional complete non-interacting collisions into the sequences mentioned in Lemma 2 are also not possible.

$(13)(12)^i(13)^i(12)^i(23)$ [L2]	$(13)(12)^i(13)^i(12)^n(23)$ [L2]
$(23)(12)^i(13)^i(12)^i(23)$ [L3]	$(23)(12)^i(13)^i(12)^n(23)$ [L2]
$(13)(12)^n(13)^i(12)^i(23)$ [RR]	$(13)(12)^n(13)^i(12)^n(23)$ [RR]
$(23)(12)^n(13)^i(12)^i(23)$ [L2]	$(23)(12)^n(13)^i(12)^n(23)$ [L1]
$(12)(13)^i(12)^i(23)^i(12)$ [L3]	$(12)(13)^i(12)^n(23)^i(12)$ [L2]
$(12)(13)^i(12)^i(23)^i(13)$ [L2]	$(12)(13)^i(12)^n(23)^i(13)$ [L1]
$(12)(13)^i(12)^i(23)^n(12)$ [RR]	$(12)(13)^i(12)^n(23)^n(12)$ [RR]
$(12)(13)^i(12)^i(23)^n(13)$ [L1]	$(12)(13)^i(12)^n(23)^n(13)$ [RR]

Since every sequence violates some restriction, the theorem is proved. Q.E.D.

## REFERENCES

1. E.G.D. Cohen, *Recent Advances in Engineering Science*, A.C. Eringen, ed., Gordon and Breach, New York, 1968, p.125.
2. J.R. Dorfman and E.G.D. Cohen, *J. Math. Phys.* 8, 282 (1967).
3. J.V. Sengers, *Recent Advances in Engineering Science*, Vol.III, A.C. Eringen, ed., Gordon and Breach, New York, 1968, p.153.
4. S. Chapman and T.G. Cowling, *The Mathematical Theory of Nonuniform Gases*, Cambridge Univ. Press, London and New York, 2nd ed., 1952.
5. J.O. Hirschfelder, C.F. Curtiss and R.B. Bird, *Molecular Theory of Gases and Liquids*, John Wiley, New York, 1954.
6. J.V. Sengers, *Triple Collision Effects in the Thermal Conductivity and Viscosity of Moderately Dense Gases*, AEDC-TR-69-68, Arnold Engineering Development Center, Tennessee, 1969.
7. Ref. 4, Chapter 16 and Ref. 5, Chapter 9.
8. H.J.M. Hanley, R.D. McCarty and J.V. Sengers, *J. Chem. Phys.* 50, 857 (1969).
9. M.H. Ernst, J.R. Dorfman, W.R. Hoegy and J.M.J. Van Leeuwen, *Physica* 45, 127 (1969).
10. E.G.D. Cohen, *Fundamental Problems in Statistical Mechanics*, North-Holland, Amsterdam, 1962, p.110.
11. J.V. Sengers and E.G.D. Cohen, *Physica* 27, 230 (1961).
12. J.V. Sengers, *Boulder Lectures in Theoretical Physics*, Vol.9C, W.E. Brittin, ed., Gordon and Breach, New York, 1967, p.335.
13. J.V. Sengers, *Proceedings of the Symposium on Kinetic Equations*, Cornell Univ. 1969, R. Liboff and N. Rostoker, eds., Gordon and Breach, New York, 1970, p.137.
14. G. Sandri, R.D. Sullivan and P. Norem, *Phys. Rev. Letters*, 13, p.743 (1964);  
G. Sandri and A.H. Kritz, *Phys. Rev.* 150, 92 (1966).

15. E.G.D. Cohen, *Boulder Lectures in Theoretical Physics*, Vol.8A, Univ. of Colo. Press, Boulder, Colo., 1966, p. 170;  
T.J. Murphy, "A Theorem on Three Hard Spheres", preprint.
16. T.J. Murphy, private communication.
17. J.V. Sengers, D.T. Gillespie and W.R. Hoegy, *Physics Letters*, 32A, 387 (1970).
18. W.R. Hoegy and J.V. Sengers, *Phys. Rev.* (to appear in December 1970 issue).
19. M.H. Ernst, L.K. Haines and J.R. Dorfman, *Rev. Mod. Phys.*, 41, 296 (1969).
20. M.S. Green, *J. Chem. Phys.*, 25, 836 (1956).
21. E.G.D. Cohen, *J. Math. Phys.*, 4, 183 (1963).
22. J.V. Sengers, *Phys. Fluids*, 9, 1333 (1966).
23. M.S. Green, *Phys. Rev.*, 136, A905 (1964).
24. G. Marsaglia and T. Bray, "One-Line Random Number Generators and their Use in Combinations", Boeing Scientific Research Laboratories Document D1-82-0689 (1968).
25. J.M. Hammersley and D.C. Handscomb, *Monte Carlo Methods*, Methuen, London, 1964.
26. D.T. Gillespie, "Monte Carlo Techniques for Analyzing Elementary Particle Reaction Mechanisms", Department of Physics Report, Johns Hopkins University, 1968.
27. B.J. Alder and T.E. Wainwright, *Phys. Rev. Letters* 18, 988 (1967).

## DOCUMENT CONTROL DATA - R &amp; D

(Security classification of title, body of abstract and indexing annotation must be entered when the overall report is classified)

1. ORIGINATING ACTIVITY (Corporate author) Institute for Molecular Physics University of Maryland College Park, Maryland 20742		2a. REPORT SECURITY CLASSIFICATION <b>UNCLASSIFIED</b>	
		2b. GROUP N/A	
3. REPORT TITLE TRIPLE COLLISION EFFECTS IN THE THERMAL CONDUCTIVITY AND VISCOSITY OF MODERATELY DENSE GASES. PART II.			
4. DESCRIPTIVE NOTES (Type of report and inclusive dates) September 1, 1968 - September 1, 1970 - Interim Report			
5. AUTHOR(S) (First name, middle initial, last name) Daniel T. Gillespie and Jan V. Sengers			
6. REPORT DATE March 1971	7a. TOTAL NO. OF PAGES 167	7b. NO. OF REFS 27	
8a. CONTRACT OR GRANT NO. F40600-69-C-0002	9a. ORIGINATOR'S REPORT NUMBER(S) AEDC-TR-71-51		
b. PROJECT NO. 8951			
c. Program Element 61102F	9b. OTHER REPORT NO(S) (Any other numbers that may be assigned this report) N/A		
d.			
10. DISTRIBUTION STATEMENT This document has been approved for public release and sale; its distribution is unlimited.			
11. SUPPLEMENTARY NOTES Part I of this title is available as AEDC-TR-69-68. Available in DDC	12. SPONSORING MILITARY ACTIVITY Arnold Engineering Development Center, Air Force Systems Command, Arnold Air Force Station, Tennessee		
13. ABSTRACT Calculations of transport properties of dilute gases are always based on the Boltzmann equation. The Boltzmann equation accounts only for the effects of collisions between two gas molecules. To predict transport properties of moderately dense gases one needs to determine the effects of collisions among more than two gas molecules. The present report studies the contributions to the transport properties caused by collisions among three gas molecules. It is demonstrated that the first density correction to the transport properties can be represented by a series of collision integrals associated with one, two, three and four collisions between three gas molecules. Numerical studies for calculating the dominant collision integrals are made for a gas of hard spherical molecules.			

14. KEY WORDS	LINK A		LINK B		LINK C	
	ROLE	WT	ROLE	WT	ROLE	WT
transport properties thermal conductivity viscosity triple collisions dense gases hard spheres						
1. Gases --     ↙						
2 4     --     ↙						
3   "     --     ↙						
4   "     --     ↙						
<del>5   "     --     ↙</del>						